The stability of a fluid film on the surface of a cone

Michael John Holgate

THE STABILITY OF A FLUID FILM ON THE SURFACE OF A CONE

by

Michael John Holgate, M.A. (Cantab)

Thesis submitted for the degree of
Doctor of Philosophy
in the
University of Durham

Department of Engineering Science,
The University,
Durham.

May 1971

ABSTRACT

The flow is studied of a fluid film originating from a source at the apex of a right circular cone, and flowing under gravity over its outer surface. A modified Orr-Sommerfeld equation is derived for the flow. This and the corresponding boundary conditions contain terms introducing distance along the cone generator as a parameter. The system of equations is solved for small wave number to give a stability criterion, which shows the flow to be unstable for all practical values of Reynolds number.

Results of experiments on a 60° included angle cone are presented, giving the pattern of behaviour of the main film and waveform characteristics. Mean film thickness is expressed as a function of Reynolds number only and found to be less than that of an undisturbed laminar film. Wave amplitude is shown to reach a limiting value and thereafter decline. Wave number is shown to be linearly related to a non-dimensional parameter incorporating viscosity, surface tension and slope derived from one proposed by Berbente and Ruckenstein whose theory also matches well the limiting amplitudes measured. Wave speed and wavelength are also measured and discussed.

ACKNOWLEDGEMENTS

The work reported here would not have been possible without the help of many people. Sincere thanks are extended to all, but of those involved the following played the largest parts, they are listed in the order of their appearance. Professor Russell Hoyle suggested the problem, supervised its early stages and provided continued and much appreciated encouragement throughout. Mr. D. Dryden assisted with the design of the basic experimental rig which was made by Mr. F. Venmore and the staff of the University Science Site Workshop, and maintained and further elaborated by Mr. C.J.F. Campbell and the technical staff of the Department of Engineering Science. Professor H. Naylor provided much helpful comment and discussion in his supervision of the later stages. Mr. T. Brown helped with the cinephotography, and Mrs. Gina Ribchester speedily deciphered and typed my manuscript.

Thanks must also be extended to the two successive Chairmen of the Board of Studies in Engineering Science, Professor Russell Hoyle and Professor G.R. Higginson for allowing the use of the facilities of that department. Finally no catalogue of indebtedness would be complete without my thanks to Pauline and the children who have had to be so patient of late.

CONTENTS

	Abstract	i
	Acknowledgements	ii
	Contents	iii, iv
	List of Figures	v
1	Introduction	1
1.1	Historical Survey	1
1.2	The Present Work	5
2	Theory	7
2.1	The Co-ordinate System	7
2.2	The Equations of Motion	8
2.2.1	The Navier Stokes Equations in terms of XYΘ	9
2.2.2	The Continuity Equation	13
2.2.3	The Elimination of Higher Order Small Terms	15
2.2.4	Body and Pressure Force Terms	17
2.2.5	Non-Dimensional Forms of the Equation of Motion	17
2.3	The Undisturbed Mean Flow	20
2.4	The Disturbed Flow	25
2.4.1	Introduction	25
2.4.2	Equations of Motion for the Disturbance Isolated from the Mean Flow	26
2.5	Boundary Conditions	32
2.5.1	At the Cone Surface	32
2.5.2	Shear Stress at the Free Surface	33
2.5.3	Continuity of Normal Stress at the Free Surface	35
2.6	Solution	39
2.6.1	Introduction	39
2.6.2	Solution for Zero Reynolds Number	40
2.6.3	Solution for Small Reynolds Number	44
2.6.4	Discussion of the Stability Criterion	47
3	Experimental Work	50
3.1	Film Flow Rig	50
3.1.1	The Cone	50
3.1.2	The Water Supply	52
3.1.3	The Measuring Station	53
3.2	Instrumentation	55
3.2.1	The Capacitance Measuring System	55
3.2.2	The Probe	58
3.2.3	The Amplifier	60
3.2.4	Recording	61

3.3 Photography 63
3.3.1 Still Photography 63
3.3.2 Cine Photography 63

3.4 Cone Setting 65
3.4.1 Levelling 65
3.4.2 Film Uniformity 66

3.5 Calibration of the Instrumentation 71
3.5.1 Static Voltmeter Calibration 71
3.5.2 Static Recorder Calibration 76
3.5.3 Dynamic Voltmeter and Recorder Comparison 78

3.6 Tests 81
3.6.1 Mean Film Thickness 81
3.6.2 Wave Measurements - Amplitude and Frequency 84
3.6.3 Wave Measurements - Wavespeed and Wavelength 85

3.7 Wave Analysis 87
3.7.1 Trials with a Wave Analyser 87
3.7.2 Fourier Analysis 87
3.7.3 Statistical Analysis Program 90

4 Results and Discussion 92

4.1 Mean Film Thickness 92
4.2 Wave Amplitude 100
4.2.1 Peak Amplitude 100
4.2.2 Root Mean Square Amplitude 106
4.2.3 Comparison with Inclined Plane Flow Predictions 109
4.3 Wave Speed and Wavelength 114
4.3.1 Wave Speed 114
4.3.2 Spectral Density 119
4.3.3 Wavelength 123
4.4 Wave Number 126

5 Conclusions 131

Notation 135

Bibliography 138

Appendices -

I Shape Correction for Capacitance Probe 141
II Fourier Analysis Program 146
III Statistical Analysis Program 147

LIST OF FIGURES

2.1.1	The co-ordinate system	7
2.2.1	The continuity element	13
3.1.1	Film flow rig	51
3.2.1	Block diagram of Wayne Kerr Distance Meter	56
3.2.2	Probe capacitor diagram	57
3.2.3	Probe	59
3.2.4	Amplifier circuit	60
3.2.5	Recorder supply circuit	61
3.2.6	Block diagram of complete instrumentation	62
3.4.1	Generator labelling diagram	65
3.4.2	Cone cap section	66
3.4.3	Graph - mean film thickness at 4 Quadrature points	69
3 5.1	Calibration arrangement	73
3.5.2	Graph - probe calibration factor ∽. check circuit voltage	75
3.5.3	Graph - voltmeter reading ∽. mean recorder deflection	79
4.1.1	Graph - mean film thickness ∽. flowrate	94
4.1.2	Graph - mean film thickness ∽. diameter	96
4.1.3	Graph - mean film thickness ∽. Reynolds number	98
4.2.1	Sample recorder traces	101
4.2.2	Graphs - peak and trough film thickness	102
4.2.3	Graphs - peak amplitude variation	105
4.2.4	Graphs - r.m.s. amplitude variation	107
4.2.5	Graphs - wave intensity variation	108
4.2.6	Graph - amplitude ∽. Reynolds number	110
4.2.7	Graph - amplitude ∽. ψ_{GR}	112
4.3.1	Graphs - wave speed variation	115-117
4.3.2	Graphs - spectral densities	120
4.3.3	Graph - peak frequency ∽. diameter	122
4.3.4	Graphs - wavelength variation	124
4.4.1	Graph - wave number ∽. diameter	127
4.4.2	Graph - wave number ∽. ψ_{GR}	129
4.4.3	Graph - constant of proportionality ∽. flowrate	130
App.I.1	Graph - correction factor variation	145

1

INTRODUCTION

1 INTRODUCTION

1.1 Historical Survey

The behaviour of thin films flowing under gravity is a problem which has interested many investigators over the years. Their interest has been seized by a number of different aspects from the purely academic unravelling of the governing mathematics to the more commercially applicable interest in the film's effect on heat and mass transfer rates. For such films are to be found in abundance in industrial process plant. Films of condensate drain down the walls and tubes of condensers. Absorbent liquid films flow under gravity through gas cleaning and cooling towers. In other related cases the primary influence of gravity is replaced by, or becomes subordinate to, other accelerating forces, notably that induced by spinning.

The first published work on film flow was that of Hopf ('10)* who investigated flows in an open channel of shallow slope. The films were fairly thick, so that despite the shallowness of the slope and consequent low velocity the Reynolds numbers recorded were upwards of 150. Nusselt ('16) published the first paper on the effect of condensate films on heat transfer. In this paper he derived the semi-parabolic velocity profile for undisturbed viscous flow for the first time. Interest then declined until the 1930s when first Warden ('30) then Kirkbride ('34), Cooper, Drew and Macadams ('34) and Fallah, Hunter and Nash ('34) all published work on falling films. They chiefly reported experimentally determined film thicknesses, and were all concerned with flow on vertical plates or on the inside or outside of vertical tubes.

---

*The figure in brackets refers to the year of publication in this century. Details may be found in the Bibliography.

Kirkbride and later Friedman and Miller ('41) and Grimley ('45) found that flow at very low Reynolds number appeared entirely smooth. Consequently efforts were made to establish the value of a critical Reynolds number, above which waves appeared. These efforts, culminating with that of Binnie ('57), were generally inconclusive since different workers with different techniques arrived at different values. Those obtained however were generally in the range of Reynolds numbers between 4 and 10.

All the above work was primarily experimental, the theoretical treatment extending little beyond Nusselt's semi-parabolic velocity distribution derivation. Kapitza ('48 - 1) laid down equations of motion for the flow from which he obtained an approximate periodic solution. He obtained also expressions for the wave profile, its phase velocity and amplitude. In a second paper, Kapitza ('48 - 2) he examined the effect of a gas flow above the film, which had been the subject also of some of the experimental work listed above. Finally, Kapitza and Kapitza ('49), he reported the result of experimental work carried out jointly with his son on flow down the outside of a vertical cylinder, which substantially bore out his theoretical predictions within the rather wide error limits of his experiments and approximation. In addition to fairly regular periodic waves, he observed under similar flow conditions, single waves at long intervals.

The next major theoretical step forward was made at about the same time by Benjamin ('57) and Yih ('54 and '63). By different methods, they examined the stability characteristics of full equations of motion derived from the Navier-Stokes equations. They

supposed a periodic disturbance and found it to be governed by an equation of the type previously examined by Orr ('27) and Sommerfeld ('08) for two dimensional Couette flow, now known as the Orr-Sommerfeld Equation, together with appropriate boundary conditions. Both Benjamin and Yih related their work specifically to flow down an inclined plane. Benjamin sought an approximate solution using a series approximation method. Yih used a more elegant perturbation method. Both arrived at an identical criterion for stability based on wave number and Reynolds number. This showed that the flow is unstable, that is waves could form, at any finite value of Reynolds number. That the surface appears unaffected at very low Reynolds number is due to the fact that the rate of amplification of the wave disturbances becomes very small at small Reynolds number, and the disturbances remain undetected.

Yih's analytical method has remained the most popular approach adopted by numerous workers since for the investigation of special problems, many of which have been examined. Yih ('65) carried out an analysis for a non-Newtonian fluid, and Yih ('67) looked at the effect of viscosity stratification in the film. Much has been published on the effect of surface active agents in reducing waviness: Benjamin ('64), Whitaker ('64) and Anshus and Acrivos ('67). The effect of visco-elasticity has been studied by Jones and Whitaker ('66), Whitaker and Jones ('66), Gupta ('67) and Gupta and Rai ('67). Variation of the underlying solid boundary received attention from Buevich and Gupalo ('67) who examined the effect of curvature, and Gupta ('66) who allowed for flexibility. Mainly experimental work

by Portalski ('64. 1 and 2) concentrated on the determination of velocities and behaviour in eddies under the waves; while Ruckenstein and Berbente ('65) continued the earlier interest in the effect of the waviness of the film on greatly increasing heat and mass transfer rates. A very recent investigation by Telles and Dukler ('70) used statistical techniques in a manner similar to the author to try to resolve the problem of a lack of a dominant periodicity at higher Reynolds numbers.

On the theoretical front Massot, Irani and Lightfoot ('66) examined the effect of surface tension, finding that the Weber number is an important governing parameter. More recently still attempts have been directed towards a theoretical prediction of wave amplitudes. Berbente and Ruckenstein ('68) derived a complex non-dimensional parameter whose effect on amplitude they examined. This highly complex parameter may in fact be simply reduced to a much simpler combination of Reynolds number and Weber number, a fact also spotted by Krantz and Goren ('70) who present a similar group as a basis for determining amplitude. Lee ('69) updated and strengthened Kapitza's analysis. In two very significant recent papers Lin ('69 and '70) has shown that the unstable film develops finite amplitude waves that then stabilise at a particular amplitude. This amplitude and the corresponding wave speed he then predicts in terms of the primary parameters of film thickness, wavelength, mean film speed and fluid properties.

The subject has been well served by bibliographers. Both Fulford ('64) and Chien and Ibele ('67) present fuller comparative surveys than is possible in this brief historical sketch.

1.2 The Present Work

The author's introduction to the problem came as part of a larger research project under the supervision of Professor Russell Hoyle. This sought to examine the heat transfer rates associated with condensation on a rotating conical surface. It followed earlier investigations by Hoyle and Matthews ('64. 1 and 2) into condensation on a rotating cylinder, and Espig and Hoyle ('67) into condensation on a rotating disc. The conical surface, Howe and Hoyle ('70) and Robson ('70) followed naturally as representing a shape intermediate between the extremes of cylinder and disc. Such heat transfer rates will clearly be affected by the presence of a film of condensate on the cool rotating body, and the mechanism of its drainage is of great importance. Thus was conceived the idea of examining this drainage as a separate problem, whose own complexity and interest became rapidly apparent. Exact correspondence with the condensate film problem is only possible with a continuous supply of fluid to the film at all points of the surface. This might be possible using a porous cone, but the author chose instead to follow the simpler case of a single source of fluid supply at the apex of the cone, from which the fluid spreads out over the conical surface. This leads to a situation of interest in its own right, since the fluid film becomes thinner as it progresses downwards over the widening surface area. Associated with this thinning is a reduction of the film's Reynolds number, the parameter which all investigations to date have suggested is of paramount importance in determining the waviness of the film.

In respect of this thinning, the film differs from those on which work has been published to date, namely films flowing down

inclined or vertical plates, or on the inside or outside of vertical cylindrical tubes. A few publications which have referred to a situation where thinning occurs have been those of Hinze and Milborn ('50), Nikolaev, Vachagin and Baryshev ('67) and Voinov and Khapilova ('69), all of which were on flow inside a spinning conical cup. These were chiefly concerned with flow characteristics within the film, and its atomisation at the cup rim, rather than with the behaviour of the film surface.

The present work, therefore, was undertaken with two primary aims. First, it aimed at deriving the equation of motion and boundary conditions for the film flow external to a conical surface, introducing in particular the effect of a coordinate in the direction of flow indicative of a reduction in mean film thickness. The equations were then solved using a perturbation method to determine the effect of conicity, as compared with flow over a plane surface. Secondly, an experimental investigation aimed at establishing the main dimensional characteristics of the film.

2

THEORY

2 THEORY

2.1 The Co-ordinate System

While it would be possible to describe the problem in terms of any 3 co-ordinate system, it is most convenient to adopt a system based on co-ordinates:-

X - along a generator of the cone, which is the direction of the main undisturbed flow.

Y - normal to the cone surface, and consequently normal to the main flow direction.

Θ - giving angular position; since in the case of a stationary cone the problem is essentially axisymmetric, this co-ordinate is included for the sake of completeness at this stage, but is later found unnecessary.

Fig. 2.1.1 thus defines the co-ordinate system adopted.

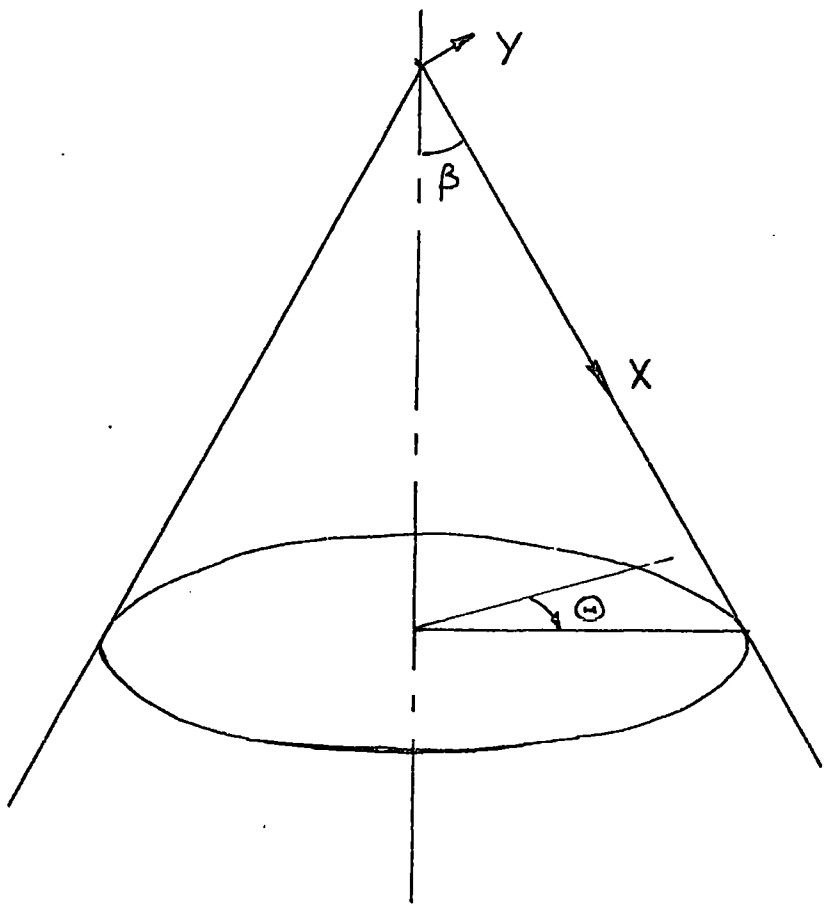

It is worth noting at this stage that all authors to date who have considered the problem of stability of falling films have chosen to take the origin of the coordinate normal to the main flow direction, Y above, at the undisturbed free surface, with the +ve direction of the coordinate into the film. They have however been concerned with flow along a plane surface, so that the undisturbed free surface is itself a plane in steady flow. Adoption of such a system somewhat simplifies the boundary conditions. In the present case, however, the author thought it more satisfactory to take the cone surface as origin with the +ve direction outwards through the film. This is on account of the additional curvature, albeit small, of the undisturbed free surface in the meridional plane of the cone.

Also defined by Fig. 2.1.1 is β, the half angle of the cone.

2.2 The Equations of Motion

It is necessary to assume from the outset that flow is laminar, and also essentially steady but for the presence of small disturbances. The stability of those disturbances is then studied in order to obtain information as to what conditions will aid the growth of such disturbances and result in the appearance of waves on the surface of the fluid.

Following from the assumption that flow is laminar, a set of Navier-Stokes equations appropriate to the coordinates chosen can be derived from the generalised vectorial form of the equation. This is done for the full 3 dimensional case in section 2.2.1. Section 2.2.2

contains a derivation of the corresponding continuity equation. These full equations are exceedingly lengthy and by an order of magnitude assessment can be considerably reduced. This reduction, together with the assumptions of axial symmetry and steady flow yields the three simplified equations of motion at the end of Section 2.2.3.

2.2.1 The Navier Stokes Equations in terms of X Y Θ

The general vectorial form of the Navier Stokes equation is

$$\frac{d\tilde{v}}{dt} - \tilde{v}\times\tilde{\omega} = \tilde{F} - \text{grad}\left(\frac{p}{\rho} + \frac{1}{2}v^2\right) + \nu\left(\text{grad div } \tilde{v} - \text{curl } \tilde{\omega}\right) \qquad - 2.2.1.$$

where $\tilde{v}$ is the velocity vector

$\tilde{\omega}$ is the vorticity vector

$\tilde{F}$ is the body force/unit mass vector

Following Lamb ('32 p.156) consider the generalised curvilinear co-ordinates α , β , γ , which have elemental increases of length in their respective directions of $h_1 d\alpha$, $h_2 d\beta$, $h_3 d\gamma$. Equating our coordinates X, Y, Θ , to α , β , γ we find

$$h_1 = h_2 = 1 \qquad h_3 = X\sin\beta + Y\cos\beta = R$$

If the components of velocity in the coordinate directions are U, V, W and the components of vorticity ξ , η , ζ , then each term in the above vectorial equation may be split into the components as follows.

$\frac{d\tilde{v}}{dt}$	$\frac{\partial U}{\partial t}$	$\frac{\partial V}{\partial t}$	$\frac{\partial W}{\partial t}$
$\tilde{v}\times\tilde{\omega}$	$V\zeta - W\eta$	$W\xi - U\zeta$	$U\eta - V\xi$
$\text{grad}(\ )$	$\frac{1}{h_1}\frac{\partial}{\partial X}(\ )$	$\frac{1}{h_2}\frac{\partial}{\partial Y}(\ )$	$\frac{1}{h_3}\frac{\partial}{\partial \Theta}(\ )$

curl $\tilde{\omega}$ $\quad \frac{1}{h_2 h_3}\left[\frac{\partial}{\partial Y}(h_3\zeta) - \frac{\partial}{\partial\Theta}(h_2\eta)\right]$

$$\frac{1}{h_3 h_1}\left[\frac{\partial}{\partial\Theta}(h_1\xi) - \frac{\partial}{\partial X}(h_3\zeta)\right]$$

$$\frac{1}{h_1 h_2}\left[\frac{\partial}{\partial X}(h_2\eta) - \frac{\partial}{\partial Y}(h_1\xi)\right]$$

and since $\quad \tilde{\omega} = \text{curl } \tilde{G}$

we have for the components of $\tilde{\omega}$

$$\xi = \frac{1}{h_2 h_3}\left[\frac{\partial}{\partial Y}(h_3 W) - \frac{\partial}{\partial\Theta}(h_2 V)\right]$$

$$= \frac{\partial W}{\partial Y} + \frac{1}{R}\left[W\cos\beta - \frac{\partial V}{\partial\Theta}\right]$$

$$\eta = \frac{1}{h_3 h_1}\left[\frac{\partial}{\partial\Theta}(h_1 U) - \frac{\partial}{\partial X}(h_3 W)\right]$$

$$= -\frac{\partial W}{\partial X} - \frac{1}{R}\left[W\sin\beta - \frac{\partial U}{\partial\Theta}\right]$$

$$\zeta = \frac{1}{h_1 h_2}\left[\frac{\partial}{\partial X}(h_2 V) - \frac{\partial}{\partial Y}(h_1 U)\right]$$

$$= \frac{\partial V}{\partial X} - \frac{\partial U}{\partial Y}$$

In addition we have

$$\text{div } \tilde{G} = \frac{1}{h_1 h_2 h_3}\left[\frac{\partial}{\partial X}(h_2 h_3 U) + \frac{\partial}{\partial Y}(h_3 h_1 V) + \frac{\partial}{\partial\Theta}(h_1 h_2 W)\right]$$

$$= \frac{1}{R}\left[U\sin\beta + R\frac{\partial U}{\partial X} + V\cos\beta + R\frac{\partial V}{\partial Y} + \frac{\partial W}{\partial\Theta}\right]$$

$$= \frac{\partial U}{\partial X} + \frac{\partial V}{\partial Y} + \frac{1}{R}\left[U\sin\beta + V\cos\beta + \frac{\partial W}{\partial\Theta}\right]$$

These then are the basic components from which it is possible to build the Navier-Stokes equation for each coordinate direction term by term.

The equation in the X direction then is

$$\frac{\partial u}{\partial t} - (V\zeta - W\eta) = F_x - \frac{1}{h_1}\frac{\partial}{\partial x}\left[\frac{P}{\rho} + \frac{1}{2}(u^2+V^2+W^2)\right] + \nu\left[\frac{1}{h_1}\frac{\partial}{\partial x}(\operatorname{div}\vec{v}) - \frac{1}{h_2h_3}\left\{\frac{\partial}{\partial y}(h_3\zeta) - \frac{\partial}{\partial\Theta}(h_2\eta)\right\}\right]$$

Taking these terms one by one for simplification

$$V\zeta - W\eta = V\frac{dV}{dX} - V\frac{dU}{dY} + W\frac{dW}{dX} + \frac{W}{R}\left[W\sin\beta - \frac{\partial U}{\partial\Theta}\right]$$

$$\frac{1}{h_1}\frac{\partial}{\partial X}\left[\frac{P}{\rho} + \frac{1}{2}(U^2+V^2+W^2)\right] = \frac{1}{\rho}\frac{\partial P}{\partial X} + U\frac{\partial U}{\partial X} + V\frac{\partial V}{\partial X} + W\frac{\partial W}{\partial X}$$

$$\frac{1}{h_1}\frac{\partial}{\partial X}(\operatorname{div}\vec{v}) = \frac{\partial}{\partial X}\left[\frac{\partial U}{\partial X} + \frac{\partial V}{\partial Y} + \frac{1}{R}\left\{U\sin\beta + V\cos\beta + \frac{\partial W}{\partial\Theta}\right\}\right]$$

$$= \frac{\partial^2 U}{\partial X^2} + \frac{\partial^2 V}{\partial X\partial Y} + \frac{1}{R}\left[\frac{\partial U}{\partial X}\sin\beta + \frac{\partial V}{\partial X}\cos\beta + \frac{\partial^2 W}{\partial X\partial\Theta}\right] - \frac{\sin\beta}{R^2}\left[U\sin\beta + V\cos\beta + \frac{\partial W}{\partial\Theta}\right]$$

$$\frac{1}{h_2h_3}\left[\frac{\partial}{\partial Y}(h_3\zeta) - \frac{\partial}{\partial\Theta}(h_2\eta)\right] = \frac{1}{R}\left[R\frac{\partial\zeta}{\partial Y} + \zeta\cos\beta - \frac{\partial\eta}{\partial\Theta}\right]$$

$$= \frac{\partial^2 V}{\partial Y\partial X} - \frac{\partial^2 U}{\partial Y^2} + \frac{\cos\beta}{R}\left[\frac{\partial V}{\partial X} - \frac{\partial U}{\partial Y}\right] + \frac{1}{R}\frac{\partial^2 W}{\partial\Theta\partial X} + \frac{1}{R^2}\left[\frac{\partial W}{\partial\Theta}\sin\beta - \frac{\partial^2 U}{\partial\Theta^2}\right]$$

Assembling these terms, we get after some reduction and reorganisation

$$\frac{\partial U}{\partial t} + U\frac{\partial U}{\partial X} + V\frac{\partial U}{\partial Y} + \frac{W}{R}\left(\frac{\partial U}{\partial \Theta} - W\sin\beta\right)$$

$$= F_x - \frac{1}{\rho}\frac{\partial P}{\partial X} + \nu\left[\frac{\partial^2 U}{\partial X^2} + \frac{\partial^2 U}{\partial Y^2} + \frac{1}{R}\left\{\frac{\partial U}{\partial X}\sin\beta + \frac{\partial U}{\partial Y}\cos\beta\right\}\right.$$

$$\left. -\frac{1}{R^2}\left\{\left(U\sin\beta + V\cos\beta + 2\frac{\partial W}{\partial \Theta}\right)\sin\beta - \frac{\partial^2 U}{\partial \Theta^2}\right\}\right]$$

- 2.2.2.

A similar approach yields for the equation in the Y direction

$$\frac{\partial V}{\partial t} + U\frac{\partial V}{\partial X} + V\frac{\partial V}{\partial Y} + \frac{W}{R}\left(\frac{\partial V}{\partial \Theta} - W\cos\beta\right)$$

$$= F_y - \frac{1}{\rho}\frac{\partial P}{\partial Y} + \nu\left[\frac{\partial^2 V}{\partial X^2} + \frac{\partial^2 V}{\partial Y^2} + \frac{1}{R}\left\{\frac{\partial V}{\partial X}\sin\beta + \frac{\partial V}{\partial Y}\cos\beta\right\}\right.$$

$$\left. -\frac{1}{R^2}\left\{\left(U\sin\beta + V\cos\beta + 2\frac{\partial W}{\partial \Theta}\right)\cos\beta - \frac{\partial^2 V}{\partial \Theta^2}\right\}\right]$$

- 2.2.3.

and in the Θ direction

$$\frac{\partial W}{\partial t} + U\frac{\partial W}{\partial X} + V\frac{\partial W}{\partial Y} + \frac{W}{R}\left(\frac{\partial W}{\partial \Theta} + U\sin\beta + V\cos\beta\right)$$

$$= F_\Theta - \frac{1}{R\rho}\frac{\partial P}{\partial \Theta} + \nu\left[\frac{\partial^2 W}{\partial X^2} + \frac{\partial^2 W}{\partial Y^2} + \frac{1}{R}\left\{\frac{\partial W}{\partial X}\sin\beta + \frac{\partial W}{\partial Y}\cos\beta\right\}\right.$$

$$\left. +\frac{1}{R^2}\left\{2\frac{\partial U}{\partial \Theta}\sin\beta + 2\frac{\partial V}{\partial \Theta}\cos\beta + \frac{\partial^2 W}{\partial \Theta^2} - W\right\}\right]$$

- 2.2.4.

2.2.2 The Continuity Equation

This is most easily derived by considering the mass flux through a small element of volume as shown in Figure 2.2.1. Since the fluid is incompressible there can be no gain in mass within the element. That is

$$\int_{Area} \rho \tilde{v} \cdot d\tilde{A} = 0$$

or where the area can be divided into n distinct faces

$$\sum_{m=1}^{n} V_m A_m = 0$$

where V_m is the velocity normal to the face of area A_m

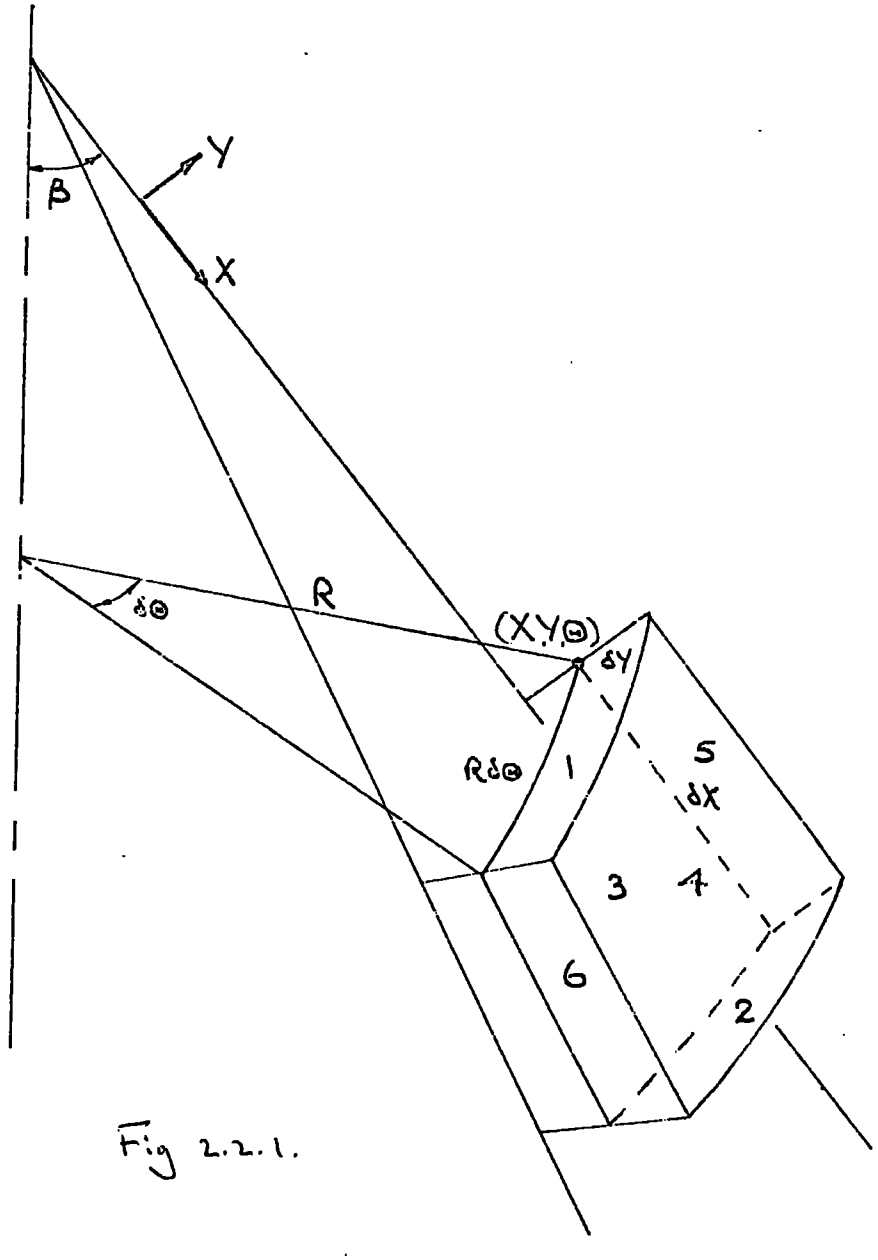

Fig 2.2.1.

Consider the $V_m A_m$ product for the faces numbered as shown

m	V_m (+ve outwards)	A_m
1	$-U$	$\left(R + \frac{1}{2}\frac{\partial R}{\partial Y}\delta Y\right)\delta\Theta . \delta Y$
2	$U + \frac{\partial U}{\partial X}\delta X$	$\left(R + \frac{\partial R}{\partial X}\delta X + \frac{1}{2}\frac{\partial R}{\partial Y}\delta Y\right)\delta\Theta . \delta Y$

Now $R = X\sin\beta + Y\cos\beta$

$\therefore \quad \frac{\partial R}{\partial X} = \sin\beta \qquad \frac{\partial R}{\partial Y} = \cos\beta$

Hence $V_1A_1 + V_2A_2 = \left[U\sin\beta + R\frac{\partial U}{\partial X}\right]\delta X . \delta Y . \delta\Theta + O(\delta^4)$

Similarly for faces 3 and 4

$$V_3A_3 + V_4A_4 = \left[V\cos\beta + R\frac{\partial V}{\partial Y}\right]\delta X . \delta Y . \delta\Theta + O(\delta^4)$$

Faces 5 and 6 both have area $\delta X . \delta Y$

Hence

$$V_5A_5 + V_6A_6 = \frac{\partial W}{\partial\Theta} . \delta X . \delta Y . \delta\Theta$$

$\therefore$ Summing for all faces

$$\sum_{m=1}^{6} V_m A_m = \left[U\sin\beta + V\cos\beta + R\left(\frac{\partial U}{\partial X} + \frac{\partial V}{\partial Y}\right) + \frac{\partial W}{\partial\Theta}\right]\delta X . \delta Y . \delta\Theta$$

$$= 0$$

$\therefore$ the continuity equation is

$$\frac{\partial U}{\partial X} + \frac{\partial V}{\partial Y} + \frac{1}{R}\left[U\sin\beta + V\cos\beta + \frac{\partial W}{\partial\Theta}\right] = 0$$

2.2.3 The Elimination of Higher Order Small Terms

The Navier-Stokes equations as presented in 2.2.1. contain a large number of terms which vary considerably in their orders of magnitude. The problem under consideration is that of the flow of a thin film of fluid over a comparatively large surface area. Thus it follows that the maximum value of the coordinate Y within the film is small compared with the range of X to be considered. In particular, in the expression

$$R = X\sin\beta + Y\cos\beta$$

the contribution of the Y term is negligible compared with that of the X term, so long as β does not approach zero; and so we may approximate as follows

$$R = X\sin\beta$$

Since X, and consequently R, is large compared with the film thickness, which is in terms of the local flow our chief characteristic dimension, terms of order $1/R^2$ are very small and will be subsequently ignored.

Just as values of Y are small compared with those of X, so also are the values of the Y component of velocity compared with the components in the X and Θ directions. For V only exists in the context of a disturbance to the mean flow, while the effect of a disturbance on U and W is to produce an initially small variation in what may be a relatively large value of the component corresponding to the mean flow. However, we are, in later sections, to examine the dynamics of the disturbance alone, so all velocity and velocity derivative terms are for the present retained.

Thus on making the approximation for R and eliminating $O(1/R^2)$ terms, we have :-

X direction

$$\frac{\partial u}{\partial t} + u\frac{\partial u}{\partial x} + v\frac{\partial u}{\partial y} + \frac{w}{x \sin\beta}\frac{\partial u}{\partial \theta} - \frac{w^2}{x}$$

$$= F_x - \frac{1}{\rho}\frac{\partial p}{\partial x} + \nu\left[\frac{\partial^2 u}{\partial x^2} + \frac{\partial^2 u}{\partial y^2} + \frac{1}{x}\left\{\frac{\partial u}{\partial x} + \frac{\partial u}{\partial y}\cot\beta\right\}\right]$$

- 2.2.6.

Y direction

$$\frac{\partial v}{\partial t} + u\frac{\partial v}{\partial x} + v\frac{\partial v}{\partial y} + \frac{w}{x \sin\beta}\frac{\partial v}{\partial \theta} - \frac{w^2}{x}\cot\beta$$

$$= F_y - \frac{1}{\rho}\frac{\partial p}{\partial y} + \nu\left[\frac{\partial^2 v}{\partial x^2} + \frac{\partial^2 v}{\partial y^2} + \frac{1}{x}\left\{\frac{\partial v}{\partial x} + \frac{\partial v}{\partial y}\cot\beta\right\}\right]$$

- 2.2.7.

θ direction

$$\frac{\partial w}{\partial t} + u\frac{\partial w}{\partial x} + v\frac{\partial w}{\partial y} + \frac{w}{x}\left[u + v\cot\beta + \frac{\partial w}{\partial \theta}\operatorname{cosec}\beta\right]$$

$$= F_\theta - \frac{1}{\rho}\frac{\partial p}{\partial \theta} + \nu\left[\frac{\partial^2 w}{\partial x^2} + \frac{\partial^2 w}{\partial y^2} + \frac{1}{x}\left\{\frac{\partial w}{\partial x} + \frac{\partial w}{\partial y}\cot\beta\right\}\right]$$

- 2.2.8.

Equation of Continuity

$$\frac{\partial u}{\partial x} + \frac{\partial v}{\partial y} + \frac{1}{x}\left[u + v\cot\beta + \frac{\partial w}{\partial \theta}\operatorname{cosec}\beta\right] = 0$$

- 2.2.9.

2.2.4 Body and Pressure Force Terms

For a stationary cone with its axis vertical and vertex upwards, the only body force acting is that due to gravity. The existence of the gravitational force produces in the film a pressure variation of the simple hydrostatic form, superimposed upon which will be local variations as a result of disturbances and also due to surface effects. The author has chosen therefore to retain a body force term, which might be considered to represent the hydrostatic component of pressure, leaving the pressure term P, or p as it later appears in non-dimensional form, to relate to the remaining components of pressure.

We have then:-

$$F_x = g\cos\beta$$
$$F_r = -g\sin\beta$$
$$F_\theta = 0$$

Note that these are forces/unit mass in accordance with the other terms of the Navier-Stokes Equations.

2.2.5 Non-Dimensional Forms of the Equations of Motion

It is convenient before going further to rewrite the equations in non-dimensional form. This has the immediate effect of introducing both Reynolds and Froude numbers, and rather more importantly it paves the way for a consideration of the flow as being semi-uniform in nature. This latter point is discussed in greater detail in section 2.3 where the undisturbed mean flow is considered.

The equations are purely kinematic in form. The only variables involving mass are those of pressure, and here the division by density

reduces them to a combination with dimensions (LT^{-2}). Therefore in order to make all terms dimensionless we need only two reference quantities, one involving length, the other time. The introduction of a Reynolds number involves also the choice of a characteristic reference dimension or length and also one of velocity. Since these latter reference quantities satisfy the former requirements, it is clearly both desirable and convenient that the same quantities be used for both purposes. Previous authors have predominantly, though not exclusively, based Reynolds number on the mean film thickness, and the mean velocity in the film; and the present author has followed this practice.

Calling the mean film thickness δ , and the mean film velocity $\bar{u}$ we have then, using lower case symbols to indicate non-dimensional quantities :-

$$u = \frac{u}{\bar{u}} \qquad v = \frac{V}{\bar{u}} \qquad w = \frac{W}{\bar{u}}$$

$$x = \frac{X}{\delta} \qquad y = \frac{Y}{\delta} \qquad \theta = \frac{\Theta}{\Theta_w}$$

$$\tau = \frac{t\bar{u}}{\delta} \qquad p = \frac{P}{\rho} \cdot \frac{1}{\bar{u}^2}$$

$$R_e = \frac{\bar{u}\delta}{\nu} \qquad F^2 = \frac{\bar{u}^2}{g\delta}$$

Making these substitutions yields for the non-dimensional forms of the equations of motion

$$\frac{\partial u}{\partial \tau} + u\frac{\partial u}{\partial x} + v\frac{\partial u}{\partial y} + \frac{w}{x\sin\beta}\frac{\partial u}{\partial \theta} - \frac{w^2}{x}$$

$$= -\frac{\cos\beta}{F^2} - \frac{\partial p}{\partial x} + \frac{1}{Re}\left[\frac{\partial^2 u}{\partial x^2} + \frac{\partial^2 u}{\partial y^2} + \frac{1}{x}\left\{\frac{\partial u}{\partial x} + \frac{\partial u}{\partial y}\cot\beta\right\}\right]$$

- 2.2.10.

$$\frac{\partial v}{\partial \tau} + u\frac{\partial v}{\partial x} + v\frac{\partial v}{\partial y} + \frac{w}{x\sin\beta}\frac{\partial v}{\partial \theta} - \frac{w^2}{x}\cot\beta$$

$$= -\frac{\sin\beta}{F^2} - \frac{\partial p}{\partial y} + \frac{1}{Re}\left[\frac{\partial^2 v}{\partial x^2} + \frac{\partial^2 v}{\partial y^2} + \frac{1}{x}\left\{\frac{\partial v}{\partial x} + \frac{\partial v}{\partial y}\cot\beta\right\}\right]$$

- 2.2.11.

$$\frac{\partial w}{\partial \tau} + u\frac{\partial w}{\partial x} + v\frac{\partial w}{\partial y} + \frac{w}{x}\left[u + v\cot\beta + \frac{\partial w}{\partial \theta}\operatorname{cosec}\beta\right]$$

$$= -\frac{\partial p}{\partial \theta} + \frac{1}{Re}\left[\frac{\partial^2 w}{\partial x^2} + \frac{\partial^2 w}{\partial y^2} + \frac{1}{x}\left\{\frac{\partial w}{\partial x} + \frac{\partial w}{\partial y}\cot\beta\right\}\right]$$

- 2.2.12.

$$\frac{\partial u}{\partial x} + \frac{\partial v}{\partial y} + \frac{1}{x}\left[u + v\cot\beta + \frac{\partial w}{\partial \theta}\operatorname{cosec}\beta\right] = 0$$

- 2.2.13.

2.3 The Undisturbed Mean Flow

Now that the equations of motion are in non-dimensional form, with no disturbance to the mean motion, y varies between 0 and 1 at all sections. Similarly u varies between 0 at the solid surface, and a maximum value which we might expect to be constant at all sections. That is, the maximum real velocity might be expected to be a fixed multiple of the mean velocity. This is a normal result in laminar flow, and we expect the flow of the thin undisturbed film to be laminar. Thus while we fully expect real velocity and mean film thickness, U and δ to vary with X, our non-dimensional variable u is found to be independent of x; we have then $u = f(y)$ only. This is exactly equivalent to the assumption that the velocity profile at all sections is similar. In the case of real values of U there is a decrease of scale of the profile in the X direction. In the case of the non-dimensional coordinates, there is no such scaling and the flow may be considered semi-uniform. In what follows it will be shown that $\bar{U}$ and δ vary relatively slowly with X, the problem may be considered to fall into what Betchov and Criminale ('67) call a category of quasi-parallel flow.

For the undisturbed mean flow then, x is not so much a variable as a parameter of the equations of motion. For the mean flow on a stationary cone we have :-

$$\frac{\partial}{\partial t} = 0 \qquad \frac{\partial}{\partial x} = 0 \qquad \frac{\partial}{\partial \theta} = 0$$

and therefore $\frac{\partial}{\partial y}$ may be replaced by $\frac{d}{dy}$, also

$$v = w = 0$$

Hence the equations of motion reduce to :-

$$0 = \frac{\cos\beta}{F^2} + \frac{1}{Re}\left[\frac{d^2u}{dy^2} + \frac{1}{x}\frac{du}{dy}\cot\beta\right]$$

$$0 = -\frac{\sin\beta}{F^2} - \frac{dp}{dy}$$

$$0 = 0$$

$$\frac{u}{x} = 0$$

Of these equations, the first will allow us to determine the way in which u varies with y. The second gives the form of the pressure distribution. The equation in the θ direction has disappeared entirely as is to be expected for this axisymmetric flow. The final equation is somewhat strange, and would seem to imply that $u = 0$ which we cannot accept. The only possible interpretation would seem to be that u is very small compared with x, and that the equation must be regarded as an order of magnitude indication. When it is remembered that in making the quantities non-dimensional we divided the relatively large X by the small δ to get x, whereas U was divided by a $\bar{U}$ of the same order of magnitude to obtain u, this seems to represent a proper interpretation of the equation. This indication of the magnitude of x further reinforces our neglect of terms of $O(\frac{1}{x^2})$ at an earlier stage.

The first of the above equations may be rewritten as

$$\left(D^2 + \frac{\cot\beta}{x}D\right)u = -\frac{Re\cos\beta}{F^2}$$

where the operator $D = \frac{d}{dy}$

Now we have seen that x is very large, hence $\frac{\cot\beta}{x}$ is small compared with the other terms of the differential equation, which we may approximate

$$D^2u = -\frac{Re\cos\beta}{F^2}$$

This may be integrated directly to give

$$u = -\frac{Re\cos\beta}{2F^2}\cdot y^2 + Ay + B$$

where A and B are constants of integration whose values are given by considering the boundary conditions :-

(i) $u = 0$ at $y = 0$ i.e. zero relative velocity at the solid surface.

(ii) $\frac{du}{dy} = 0$ at $y = 1$ i.e. no velocity gradient at the free surface, which follows if it is assumed that there is no shear stress due to air drag on the surface.

These conditions yield :-

$$B = 0$$

$$A = \frac{Re\cos\beta}{F^2}$$

$$\therefore \quad u = \frac{Re\cos\beta}{2F^2}(2y - y^2)$$

Or on reverting to dimensional quantities

$$U = \frac{g\delta^2\cos\beta}{2\nu}\cdot\left(2\frac{Y}{\delta} - \frac{Y^2}{\delta^2}\right)$$

The total flow/unit width of the surface

$$q = \bar{U}\delta$$

$$= \int_0^\delta U\,dY$$

$$= \frac{g\delta^3\cos\beta}{3\nu}$$

Hence $$\bar{u} = \frac{g\delta^2 \cos\beta}{3\nu} \qquad - \quad 2.3.1.$$

and $$u = \frac{3}{2}\bar{u}\left(2\frac{y}{\delta} - \frac{y^2}{\delta^2}\right)$$

or $$u = \frac{3}{2}\left(2y - y^2\right)$$

and hence $$3F^2 = Re\cos\beta \qquad - \quad 2.3.2.$$

This is the parabolic distribution of velocity that was first derived by Nusselt and has been used by virtually all authors since.

Now for the case of the cone q is dependent on X, for the total flow over the conical surface

$$Q = 2\pi X \sin\beta \cdot q$$

and we shall assume Q = constant

$$\therefore \quad Q = \frac{\pi g \delta^3 \sin 2\beta \cdot X}{3\nu}$$

or in terms of δ

$$\delta^3 = \frac{3\nu Q}{\pi g \sin 2\beta \cdot X}$$

and also

$$\bar{u} = \frac{g\cos\beta}{3\nu}\left[\frac{3\nu Q}{\pi g \sin 2\beta}\right]^{2/3} \cdot \frac{1}{X^{1/3}}$$

So that it is seen, as stated earlier, that the variation of δ and $\bar{u}$ with X is not rapid.

Summarising, we have the following results for the mean undisturbed flow :-

(i) The velocity profile is given by

$$u = \frac{3}{2}(2y - y^2) \qquad - \quad 2.3.3.$$

(ii) The variation in mean film thickness with distance down the cone is

$$\delta = \left[\frac{3\nu Q}{\pi g \sin 2\beta}\right]^{1/3} \cdot \frac{1}{X^{1/3}} \qquad - \quad 2.3.4.$$

(iii) The variation in mean velocity with distance down the cone is

$$\bar{u} = \left[\frac{g \cos\beta \, Q^2}{12\pi^2 \nu \sin^2\beta}\right]^{1/3} \cdot \frac{1}{X^{2/3}} \qquad - \quad 2.3.5.$$

(iv) Consequently the variation in Reynolds number with distance down the cone is given by

$$Re = \frac{Q}{2\pi\nu \sin\beta} \cdot \frac{1}{X} \qquad - \quad 2.3.6.$$

And $F^2 = \frac{1}{3} Re \cos\beta$, indicates a similar decrease in Froude number with passage down the cone's surface.

2.4 The Disturbed Flow

2.4.1 Introduction

Section 2.3 was based on a neglect of all motion other than that in the primary flow direction. It did not therefore take into account the possibility of any surface disturbance which could lead to the formation of waves. This led then to a one dimensional solution which is valuable in that it gives information as to the behaviour of a flow without disturbances. In the first instance the magnitude of disturbance modifications to the velocity components will be small compared with the undisturbed values. Hence the one dimensional solution does yield useful information as to the mean flow pattern; in particular it gives a useful indication of the nature of the velocity profile within the film.

To study the stability of the flow, however, it is necessary to examine the behaviour of a disturbance. This is most readily done by postulating a disturbance and then studying its change as it travels through time and space. If it decreases in magnitude, in other words if the flow tends to return to the undisturbed mean state, it can be concluded that the flow is stable. On the other hand if the disturbance grows, the flow must be considered unstable.

If a disturbance is to grow, it is to be expected that it will propagate laterally over the cone's surface as well as in the main flow direction. For a stationary cone, with a vertical axis, for which the undisturbed flow is axisymmetric, it may reasonably be assumed that such lateral propagation will be symmetrical about the axial plane through the point of initiation of the disturbance. The behaviour of the disturbance, and its growth or otherwise,

within this axial plane can be considered to typify the behaviour of the whole disturbance. According to Squire ('33) and Yih ('55) 3 dimensional disturbances are inherently somewhat more stable than 2 dimensional ones. Therefore by concentrating on a 2 dimensional analysis of stability the error, if any, is on the right side. That is, instability will be predicted if anything somewhat earlier than it should.

To summarise then, the stability examination which follows is based on consideration of a stationary cone and is limited to behaviour in the Oxy plane.

2.4.2 Equations of Motion for the Disturbance Isolated from the Mean Flow

Using subscripts to indicate partial differentiation the equations of motion in the Oxy plane may be rewritten as

$$u_t + u u_x + v u_y = \frac{1}{F^2}\cos\beta - p_x + \frac{1}{Re}\left[u_{xx} + u_{yy} + \frac{1}{x}(u_x + u_y \cot\beta)\right] \quad - \quad 2.4.1$$

$$v_t + u v_x + v v_y = -\frac{1}{F^2}\sin\beta - p_y + \frac{1}{Re}\left[v_{xx} + v_{yy} + \frac{1}{x}(v_x + v_y \cot\beta)\right] \quad - \quad 2.4.2$$

$$u_x + v_y + \frac{1}{x}(u + v\cot\beta) = 0 \quad - \quad 2.4.3$$

It is appropriate at this stage to compare the orders of magnitude of the bracketed terms in the continuity equation. Since $x \gg y$ it follows that in the absence of forces causing large accelerations in the y direction, v will in general be small compared with u. The continuity equation may therefore be simplified to

$$u_x + v_y + \frac{1}{x}\cdot u = 0$$

It should however be borne in mind that this neglect of the $v\cot\beta$ term may no longer be valid for very small β, and care must be taken in drawing any conclusions in the limit $\beta = 0$ from what follows.

Totally undisturbed flow must satisfy the above equations. Using superscript $^\circ$ to indicate undisturbed flow quantities, and making the appropriate substitutions

$$u = u^\circ \qquad v = 0 \qquad p = p^\circ$$

and bearing in mind that the undisturbed flow is steady, i.e. $u^\circ_t = 0$ gives

$$u^\circ u^\circ_x = \frac{1}{F^2}\cos\beta - p^\circ_x + \frac{1}{Re}\left[u^\circ_{xx} + u^\circ_{yy} + \frac{1}{x}\left(u^\circ_x + u^\circ_y \cot\beta\right)\right] \qquad - \ 2.4.4$$

$$0 = -\frac{1}{F^2}\sin\beta - p^\circ_y \qquad - \ 2.4.5$$

$$u^\circ_x + \frac{1}{x}u^\circ = 0 \qquad - \ 2.4.6$$

Using unsuperscripted quantities to indicate the contribution to the velocity components of the disturbance alone, requires substitution in 2.4.1 - 3 of $u^\circ+u$, v, $p^\circ+p$ and yields for the total flow :-

$$u_t + (u^\circ+u)(u^\circ_x+u_x) + v(u^\circ_y+u_y) = \frac{1}{F^2}\cos\beta - (p^\circ_x + p_x) + \frac{1}{Re}\left[(u^\circ_{xx}+u_{xx}) + (u^\circ_{yy}+u_{yy}) + \frac{1}{x}\left\{(u^\circ_x+u_x) + (u^\circ_y+u_y)\cot\beta\right\}\right]$$

$$v_t + (u^\circ+u)v_x + vv_y = -\frac{1}{F^2}\sin\beta - (p^\circ_y + p_y) + \frac{1}{Re}\left[v_{xx} + v_{yy} + \frac{1}{x}\left\{v_x + v_y\cot\beta\right\}\right]$$

$$(u^\circ_x + u_x) + v_y + \frac{1}{x}(u^\circ+u) = 0$$

Subtracting the undisturbed flow and remembering that u° does not vary with x gives for the disturbance only, the equations of motion :-

$$u_t + (u^\circ + u)u_x + v(u^\circ_y + u_y)$$
$$= -p_x + \frac{1}{Re}\left[u_{xx} + u_{yy} + \frac{1}{x}(u_x + u_y \cot\beta)\right]$$

$$v_t + (u^\circ + u)v_x + v v_y$$
$$= -p_y + \frac{1}{Re}\left[v_{xx} + v_{yy} + \frac{1}{x}(v_x + v_y \cot\beta)\right]$$

$$u_x + v_y + \frac{1}{x}u = 0$$

As the disturbance terms are small, products of these terms may be neglected, and the equations simplified to :-

$$u_t + u^\circ u_x + u^\circ_y v = -p_x + \frac{1}{Re}\left[u_{xx} + u_{yy} + \frac{1}{x}(u_x + u_y \cot\beta)\right]$$

$$v_t + u^\circ v_x = -p_y + \frac{1}{Re}\left[v_{xx} + v_{yy} + \frac{1}{x}(v_x + v_y \cot\beta)\right]$$

$$u_x + v_y + \frac{1}{x}u = 0$$

The number of variables, and equations, may be reduced if a stream function $\psi(x,y)$ exists which satisfies the continuity equation. Such a stream function is given by

$$u = \frac{1}{x}\psi_y \qquad v = -\frac{1}{x}\psi_x \qquad - \quad 2.4.7$$

Substituting for this gives :-

$$\left(-\frac{1}{x^2}u^\circ\psi_y + \frac{1}{x}\psi_{yt}\right) + u^\circ\left(-\frac{1}{x^2}\psi_y + \frac{1}{x}\psi_{yx}\right) - u^\circ_y\frac{1}{x}\psi_x$$
$$= -p_x + \frac{1}{Re}\left[\left(\frac{2}{x^3}\psi_y - \frac{2}{x^2}\psi_{yx} + \frac{1}{x}\psi_{yxx}\right) + \frac{1}{x}\psi_{yyy}\right.$$
$$\left. + \frac{1}{x}\left(-\frac{1}{x^2}\psi_y + \frac{1}{x}\psi_{yx} + \frac{1}{x}\psi_{yy}\cot\beta\right)\right]$$

$$\left(\frac{1}{x^2}u^\circ\psi_x - \frac{1}{x}\psi_{xt}\right) + u^\circ\left(\frac{1}{x^2}\psi_x - \frac{1}{x}\psi_{xx}\right)$$
$$= -p_y + \frac{1}{Re}\left[\left(-\frac{2}{x^3}\psi_x + \frac{2}{x^2}\psi_{xx} - \frac{1}{x}\psi_{xxx}\right) - \frac{1}{x}\psi_{xyy}\right.$$
$$\left. + \frac{1}{x}\left(\frac{1}{x^2}\psi_x - \frac{1}{x}\psi_{xx} - \frac{1}{x}\psi_{xy}\cot\beta\right)\right]$$

Or, on collecting terms :-

$$\frac{1}{x}\left[\psi_{yt} + u^0\psi_{yx} - \frac{2}{x}u^0\psi_y - u^0_y\psi_x\right]$$
$$= -p_x + \frac{1}{x\,Re}\left[\psi_{yxx} + \psi_{yyy} - \frac{1}{x}(\psi_{yx} - \psi_{yy}\cot\beta) + \frac{1}{x^2}\psi_y\right]$$

$$-\frac{1}{x}\left[\psi_{xt} + u^0\psi_{xx} - \frac{2}{x}u^0\psi_x\right]$$
$$= -p_y - \frac{1}{x\,Re}\left[\psi_{xxx} + \psi_{xyy} - \frac{1}{x}(\psi_{xx} - \psi_{xy}\cot\beta) + \frac{1}{x^2}\psi_x\right]$$

We now make the usual assumption that the disturbance is harmonic and of the form

$$\psi = \phi(y)\exp\left[i\alpha(x - ct)\right] \qquad - \ 2.4.8$$

also that a similar solution exists for the non-dimensional pressure

$$p = f(y)\exp\left[i\alpha(x - ct)\right] \qquad - \ 2.4.9$$

The functions $\phi(y), f(y)$ allow for variation in the y direction, that is across the film, while the complex exponential term covers the harmonic variation as the disturbance progresses both down the conical surface and through time. The non-dimensional parameter α which is related to the wavelength of a disturbance on the free surface is known as the wave number. The relationship between α and wavelength is an inverse one, small α corresponds to long wavelength; in particular the limiting case of $\alpha = 0$ corresponds to a single infinitely long wave. The non-dimensional product αc is similarly a measure of frequency, from which it can be seen that c alone must have the form of a non-dimensional velocity, and it is known as the wave velocity.

Most importantly it can be seen that if the disturbance is to grow, ψ must increase with time. Such increase with time is

our criterion for instability. Therefore the flow must be considered unstable if the product $(-i\alpha c)$ has a positive real component. In general c can be complex $c = c_r + ic_i$, therefore since α is real and ≥ 0, the condition for instability is that $c_i > 0$.

Putting in the assumed harmonic disturbances gives

$$\frac{1}{\alpha}\left[-i\alpha c\phi' + u^0 i\alpha\phi' - \frac{2}{\alpha}u^0\phi' - u^0_y i\alpha\phi\right] = -i\alpha f + \frac{1}{\alpha Re}\left[-\alpha^2\phi' + \phi''' - \frac{1}{\alpha}(i\alpha\phi' - \phi''\cot\beta) + \frac{1}{\alpha^2}\phi'\right] \quad - \quad 2.4.10$$

$$-\frac{1}{\alpha}\left[\alpha^2 c\phi - u^0\alpha^2\phi - \frac{2}{\alpha}u^0 i\alpha\phi\right] = -f' - \frac{1}{\alpha Re}\left[-i\alpha^3\phi + i\alpha\phi'' - \frac{1}{\alpha}(-\alpha^2\phi - i\alpha\phi'\cot\beta) + \frac{1}{\alpha^2}i\alpha\phi\right] \quad - \quad 2.4.11$$

where $'$ indicates differentiation with respect to y

The function $f(y)$ may be eliminated by differentiating the former equation, and subtracting $i\alpha$ × the latter. Multiplication throughout by α then yields :-

$$(u^0 - c)i\alpha(\phi'' - \alpha^2\phi) - \frac{2}{\alpha}u^0(\phi'' - \alpha^2\phi) - \frac{2}{\alpha}u^0_y\phi' - u^0_{yy}i\alpha\phi = \frac{1}{Re}\left[(\phi^{IV} - 2\alpha^2\phi'' + \alpha^4\phi) + \frac{1}{\alpha}(\phi''' - \alpha^2\phi')\cot\beta - \frac{i\alpha}{\alpha}(\phi'' - \alpha^2\phi) + \frac{1}{\alpha^2}(\phi'' - \alpha^2\phi)\right]$$

Rearranging so as to separate real and imaginary coefficients

$$\phi^{IV} - 2\alpha^2\phi'' + \alpha^4\phi + \frac{1}{\alpha}(\phi''' - \alpha^2\phi')\cot\beta + \frac{1}{\alpha^2}(\phi'' - \alpha^2\phi) + \frac{2Re}{\alpha}\left[u^0(\phi'' - \alpha^2\phi) + u^0_y\phi'\right] = i\alpha\left[Re\left\{(u^0 - c)(\phi'' - \alpha^2\phi) - u^0_{yy}\phi\right\} + \frac{1}{\alpha}(\phi'' - \alpha^2\phi) - \frac{1}{\alpha^2}(\phi'' - \alpha^2\phi)\right]$$

Comparison with the standard Orr-Sommerfeld equation obtained for flow down an inclined plane shows the above to be identical but for the addition of the terms in x. It has already been shown that x is large; neglecting terms of order $\left(\frac{1}{x^2}\right)$ gives :-

$$\phi^{iv} + \frac{\cot\beta}{x}\phi''' + 2\left(\frac{R_e}{x}u^0 - \alpha^2\right)\phi'' + \left(2\frac{R_e}{x}u^0_y - \alpha^2\frac{\cot\beta}{x}\right)\phi' - \alpha^2\left(2\frac{R_e}{x}u^0 - \alpha^2\right)\phi$$

$$= i\alpha\left[R_e\left\{(u^0 - c)(\phi'' - \alpha^2\phi) - u^0_{yy}\phi\right\} + \frac{1}{x}(\phi'' - \alpha^2\phi)\right]$$

- 2.4.12

Which is the standard Orr-Sommerfeld equation with the addition of terms catering for the change of film in the x direction caused by spreading of the film over the increasing width of the cone. These terms are all of order $\left(\frac{1}{x}\right)$ and consequently small. As before it is simpler to regard x as a parameter of the equation rather than a true variable, for ϕ is a function of y only, and it is particularly desirable to think of R_e, which is in turn dependent on x, as a parameter.

2.5 Boundary Conditions

The modified Orr-Sommerfeld equation is a fourth order differential equation in $\phi(y)$. For a complete solution, therefore, it is necessary to obtain four boundary conditions from which to determine the constants of integration. Of these, two can be obtained from the no slip and no normal velocity condition at the solid cone surface. A third follows from the assumption of no shear at the free surface, and the final condition is based on a consideration of the continuity of normal stress at the free surface.

2.5.1 At the Cone Surface

For no slip at the solid cone surface,

$$u = 0 \quad \text{at} \quad y = 0$$

Hence also $\quad \frac{1}{x}\cdot\psi_y = 0$

and on substituting the assumed form of ψ

$$\frac{1}{x}\left[\phi'(0)\exp\{i\alpha(x-ct)\}\right] = 0$$

This can only be satisfied for all x and t if

$$\phi'(0) = 0 \qquad - \quad 2.5.1$$

which is therefore the first boundary condition.

For no normal velocity component at the solid cone surface

$$v = 0 \qquad \text{at} \qquad y = 0$$

Hence also $\quad -\frac{1}{x}\psi_x = 0$

which corresponds, on substituting the assumed form of ψ, as above, to

$$-\frac{1}{x}\left[\phi(0)\, i\alpha \exp\{i\alpha(x-ct)\}\right] = 0$$

Again for this to be satisfied for all x, t and α

$$\phi(0) = 0 \qquad - \quad 2.5.2$$

which is the second boundary condition.

2.5.2 Shear Stress at the Free Surface

If it is assumed that there is no air drag at the free surface of the film, then there can be no shear stress at this surface, and therefore

$$\mu\left[\frac{\partial v}{\partial x} + \frac{\partial u}{\partial y}\right] = 0$$

Or simply

$$\frac{\partial v}{\partial x} + \frac{\partial u}{\partial y} = 0$$

It is worth noting that the one dimensional analysis of section 2.3 made use of this in the simplified form

$$\frac{\partial u}{\partial y} = 0$$

and that the assumed velocity distribution

$$u = \frac{3}{2}(2y - y^2)$$

satisfies this.

This condition applies at the free surface, which in the presence of disturbances varies by a small amount either side of the mean position given by $y = 1$. Suppose then the free surface occurs at

$$y = 1 + \eta$$

where η is small. In dimensional terms this is equivalent to $Y = \delta(1 + \eta)$. Following Yih ('63) this condition gives at $y = 1$

$$\frac{\partial v}{\partial x} + \frac{\partial u}{\partial y} + \frac{\partial^2 u}{\partial y^2}\cdot\eta = 0$$

Where terms, except the one in η, are now understood to be evaluated at $y = 1$. Now the velocities referred to here are the total velocities. That is u must refer to the two components of u° the undisturbed flow and u the disturbance component. Now at $y = 1$,

$$u^\circ_y = 0 \qquad u^\circ_{yy} = -3$$

Hence using subscript notation the above may be written on introducing the values at $y = 1$.

$$v_x + u_y + u_{yy}\eta - 3\eta = 0$$

or on neglecting second order small quantities

$$v_x + u_y - 3\eta = 0$$

In terms of ψ this becomes

$$\frac{1}{x^2}\psi_x - \frac{1}{x}\psi_{xx} + \frac{1}{x}\psi_{yy} - 3\eta = 0$$

A relationship between ψ and η may be derived by considering the definition of v

$$v = \frac{dy}{dt} = \frac{d\eta}{dt}$$

$$= \frac{\partial \eta}{\partial t} + \frac{\partial \eta}{\partial x}\cdot\frac{dx}{dt}$$

$$= \eta_t + \eta_x(u^\circ + u)$$

Hence, on neglecting second order small quantities

$$-\frac{1}{x}\psi_x = \eta_t + u^\circ \eta_x$$

The form of η will be harmonic like ψ and p

Suppose $$\eta = A \exp\left[i\alpha(x - ct)\right]$$

Then $$-\frac{1}{x} i\alpha\phi = -i\alpha c A + u^\circ i\alpha A$$

i.e. $$\eta = -\frac{1}{x}\frac{\phi(y)}{u^\circ - c}\exp\left[i\alpha(x - ct)\right] \qquad - \quad 2.5.3$$

Substituting for η, ϕ, ω^0 and derivatives at $y = 1$ yields :-

$$\frac{1}{\alpha^2} i\alpha\,\phi(1) + \frac{1}{\alpha}\alpha^2\phi(1) + \frac{1}{\alpha}\phi''(1) + \frac{3}{\alpha}\cdot\frac{1}{\frac{3}{2}-c}\phi(1) = 0$$

or on substituting $c' = c - \frac{3}{2}$

$$\phi''(1) + \left[\alpha^2 - \frac{3}{c'} + \frac{i\alpha}{\alpha}\right]\phi(1) = 0 \qquad - \quad 2.5.4$$

This constitutes the third boundary condition. Comparison with that of Yih ('63) for flow down an inclined plane, shows that the dependence on α has shown itself in the appearance of an additional term, the one in $\frac{1}{\alpha}$.

2.5.3 Continuity of Normal Stress at the Free Surface

The curvature of the film surface due both to the presence of a wavelike disturbance, and to the curvature of the conical substrate gives rise to a net normal stress at the free surface which must be balanced by pressure and viscous stresses.

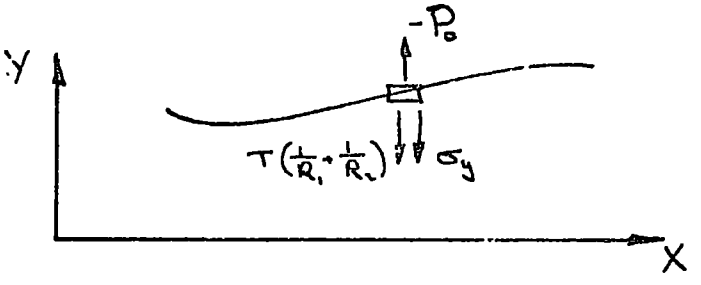

In dimensional terms, the normal stress due to curvature is given by $T\left(\frac{1}{R_1} + \frac{1}{R_2}\right)$

where T is the coefficient of surface tension

R_1 R_2 are the two radii of curvature (+ve if inwardly directed).

The radius of curvature due to the cone

$$R_1 = X \tan\beta$$

that in the OXY plane, due to the disturbance

$$R_2 = - \frac{\left[1 + \left(\frac{\partial Y}{\partial X}\right)^2\right]^{3/2}}{\frac{\partial^2 Y}{\partial X^2}}$$

The normal stress σ_y arising from pressure and viscous sheer is

$$-P + 2\mu \frac{\partial V}{\partial Y}$$

$\therefore$ for continuity of normal stress at the surface

$$-P + 2\mu \frac{\partial V}{\partial Y} + T\left[\frac{\cot\beta}{X} - \frac{\frac{\partial^2 Y}{\partial X^2}}{\left[1+\left(\frac{\partial Y}{\partial X}\right)^2\right]^{3/2}}\right] = -P_0 \qquad - \quad 2.5.5$$

where P_0 is the atmospheric pressure above the film. This expression may be rendered non-dimensional as in section 2.2.5 to give

$$-p + \frac{2}{Re} \frac{\partial v}{\partial y} + S\left[\frac{\cot\beta}{x} - \frac{\frac{\partial^2 y}{\partial x^2}}{\left[1+\left(\frac{\partial y}{\partial x}\right)^2\right]^{3/2}}\right] = -p_0$$

where $S = \frac{T}{\delta \rho \bar{u}^2}$ is the inverse of a Weber number related to mean film velocity and mean film thickness.

Now $y \ll x$, therefore

$$\left[1+\left(\frac{\partial y}{\partial x}\right)^2\right]^{3/2} = 1 + \frac{3}{2}\left(\frac{\partial y}{\partial x}\right)^2 + \ldots + O\left(\frac{\partial y}{\partial x}\right)^4$$

$$\simeq 1$$

Using subscript notation

$$-p + \frac{2}{Re} v_y + S\left[\frac{\cot\beta}{x} - y_{xx}\right] = -p_0$$

As in section 2.4.2 this can be considered to include contributions both from the disturbance and from the mean flow. Using superscript $^\circ$ to indicate a mean flow contribution and unsuperscripted variables to indicate disturbance contributions, we have for total flow

$$-p^\circ - p + \frac{2}{Re} v_y + S\left[\frac{\cot\beta}{x} - y_{xx}\right] = -p_0$$

and for mean, undisturbed flow

$$-p^\circ + S\left[\frac{\cot\beta}{x}\right] = -p_0$$

which on subtraction, leaves for the disturbance effect,

$$-p + \frac{2}{Re} v_y - S_{y_{xx}} = 0$$

Again as in the previous section it is useful to put $y = 1+\eta$ to give the above in terms of its variation η about the mean surface position.

Then $$p = p_1 + p^0_y \cdot \eta$$

where p_1 indicates the value of the disturbance component of pressure at $y = 1$ and

p^0_y is the gradient of pressure in the y direction for which the mean stream component value will be the major part.

From equation 2.4.5 $$p^0_y = -\frac{\sin\beta}{F^2}$$

Therefore

$$-p_1 + \frac{\sin\beta}{F^2}\eta + \frac{2}{Re} v_y - S_{\eta_{xx}} = 0$$

Or on taking into account $3F^2 = Re\cos\beta$

and replacing $v_y = -\frac{1}{x}\psi_{xy}$

$$-p_1 + \frac{3\tan\beta}{Re}\cdot\eta - \frac{2}{xRe}\psi_{xy} - S_{\eta_{xx}} = 0$$

Substituting for the assumed and derived forms for p, ψ and η and dividing by $\exp\left[i\alpha(x-ct)\right]$ we obtain,

$$-f(1) + \frac{3\tan\beta}{c'xRe}\phi(1) - \frac{2i\alpha}{xRe}\phi'(1) + S\left[\frac{\alpha^2}{c'x} + \frac{2i\alpha}{c'x^2} - \frac{2}{c'x^3}\right]\phi(1) = 0$$

Elimination of the first term is possible by use of 2.4.10 which when applied at $y = 1$ gives

$$\frac{1}{x}\left[-i\alpha\left(c-\tfrac{3}{x}\right)\phi'(1) - \frac{3}{x}\phi'(1)\right]$$

$$= -i\alpha f(1) + \frac{1}{xRe}\left[-\alpha^2\phi'(1) + \phi'''(1) - \frac{1}{x}\left(i\alpha\phi'(1) - \phi''(1)\cot\beta\right) + \frac{1}{x^2}\phi'(1)\right]$$

Elimination and sorting of terms gives

$$i\phi'''(1) + i\frac{\cot\beta}{x}\phi''(1) - \left[3i\alpha^2 + c'\alpha Re - \frac{\alpha}{x} - \frac{3iRe}{x} - \frac{i}{x^2}\right]\phi'(1)$$

$$+ \frac{\alpha}{c'}\left[3\tan\beta + \alpha^2 SRe + \frac{2i\alpha SRe}{x} - \frac{2SRe}{x^2}\right]\phi(1) = 0$$

Terms including $\frac{1}{x^2}$ are clearly small, and our further considerations will also be limited to relatively small values of α . Therefore the term involving $\frac{\alpha^2}{x}$ will also be small. The term in $\alpha^3 SRe$ is however retained since it is the only term in S and the joint product might be of importance in cases of high surface tension.

Thus our fourth and final boundary condition is

$$i\phi'''(1) + i\frac{\cot\beta}{x}\phi''(1) - \left[3i\alpha^2 + c'\alpha Re - \frac{\alpha}{x} - \frac{3iRe}{x}\right]\phi'(1)$$

$$+ \frac{\alpha}{c'}\left[3\tan\beta + \alpha^2 SRe\right]\phi(1) = 0 \qquad - 2.5.6$$

Comparison of the above boundary conditions with those generally accepted for flow down an inclined plane, shows that a basic similarity exists, but that the present set do contain terms in $\frac{1}{x}$ that have no place in the planar set. These are in the third and fourth boundary conditions only. More detailed comparison with the planar set as quoted by Yih ('63) shows a change of sign for the last bracket in the final condition above. This is accounted for by the reversal of the direction of the y coordinate as is the change in the value of y at the free surface.

2.6 Solution

2.6.1 The system of equations to be solved is that given by 2.4.12 together with the boundary conditions derived in 2.5., namely

$$\phi^{iv} + \kappa\phi''' + 2\left(\frac{Re}{2}u^0 - \alpha^2\right)\phi'' + \left(2\frac{Re}{2}u^0_y - \kappa\alpha^2\right)\phi' - \alpha^2\left(2\frac{Re}{2}u^0 - \alpha^2\right)\phi$$

$$= i\alpha\left[Re\left\{(u^0 - c)(\phi'' - \alpha^2\phi) - u^0_{yy}\phi\right\} + \frac{1}{2}(\phi'' - \alpha^2\phi)\right]$$

- 2.6.1

$$\phi(0) = 0 \quad - \quad 2.6.2$$

$$\phi'(0) = 0 \quad - \quad 2.6.3$$

$$\phi''(1) + \left[\alpha^2 - \frac{3}{c'} + \frac{i\alpha}{2}\right]\phi(1) = 0 \quad - \quad 2.6.4$$

$$i\phi'''(1) + \kappa i\phi''(1) - \left[3i\alpha^2 + c'\alpha Re - \frac{\alpha}{2} - 3i\frac{Re}{2}\right]\phi'(1)$$

$$+ \frac{\alpha}{c'}\left[2\tan\beta + \alpha^2 S Re\right]\phi(1) = 0 \quad - \quad 2.6.5$$

where $\kappa = \frac{\cot\beta}{2}$, $c' = c - \frac{3}{2}$

Observation of the film formed on a cone shows that the dominant waves are of much greater length than the film thickness. For such waves, the wave number $\alpha = 2\pi \cdot \frac{\text{mean film thickness}}{\text{wavelength}}$ is small.

The solution therefore proceeds on the assumption that interest lies chiefly with small values of α . The second major parameter Re occurs only divided by 2, and multiplied by α, so that for even moderately large values of Re it makes a small contribution to the system. With the above in mind a perturbation method has been adopted for the solution in which α is treated as a small perturbation quantity. This allows a first approximation to be made by solving the system for $\alpha = 0$, i.e. including only terms of $O(\alpha^0)$. A second approximation follows in which terms of $O(\alpha^1)$ are included. So as not to introduce, by implication, terms of higher order, the first approximate solution is substituted in these terms involving α^1 . In this way a second

approximation is obtained, and by an iterative procedure, higher approximations could follow. It is however found unnecessary to go beyond this second level of approximation, since this is found to reveal the stability criterion which is sought.

The solution has been divided into two parts. First a solution is found for zero R_e. This can be regarded as the limit to which any thinning film will tend , as R_e is shown in section 2.3 to decrease with α . There follows a second solution allowing for non zero but small R_e .

2.6.2 Solution for Zero Reynolds Number

As indicated above a solution is first sought for the system with zero α as well as zero R_e. The system 2.6.1-5 is thus reduced to

$$\phi^{iv} + \kappa\phi'' = 0 \qquad - \text{ 2.6.6}$$

$$\phi(0) = 0 \qquad - \text{ 2.6.7}$$

$$\phi'(0) = 0 \qquad - \text{ 2.6.8}$$

$$\phi''(1) - \frac{3}{c_1}\phi(1) = 0 \qquad - \text{ 2.6.9}$$

$$i\phi'''(1) + i\kappa\phi'(1) = 0 \qquad - \text{ 2.6.10}$$

2.6.6 yields a first approximation solution

$$\phi_o = Ae^{-\kappa y} + By^2 + Cy + D$$

where the constants of integration are found by substitution in the boundary conditions, which gives

$$\begin{aligned} A \qquad\qquad\qquad + D &= 0 \\ -\kappa A \qquad + C &= 0 \\ (\kappa^2 - \tfrac{3}{c_1})e^{-\kappa}A + (2 - \tfrac{3}{c_1})B - \tfrac{3}{c_1}C - \tfrac{3}{c_1}D &= 0 \\ 2i\kappa B &= 0 \end{aligned}$$

From which $B = 0$, and either $A = C = D = 0$

or $$\left(\kappa^2 - \frac{3}{c_1}\right)e^{-\kappa} - \frac{3}{c_1}\kappa + \frac{3}{c_1} = 0$$

i.e. $$c' = \frac{3}{\kappa^2} \cdot \frac{e^{-\kappa} + \kappa - 1}{e^{-\kappa}}$$

$$= \frac{3}{2} + \kappa + O\left(\frac{1}{\kappa^2}\right)$$

$\therefore$ for a non trivial first approximation,

$$c_0' = \frac{3}{2} + \kappa$$

And since $D = -A \quad C = \kappa A$

$$\phi_0 = A\left[e^{-\kappa y} + \kappa y - 1\right]$$

On again expanding $e^{-\kappa y}$ in the series form and neglecting terms of $O\left(\frac{1}{\kappa^2}\right)$

$$\phi_0 = A \cdot \frac{\kappa^2}{2} \cdot y^2$$

No further information is available for the exact determination of A. So as is common, the eigen function ϕ_0 is determined only up to a multiplicative constant. For simplicity take $A = \frac{2}{\kappa^2}$ and we have

$$\phi_0 = y^2 \qquad - 2.6.11$$

It is worth noting that while this is identical to the first approximation obtained in the case of flow over a plane surface, there is in the assumed value for A a dependence on the value of κ which is a function both of the slope β and distance down the cone x.

For the second approximation, terms of first power in α are included in the system.

$$\phi^{iv} + \kappa\phi''' = \frac{i\alpha}{2c}\phi''$$

$$\phi(0) = 0$$

$$\phi'(0) = 0$$

$$\phi''(1) - \frac{3}{c_1}\phi(1) = -\frac{i\alpha}{2}\phi(1)$$

$$i\phi'''(1) + i\kappa\phi''(1) = -\frac{\alpha}{\kappa}\phi'(1) - \frac{\alpha}{c'}(3\tan\beta + \alpha^2 S R_e)\phi(1)$$

Terms in α have been put on the right hand sides of the above equations. Now this system is expected to yield a higher approximation in ϕ than ϕ_0, one that involves α. If this is substituted in the right hand sides, these will contain terms in α^2 implying a higher approximation still. Therefore ϕ_0 is substituted in all those terms involving α. Note also that the term in $\alpha^2 S R_e$ has not been rejected as could be expected on grounds of the power of α involved. This is the only term introducing S the surface tension factor, and if it is regarded as a group $\alpha^2 S R_e$, its retention causes no difficulty and provides a result which gives an indication of the effect of surface tension. The system is therefore :-

$$\phi^{IV} + \kappa\phi'' = 2\frac{i\alpha}{\kappa} \qquad - \quad 2.6.12$$

$$\phi(0) = 0$$

$$\phi'(0) = 0$$

$$\phi''(1) - \frac{3}{c'}\phi(1) = -\frac{i\alpha}{\kappa}$$

$$i\phi'''(1) + i\kappa\phi''(1) = -2\frac{\alpha}{\kappa} - \frac{\alpha}{c'}(3\tan\beta + \alpha^2 S R_e)$$

Not only does this system yield a higher approximation in ϕ, but it will also give an updated value for c'.

Suppose $\quad c' = c_0' + \Delta c_1'$

Then $\quad -\frac{3}{c'} = -\frac{3}{c_0' + \Delta c_1'} = -\frac{3}{c_0'}\left[1 + \frac{\Delta c_1'}{c_0'}\right]^{-1}$

$$= -\frac{3}{c_0'} + \frac{3\Delta c_1'}{c_0'^2} + O(\alpha^2)$$

So by similar considerations to those adopted for ϕ in relation to α, third and fourth boundary conditions become

$$\phi''(1) - \frac{3}{c_0'}\phi(1) = -\frac{3\Delta c_1'}{c_0'^2} - \frac{i\alpha}{\kappa}$$

and $$i\phi'''(1) + i\kappa\phi''(1) = -2\frac{\alpha}{\kappa} - \frac{\alpha}{c_0'}(3\tan\beta + \alpha^2 SR_e)$$

The solution of 2.6.12 is $\phi = \phi_0 + \phi_1$

where $$\phi_1 = \frac{i\alpha}{3\kappa\kappa} y^3 + \Delta A e^{-\kappa y} + \Delta B y^2 + \Delta C y + \Delta D$$

Where in addition to the particular integral $\frac{i\alpha}{3\kappa\kappa} y^3$ the Δ terms are included to cater for the changed boundary conditions. Substitution of this solution in the boundary conditions yields after subtraction of the set obtained in the first approximation :-

$$\Delta A + \Delta D = 0$$

$$-\kappa\Delta A + \Delta C = 0$$

$$(\kappa^2 - \tfrac{3}{c_0'})e^{-\kappa}\Delta A + (2 - \tfrac{3}{c_0'})\Delta B - \tfrac{3}{c_0'}\Delta C - \tfrac{3}{c_0'}\Delta D = -\frac{3\Delta c_1'}{c_0'^2} - \frac{i\alpha}{\kappa} - \frac{2i\alpha}{\kappa\kappa} + \frac{1}{c_0'}\frac{i\alpha}{\kappa\kappa}$$

$$2i\kappa\Delta B = -2\frac{\alpha}{\kappa} + 2\frac{\alpha}{\kappa\kappa} + 2\frac{\alpha}{\kappa} - \frac{\alpha}{c_0'}(3\tan\beta + \alpha^2 SR_e)$$

The same relationship holds between ΔA, ΔC and ΔD as did between A, C and D in the first approximation. So just as $Ae^{-\kappa y} + Cy + D \longrightarrow Ay^2$ so will $\Delta A e^{-\kappa y} + \Delta C y + \Delta D \longrightarrow \Delta A y^2$

Now A was chosen arbitrarily since its value could not be exactly determined, and any attempt to put an exact value on ΔA is clearly pointless $\therefore$ set $\Delta A = 0$

Eliminating ΔB then gives

$$\frac{3\Delta c_1'}{c_0'} - \frac{i\alpha}{\kappa\kappa} + c_0'\frac{i\alpha}{\kappa\kappa}(2+\kappa) = -\frac{i\alpha}{c_0'}(3\tan\beta + \alpha^2 SR_e) + \frac{2i\alpha}{\kappa\kappa}$$

i.e. $$\Delta c_1' = -i\alpha(\tan\beta + \tfrac{\alpha^2}{3}SR_e) + \frac{i\alpha}{\kappa\kappa}(c_0' - \tfrac{2+\kappa}{3}c_0'^2)$$

$$= -i\alpha\left[\tan\beta + \frac{7}{4\kappa} + \tfrac{1}{3}\alpha^2 SR_e\right] + O(\tfrac{1}{\kappa^2})$$

Then for $c = c_r + i c_i$

$$= c' + \frac{3}{2} = c_0' + \Delta c_1' + \frac{3}{2}$$

$$c_r = 3 + \frac{\cot\beta}{\alpha}$$

$$c_i = -\alpha\left[\tan\beta + \frac{7}{4\alpha} + \frac{1}{3}\alpha^2 S R_e\right] \qquad -2.6.13$$

The original assumed disturbance was of the form

$$\psi = \phi(y)\exp\left[i\alpha(x - ct)\right]$$

So a negative c_i as found corresponds to an exponential function which decreases with time.

Therefore the assumed disturbance will decrease in magnitude with time, and the motion is stable for zero Reynolds number. All three elements of the expression for c_i are seen to exert a stabilising influence, though it is seen that this influence diminishes with the growth of α. It can also be seen that as the cone degenerates to a vertical cylinder $\beta = 0$, the only remaining stabilising influence is that of surface tension.

2.6.3 Solution for Small Reynolds Number

This is obtained as above for small values of α also. The first approximation ϕ_0 obtained for $\alpha = 0$ $R_e = 0$ is again taken as the starting point. Now however both first order terms in α and in R_e are included. As noted in 2.6.1. R_e appears as either the quotient R_e/α which due to the largeness of α, is small for even quite large R_e, or as the product αR_e. The latter is therefore not disregarded as being a second order small quantity but is retained, thus again allowing for quite reasonably sized values of R_e. It

is further important to note that no higher power values of R_e occur, so that neither is a higher level of approximation possible, nor are any large values implied by these higher values of R_e raised to higher powers being neglected.

The system to be solved is therefore now

$$\phi^{iv} + \kappa\phi''' = -2\frac{R_e}{\pi}\left[u^0\phi_0'' + u^0_y\phi_0'\right] + i\alpha\left[R_e\{(u^0 - c_0)\phi_0'' - u^0_{yy}\phi_0\} + \frac{1}{\pi}\phi_0'\right]$$

$$\phi(0) = 0$$

$$\phi'(0) = 0$$

$$\phi''(1) - \frac{3}{c_0'}\phi(1) = -\frac{3\Delta c_1'}{c_0'^2}\phi_0(1) - \frac{i\alpha}{\pi}\phi_0(1)$$

$$i\phi'''(1) + i\kappa\phi''(1) = \left[c_0'\alpha R_e - \frac{\alpha}{\pi} - 3i\frac{R_e}{\pi}\right]\phi_0'(1) - \frac{\alpha}{c_0'}\left[3\tan\beta + \alpha^2 S R_e\right]\phi_0(1)$$

Substituting for $\phi_0 = y^2$

$$u^0 = \tfrac{3}{2}(2y - y^2)$$

gives

$$\phi^{iv} + \kappa\phi''' = -6\frac{R_e}{\pi}y^2 + i\alpha R_e\left[6y - 6 - 2\kappa\right] + 2\frac{i\alpha}{\pi} \qquad 2.6.14$$

$$\phi(0) = 0$$

$$\phi'(0) = 0$$

$$\phi''(1) - \frac{3}{c_0'}\phi(1) = -\frac{3}{c_0'^2}\Delta c_1' - \frac{i\alpha}{\pi}$$

$$i\phi'''(1) + i\kappa\phi''(1) = 2\left[c_0'\alpha R_e - \frac{\alpha}{\pi} - 3i\frac{R_e}{\pi}\right] - \frac{\alpha}{c_0'}\left[3\tan\beta + \alpha^2 S R_e\right]$$

The solution of 2.6.14 will be

$$\phi = \phi_0 + \phi_2$$

where ϕ_2 consists of a particular integral together with terms modifying the basic ones of ϕ_0 to fit the revised boundary conditions. The particular integral is

$$\phi_{2P_1} = Ly^5 + My^4 + Ny^3$$

where $$L = -\frac{1}{10}\cdot\frac{R_e}{\kappa\alpha}$$

$$M = \frac{1}{2\kappa}\cdot\frac{R_e}{\kappa\alpha} + \frac{1}{4\kappa}\, i\alpha R_e$$

$$N = -\frac{2}{\kappa^2}\cdot\frac{R_e}{\kappa\alpha} - \frac{1}{3}\left(1+\frac{3}{\kappa}+\frac{3}{\kappa^2}\right) i\alpha R_e + \frac{1}{3\kappa}\cdot\frac{i\alpha}{\alpha}$$

$$\therefore \quad \phi_2 = Ly^5 + My^4 + Ny^3 + \Delta A e^{-\kappa y} + \Delta B y^2 + \Delta C y + \Delta D$$

Substitution of $\phi = \phi_0 + \phi_2$ in the boundary conditions and subtraction of the first approximation set gives

$$\Delta A + \Delta D = 0$$

$$-\kappa\Delta A + \Delta C = 0$$

$$\left(\kappa^2 - \frac{3}{c_0'}\right)e^{-\kappa}\Delta A + \left(2-\frac{3}{c_0'}\right)\Delta B - \frac{3}{c_0'}\Delta C - \frac{3}{c_0'}\Delta D = -\frac{3}{c_0'^2}\Delta c_i' - \frac{i\alpha}{\alpha} - \left[20L+12M+6N\right] + \frac{3}{c_0'}\left[L+M+N\right]$$

$$2i\kappa\Delta B = 2\left[c_0'\alpha R_e - \frac{\kappa}{\alpha} - 3i\frac{R_h}{\alpha}\right] - \frac{\alpha}{c_0'}\left[3\tan\beta + \alpha^2 S R_e\right] - i\left[60L + 24M + 6N\right] - i\kappa\left[20L+12M+6N\right]$$

As previously $\Delta A = \Delta C = \Delta D = 0$ since any other choice of value adds nothing to the arbitrary choice of value for A made in the first approximation. ΔB can then be eliminated to give :-

$$\frac{3}{c_0'}\Delta c_i' = -\frac{i\alpha}{\alpha}\left[c_0'+2\right] + 6\frac{R_e}{\alpha} + 2c_0' i\alpha R_e - \frac{i\alpha}{c_0'}\left[3\tan\beta + \alpha^2 S R_e\right] + \left[33L+9M\right]$$

This yields after substitution for L, M, N and c_0' and rearrangement

$$\Delta c_i' = \frac{R_e}{\kappa\alpha}\left[\frac{9}{\kappa 4} - \frac{3}{20} + \frac{19}{10}\kappa + 2\kappa^2\right] + i\alpha R_e\left[\frac{9}{8\kappa} + \frac{9}{4} + 2\kappa + \frac{2}{3}\kappa^2\right] - \frac{i\alpha}{\alpha}\left[\frac{7}{4} + \frac{5}{3}\kappa + \frac{1}{3}\kappa^2\right] - i\alpha\left[\tan\beta + \frac{1}{3}\alpha^2 S R_e\right]$$

Then for $c = c_r + ic_i = c_0' + \Delta c_i' + \frac{3}{2}$

we have for non zero R_e

$$c_i = \alpha\left[Re\left(\frac{9}{8}x\tan\beta + \frac{9}{4} + 2\frac{\cot\beta}{x}\right) - \frac{7}{4x} - \left(\tan\beta + \frac{1}{3}\alpha^2 S Re\right)\right] + O\left(\frac{1}{x^2}\right)$$

2.6.15

This is seen to reduce to 2.6.13 for $Re = 0$. Instability, that is an increase in the assumed disturbance with time occurs with positive c_i. 2.6.15 therefore shows that the flow will be unstable for

$$Re > \frac{\tan\beta + \frac{7}{4x}}{\frac{9}{8}x\tan\beta + \frac{9}{4} + 2\frac{\cot\beta}{x} - \frac{1}{3}\alpha^2 S}$$

- 2.6.16

2.6.4 Discussion of the Stability Criterion

The expression 2.6.16 just derived represents a condition on Re for disturbances in the film to develop and cause surface waves of long wavelength. The expression contains elements representing the slope of the conical surface, the distance travelled along a generator of that surface, the wave number and the surface tension. A quick order of magnitude assessment shows that S is small, and that for non extreme values of β the dominant term is the first term of the denominator. For large x then the criterion reduces to

$$Re > \frac{8}{9x}$$

which gives a very small critical Reynolds number indeed. For all practical purposes then the flow is at all times unstable which is in agreement with Benjamin's conclusion for the inclined plane surface.

A computational exercise was carried out to relate this criterion to the practical case of the cone on which the experiments

were carried out. The critical value of R_e, that is the value equal to the right hand side of 2.6.16. was calculated for $\beta = 30^\circ$, $\mathcal{X}$ in the range 1 to 10, α in the range 0.001 to 0.1 and the values of S corresponding to the maximum and minimum flowrates achieved during the experiments. After allowing for the variation of S with $\mathcal{X}$ due to thinning of the film and consequent variation of both mean film thickness δ and mean velocity $\bar{u}$ as indicated in 2.3. both the variation of S and of α over the whole of the range quoted were found to have insignificant effect. The critical value of Reynolds number was indeed for practical purposes a function of $\frac{1}{\mathcal{X}}$ only. The values obtained were as follows, the two extreme values of S being $6.334 \times 10^{-3}\, \mathcal{X}^{5/4}$ and $0.356 \times 10^{-3}\, \mathcal{X}^{5/4}$.

$\mathcal{X}$ =	critical R_e =
1	0.3657
2	0.2750
3	0.2168
4	0.1776
5	0.1498
6	0.1292
7	0.1135
8	0.1010
9	0.0910
10	0.0828

Not too great reliance can be placed upon the first few values above since they apply to values of $\mathcal{X}$ for which $\frac{1}{\mathcal{X}^2}$ cannot be fairly neglected as it was in the derivation of the stability criterion. Yet the results show clearly how the critical R_e falls to an extremely low value within the travelling of but a few film thicknesses down the cone, (it being remembered that distance was made non-dimensional by dividing by δ).

Two special cases corresponding to the extreme values of β deserve a mention. Firstly, that of $\beta = \frac{\pi}{2}$ corresponds to a horizontal plane with film flow radially outwards from a central point. 2.6.16 can be rewritten as

$$Re > \frac{1 + \frac{7}{4x}\cot\beta}{\frac{9}{8}x + \left(\frac{9}{4} + \frac{2\cot\beta}{x} - \frac{1}{3}\alpha^2 S\right)\cot\beta}$$

which for $\beta = \frac{\pi}{2}$ reduces to $\quad Re > \frac{8}{9x}$

This particular case then is basically similar to the general one in practical effect, though now even the nominal dependence on $\alpha^2 S$ has disappeared.

The other case of $\beta = 0$ is best approached by considering β small. 2.6.16 can now be rewritten as

$$Re > \frac{\frac{7}{4x}\tan\beta + \tan^2\beta}{\frac{2}{x} + \frac{9}{8}x\tan^2\beta + \left(\frac{9}{4} - \frac{1}{3}\alpha^2 S\right)\tan\beta}$$

Now as β is small this becomes

$$Re > \frac{\frac{7}{4x}\cdot\beta}{\frac{2}{x} + \left(\frac{9}{4} - \frac{1}{3}\alpha^2 S\right)\beta}$$

This approximates to $Re > \frac{7}{8}\beta$ for $\beta \ll x$ and suggests that the critical $Re \to 0$ as $\beta \to 0$. This implies that only in the limiting case of $Re = 0$ is the flow down the outside of a vertical cylinder stable.

3

EXPERIMENTAL WORK

3 EXPERIMENTAL WORK

3.1 Film Flow Rig

3.1.1 The Cone

The rig consisted basically of a right circular cone, included angle 60° nominal, over which a film of water is made to flow. The cone had a base diameter of 2 ft. and was a machined aluminium casting. Final machining was carried out on a vertical borer with a small depth of cut, to reduce as far as possible any non-circularity due to machining. The surface finish was good in terms of low roughness, and a cleaning procedure which involved the use of very fine 400 grade 'wet and dry' followed by 600 grade maintained and slightly improved this. Small blowholes in the casting tended to be troublesome in so far as they trapped bubbles of air underneath the water film. This problem was effectively overcome by allowing water to flow over the cone for some time at the start of a series of tests. Wiping the surface then cleared most of the bubbles and no surface irregularity was visible. The process was probably helped by the very slight porosity of the casting.

The cone was mounted on a vertical hollow shaft of stainless steel through which the supply water was fed. In order to leave the space above the cone as free as possible for observation of the film, the water feed was upwards through this shaft. To facilitate the smooth passage of this flow over onto the subsequently downward sloping conical face, the transition between shaft outer diameter and cone surface was radiused and surmounted by a small conical cap with an underside profile of matching radius. This cap served not only to assist the feed of water onto the cone surface, but

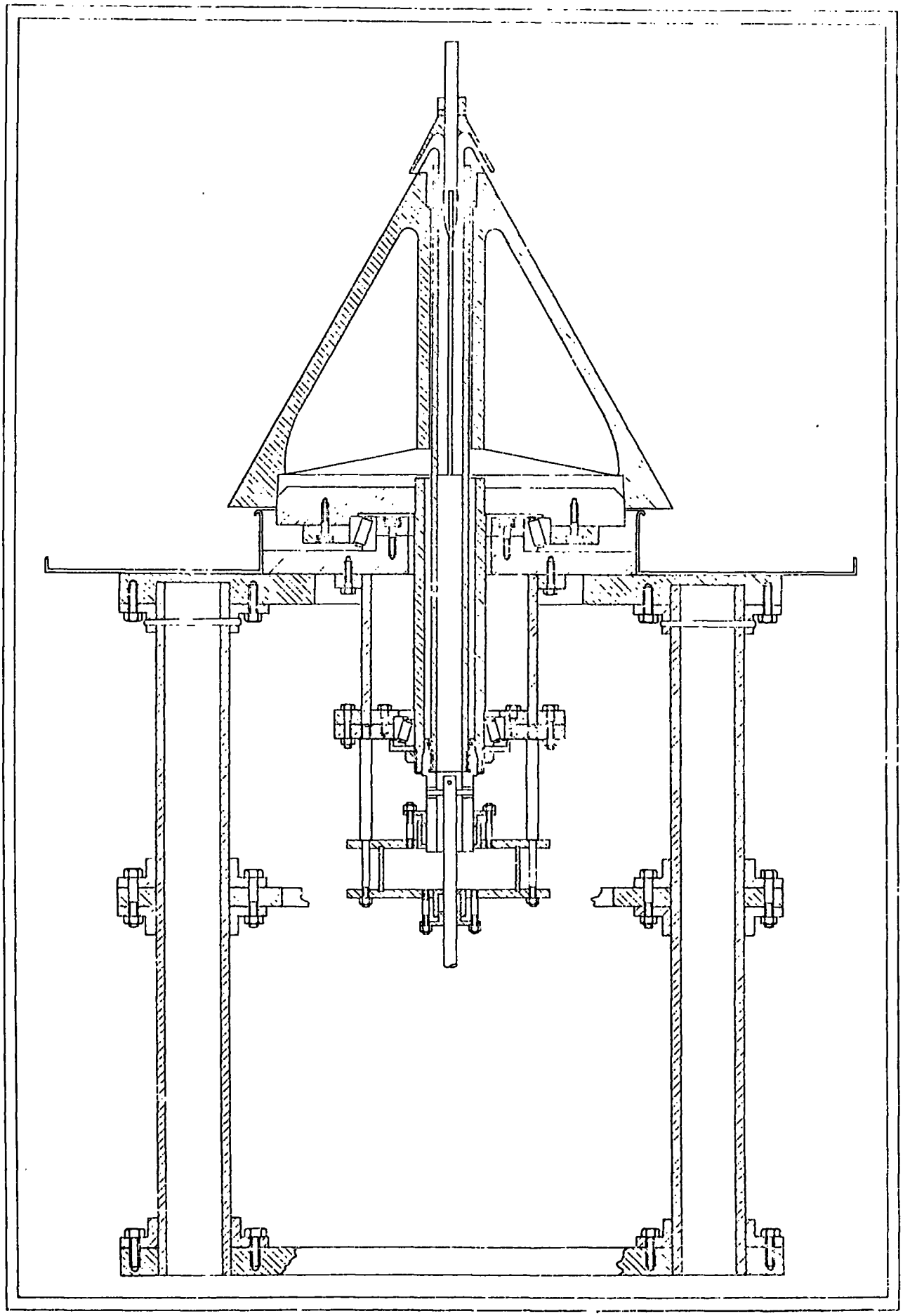

Fig. 3.1.1 Film Flow Rig

also acted as a damper of any supply fluctuations.

As can be seen in the drawing of the full rig, Fig. 3.1.1. further elaboration was necessary to allow this rig to be used for future work on the effect of rotation of the cone. For the purposes of this report however it is sufficient to say further only that the cone was supported on a very rigid structure designed to limit the effect of any free vibrations within the rig.

3.1.2 The Water Supply

The water supply was taken directly from the laboratory mains supply. This occasionally caused complications in so far as heavy use of water elsewhere in the building sometimes limited the maximum flow-rate available to an inconveniently low level. Sometimes other usage also led to regular oscillation of the supply pressure and consequent flowrate oscillation. This was very clearly detectable at a number of points in the system, and tests could not then be run. The limitation of testing to relatively quiet times was a simple and effective solution of the above problems. An independent gravity feed system from a header tank was tried, but Durham water is unusually rich in iron bacteria which multiply prolifically in static closed water systems causing discoloration and sizeable solid particles. While these can be readily killed by the addition of detergents, such an addition would have caused a marked change in the surface tension and viscosity of the water, and was eschewed.

The mains supply was taken through a micronyl filter, and hence through a rotameter for flow measurement to the cone supply line. The range of flows measured by the rotameter 10-100 gallons/hour (12.6-126 x 10^{-6} m^3/s) was ideally suited to the film conditions desired on

the cone. With flows of less than 10 galls/hr. it was found very difficult to maintain an unbroken film since the film thickness at the higher cone diameters is very small indeed as can be seen from the results presented later. Whereas above 100 galls/hr. surface wave patterns became very irregular, and some difficulty was experienced in maintaining a steady supply of this amount from the mains. Control of flowrate by the ordinary mains tap was rather surprisingly found to be very good and quite adequately sensitive. The rotameter was calibrated by the manufacturers, who supplied a calibration chart. The water leaving the cone was collected in a stainless steel drip tray and passed to drain. A thermometer in the tray drain enabled a check to be kept on water temperature which was found to vary very little during a series of tests. The day to day variation was however greater 1 - 2°C and temperatures were recorded for the accurate determination of Reynolds numbers.

3.1.3 The Measuring Station

A pair of rails parallel to a generator of the cone supported a sliding carrier to which was attached the film thickness measurement probe. This system enabled the probe, once it was mounted on its carrier, to be readily moved along a line parallel to the generator, in order to face the cone at different cone diameters. The probe axis was held normal to the cone surface, and a fixed scale allowed direct reading of the cone diameter at the point of its surface directly facing the centre of the probe. Section 3.4.2. describes initial tests to determine how representative of flow over the whole cone, was flow along the generator facing this measuring station.

Once these tests had been carried out, the cone was marked and held in a fixed position, so that all subsequent testing was carried out along this one generator of the cone.

The rails and supporting structure were sturdily constructed in order to minimise errors in the film thickness readings due to vibration. It was not found possible to position the rails with sufficient accuracy that the distance from the probe to the cone surface remained perfectly constant at all probe positions. This would be due to slight inaccuracies of form in both the rails and the cone itself which were readily displayed by the highly accurate measuring system provided by the instrumentation being used. In consequence of this, new zero readings were taken each time the probe was moved to a new diameter. A simple locking device was used to fix the probe carrier at any such required diameter.

3.2 Instrumentation

3.2.1 The Capacitance Measuring System

Of the several methods available for the measurement of film thickness, the most suitable was judged to be that based on a measurement of the capacitance between a probe held above the liquid film surface, and the cone. Such a system can be easily achieved with adequate frequency response to permit measurement and recording of instantaneous film thickness. This makes it clearly superior to those methods which yield only mean film thickness results. Indeed, some of the latter methods, such as continuous weighing, or the drainage technique whereby flow is shut off and the fluid on the surface at that instant is collected and measured, are not applicable on a conical surface where the mean film thickness varies with passage down the cone surface unlike the case of flow down a plane or cylinder for which they have successfully been used: Kamei and Oishi ('56), Cooper, Drew and McAdams ('34), Fallah, Hunter and Nash ('34), Friedman and Miller ('41), Portalski ('64). Another commonly used method, that of determining the position of the film surface with a contacting needle on a micrometer screw, is both limited and laborious despite later sophistications which have been developed whereby a comparison at various depths of the periods of contact and non contact allow an estimate of wave form to be made: Hopf ('10) Kirkbride ('34), Brauer ('56) and many others. Optical methods based on light absorption by dye in the liquid film such as used by Charvonia ('59) could not be used since the cone itself was opaque.

Another electrical method that also gives good frequency response is that of measuring the resistance between two electrodes set in, but insulated from, the solid surface and contacting the fluid film. The method however has the disadvantage of requiring fixed probes at fixed predetermined positions, and therefore lacks the flexibility of a movable capacitance probe. The use of the resistance method has been reported by Collier and Hewitt ('61) and van Rossum ('59).

The capacitance system used was based on a commercially available system produced and marketed by Messrs. Wayne Kerr Ltd., for vibration and distance measurement. The particular instrument used being a comparatively early version, a distance meter DM 100. The meter system consists of an oscillator and high gain amplifier fed by an internal H.T. power supply, together with a metering circuit and recorder output.

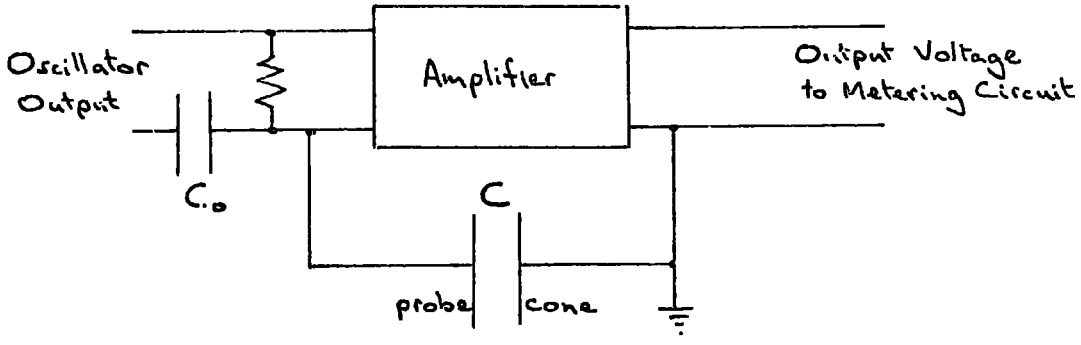

Fig. 3.2.1

The oscillator provides a reference current through a standard capacitor C_o which together with the current through the capacitance C formed between the probe and the cone is fed to the high gain amplifier. The amplifier output voltage then becomes inversely proportional to the value of C , and is therefore directly proportional to the separation of its plates, namely the probe and the cone or covering film surface facing it. The metering circuit rectifies this modulated 50 kHz

output, to give an output of fluctuating DC voltage proportional to the mean plate separation. A small internal ammeter gave a somewhat inaccurate reading of mean value. In preference to this the output was taken to a digital DC voltmeter with variable damping for mean value determination, and via an operational amplifier to an ultra violet recorder for instantaneous value recording.

The ability of this system to measure the liquid film thickness depends on the very large difference between the relative permittivity of air and water.

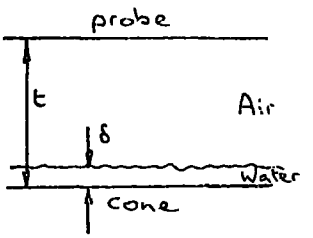

Fig. 3.2.2

For a simple parallel plate condenser as shown, the capacitance

$$C = \frac{\varepsilon_0 A}{\frac{t-\delta}{\varepsilon_1} + \frac{\delta}{\varepsilon_2}}$$

where A is the plate area

ε_0 is the permittivity of free space

ε_1 is the permittivity of air

ε_2 " " " " the fluid in the film

As stated above the output voltage of the instrument

$$V \propto \frac{1}{C}$$

$$\therefore \quad V \propto \varepsilon_2(t-\delta) + \varepsilon_1\delta$$

Now for water ε_2 varies between 82.22 at 15°C and 80.36 at 20°C while for air, even with a high water vapour content ε_1 will not exceed 1.01. Also δ did not for the most part exceed 10% of t, so that on two counts $\varepsilon_1\delta$ was small compared with $\varepsilon_2(t-\delta)$.

Hence $$V \propto (t-\delta)$$

and by subtraction of readings for V from a zero reading obtained with a dry cone ($\delta = 0$), δ could be determined after some calibration to find the constant of proportionality.

The probe used however did not form part of a simple parallel plate condenser as considered above. For although the probe itself had a plane surface, it faces the surface of the cone which was curved in one direction, and what is more curved to a varying degree. Appendix I contains an analysis of this problem, in which the factor by which the actual capacitance of the gap varies from that formed by a plane surface at the same distance as the cone, is derived. Numerical values of this factor for various values of plate separation and cone diameter were obtained, and the error introduced by the non plane surface was found to be small, less than 3% for virtually all the readings taken.

3.2.2 The Probe

The expression for capacitance above in 3.2.1 shows that

$$C \propto \frac{A}{t}$$

so that for 'similar' operation of the instrument a reduction in A, probe area, must be accompanied by a reduction in plate separation t. Now for good resolution of small wavelengths the probe area should be as small as possible. However there is a practical limitation on

the smallness of t. For if t is too small there is little clearance between the probe and the water film, and the probe becomes liable to flooding when the flow is started. That is contact between the probe and film is made and the action of surface tension causes the film to be drawn up over the whole probe surface, and to remain so. The standard probes produced by Wayne Kerr are circular, and spanned a rather greater distance along the main flow direction than was desired. A special probe was therefore designed and produced with a much shorter dimension in this direction. The requisite area was provided by making it longer in the direction normal to this, across the cone. For ease of manufacture the shape chosen for the active area was a rectangle with semi circular ends. Fig. 3.2.3. shows this probe complete with its necessary guard ring to maintain parallel lines of flux. This probe of width 4.8 mm was equivalent to a circular probe of diameter 11 mm.

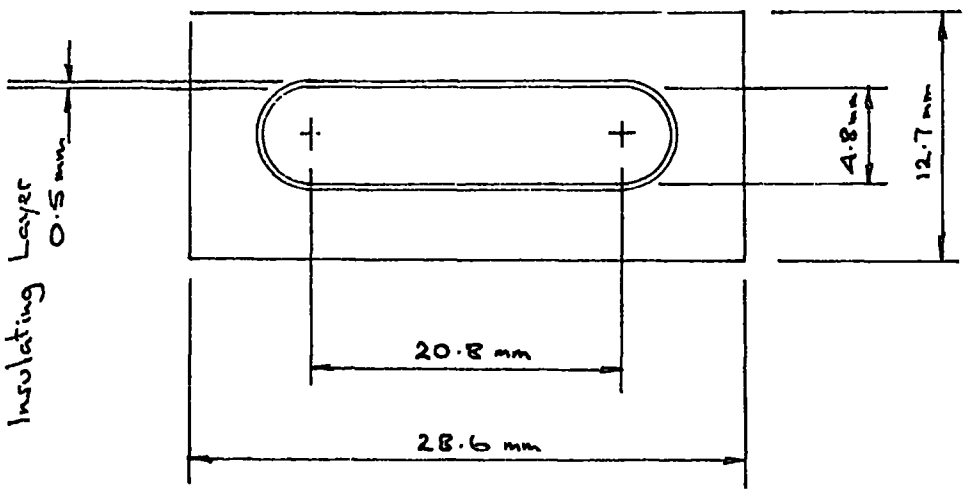

Fig. 3.2.3

3.2.3 The Amplifier

Output from the Wayne Kerr meter was in the form of a current of the order 1 mA which was proportional to the distance of the probe from the cone or its superimposed liquid film. The current was fed through a 1 kΩ reference resistor, and the voltage V_1 across this used for further processing. V_1 consisted of two components, a relatively high mean value $\bar{V}_1$, corresponding to the mean air gap thickness, together with a variable smaller amount δV_1 reflecting the variation in the air gap thickness due to surface waves. As already stated a DC digital voltmeter gave a reading of $\bar{V}_1$. A stabilised DC power supply and voltage dividing potentiometer were set up to produce a voltage V_o equivalent to the value of V_1 when there was no flow on the cone. V_o and V_1 were then fed to the inputs of a differential operational amplifier. Without flow on the cone then, the amplifier produced a zero output voltage. With flow, it produced an output proportional to the instantaneous film thickness.

The amplifier used was a Burr-Brown encapsulated amplifier type 3021/15. Diagrammatically the circuit is shown in fig. 3.2.4.

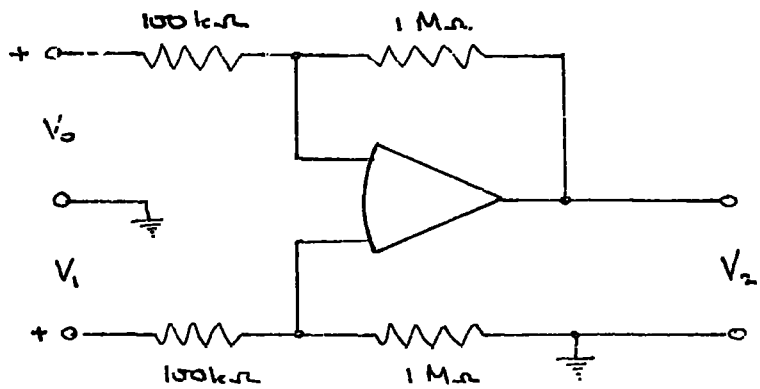

$$V_2 = \frac{10^6}{10^3}(V_1 - V_o) = -10\left[V_o - (\bar{V}_1 + \delta V_1)\right]$$ Fig. 3.2.4

i.e. $-V_2 \propto \delta$ the instantaneous film thickness

3.2.4 Recording

The output V_2 from the amplifier was recorded using a Southern Instruments type M 1300 ultra violet recording oscillograph. The matching of the amplifier output and the recording galvanometer was as follows:

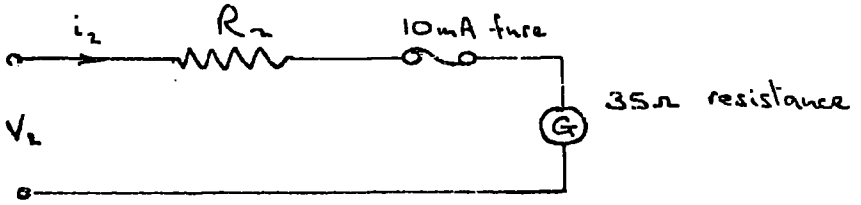

Fig. 3.2.5

The galvanometer was type SMI/M, sensitivity .050 mA/mm. It had internal fluid damping, so no parallel damping resistor was necessary. The resistor R_2 was necessary to reduce the current in the circuit to a level both acceptable to the galvanometer, and below the saturation current of the amplifier which was approximately 6.5 mA. Although this saturation level was well below the maximum current that could be tolerated by the galvanometer, the latter was nevertheless protected by a 10 mA fuse against possible accidental overloads or catastrophic failure of the amplifier. A choice of $R_2 = 375\Omega$ (for the resistor and fuse together) gave

$$V_2 = i_2 (375 + 35)$$

and galvanometer deflection in mm = i_2 in mA / .050

$$= 48.8\, V_2$$

For the wave analysis reported in 3.7 the recorder was run with a paper speed of 400 mm/s with timing marks every 0.1 s.

The completed instrumentation was then as shown in the block diagram Fig. 3.2.6.

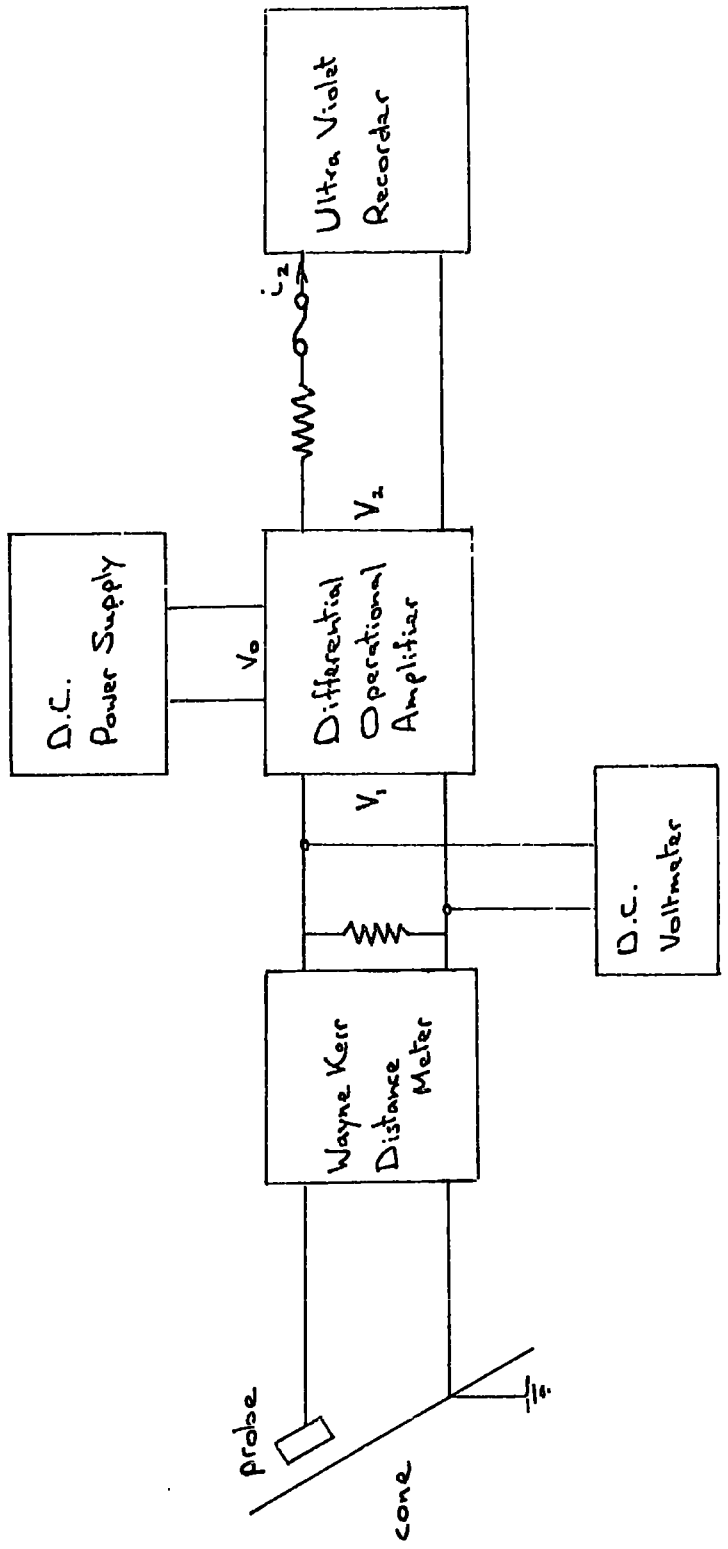

Fig. 3.2.6 Block Diagram of Complete Instrumentation

3.3 Photography

3.3.1 Still Photography

A number of still photographs were taken early in the experimental work to confirm the visual impression that roughly horizontal wavefronts were passing down the cone. Also that these wavefronts were more regular and clearly defined at the lower flowrates.

Three different cameras were used during the initial trial runs to determine exposures and lighting positions. The best quality pictures were finally obtained using a large format monorail camera, a Sinar 4" x 5" with a 150 mm lens. Use was made of the rising and tilting movements of both the lens panel and film plane of this camera to maintain a large area of the cone surface in sharp focus. Of the few lighting positions tried the best was with the single light source directly above the cone directed downwards along the cone axis, with the camera axis in the horizontal plane normal to the cone axis. The light source was a 2 μs single flash unit of 40 joules output. This provided both sufficient light and speed to "freeze" movement and allow the use of a reasonably fine grained film stock, Kodak Plus X exposed at f 5.6.

3.3.2 Cine Photography

A Hycam variable framing rate rotating prism 16 mm cine camera was used to obtain motion pictures of the flow. Although capable of very high framing rates, it was, for most of the tests, run at 30 frames/second. This gave sufficient movement of the wavefront over a few successive frames to make measurement of wave speeds possible. A mm scale placed in front of the cone surface and parallel to it just clear of the fluid film, made these measurements simple and obviated any necessity to record accurately enlargement factors in subsequent

printing.

With a $^{1}/_{10}$th shutter in the camera, the exposure for each frame was $^{1}/_{300}$s at f 2.8. The film used was Ilford FP4 developed for $4\frac{1}{2}$ minutes in Microphen at 73°F. This yielded a reasonably fine grained and high contrast image. The contrast was further improved by printing on hard paper, from which prints the measurements were made. Lighting was provided by two 500W photofloods placed as before above the cone. At very low flowrates detection of the very small waves was extremely difficult, and it was then found best to move the lights a little to the rear of the cone median plane. All cine photographs were taken opposite the 0° measuring station.

3.4 Cone Setting

3.4.1 Levelling

The cone was levelled using a Hilger and Watts clinometer, of $6\frac{1}{2}$ inches base length. With this the inclination of the conical surface to the horizontal was measured at four generators at 90° intervals. Levelling was then carried out by packing shims and wedges under the rig support structure. Three sources of irregularity were possible; irregularity of the surface, lack of coincidence of surface axis and axis of rotation, and a non-vertical axis of rotation. With possible future rotation of the cone in mind, readings were taken with the cone rotated through 90°, 180°, 270° in addition to the 0° position to get the best 'compromise level' setting.

With this done, and the cone returned to the position at which all subsequent readings were taken, the clinometer readings were as follows :

0°	59°	57'	30"
90°	60°	00'	15"
180°	59°	59'	05"
270°	59°	55'	25"

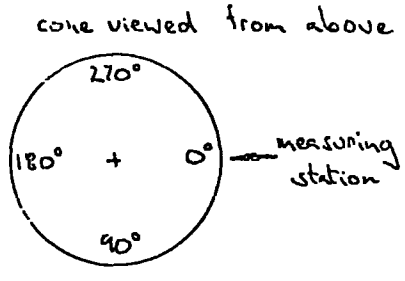

Fig. 3.4.1

Of the remaining differences in slope, about half was due to non-verticality of the axis of rotation, and half to the combination of the other two errors. The above give an average inclination to the horizontal of 59° 58' 04" with a variation of + 2'11" and - 2'49". This corresponds to a value for β of 30° 01' 56", which if approximated to

30° introduces errors of less than 0.1% in the functions $\sin\beta$, $\cos\beta$, $\sin 2\beta$.

The 0° generator was chosen for the measuring station as having the slope closest to the average value.

3.4.2 Film Uniformity

Early trials showed a fairly gross lack of uniformity in the film thickness. Errors of this sort, it was thought, might be attributable in part to errors of flow over the surface itself, and in part to non-uniformity of fluid supply to the surface. As reported in 3.1.1 the fluid supply came via a hollow central shaft up through the cone. This hollow annulus was divided by a cruciform section into four channels, so as to impart whirl to the water if the cone was rotating. But this division of the flow ended some $2\frac{1}{2}$ inches short of the top of the cone, and from that point flow should be fully annular. Again as described in 3.1.1 flow is turned onto the cone surface by an adjustable cap, see Fig. 3.4.2.

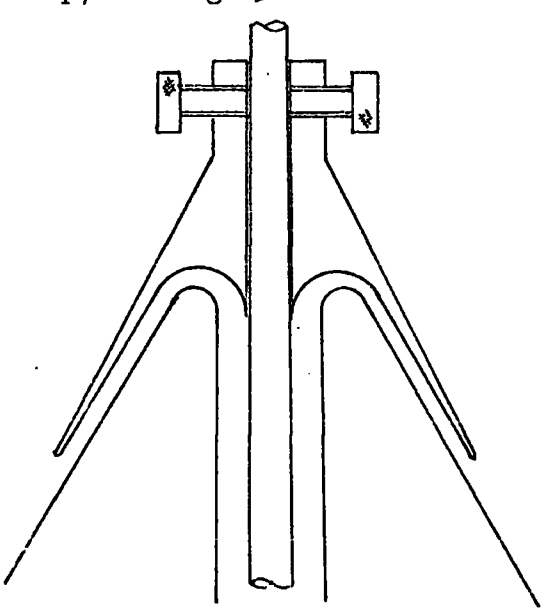

Fig. 3.4.2.

The original large error was found to be due to damage to this conical cap : the lower rim had become non-circular. This was re-machined and the large error thus rectified. The discovery however pointed to the very important role played by the cap. Its complete removal showed clearly that there was still some residual effect of the cruciform section at the cone apex. Further, without the cap, there was a very early onset of waves near the cone apex, due no doubt to the disturbances experienced in the change of direction of flow. With the cap in position, both these effects were undetectable, and its use was thus well justified. It also proved useful as both a detector, and also no doubt a damper of fluctuations in the supply flow. When occasionally these were experienced the cap, which was left free to move vertically, rattled up and down noisily. This free vertical movement was allowed partly for this reason, and partly in the expectation that this would allow for a self centering effect that would best produce an equal gap between cone and cap at the cap rim. The cap was a good sliding fit on the central shaft, and the two locking screws were adjusted so as to just allow vertical momement. A check around this gap with feeler gauges showed no lack of concentricity detectable by this method.

Checks were now repeated, taking measurements of mean film thickness for flowrates of between 10 and 100 gph for the four equally spaced generators shown in Fig. 3.4.1. The measurements were all made at 400 mm cone diameter. The results gave very good agreement at the higher flowrates, almost perfect agreement in the first instance at 80 gph. At low flowrates however there was much less satisfactory uniformity, the readings between the four generators varying over a range of up to around 15%. This was however typical of the difficulty

throughout the experimental work of obtaining good and consistent results at the lower flowrates; and it should be pointed out that it was on a very thin film of approximately 0.14 mm mean thickness that these measurements were being made.

Later recalculation of these results was carried out in the light of experience in the calibration of the instruments and the discovery of factors affecting the calibration. The recalculated results with full calibrations and also temperature allowances made showed little overall effective change. The individual results were altered slightly, but over-all the spread of readings was only slightly reduced at low flowrates, and was somewhat increased at higher ones. Fig. 3.4.3 shows a plot of the results obtained for film thickness against flowrate. It shows that the readings obtained on the 0° generator were consistently high while those at the 180° generator were consistently lower than average, with the 90° and 270° broadly similar in the middle. These discrepancies are not explicable in terms of the small residual difference in slopes. Bearing in mind that even at the highest percentage variation this only represents $\pm$ .010 mm on .134 mm, it was decided to take the precaution of maintaining the cap always in the same angular position, and to proceed with readings on the 0° generator always. In the range of flowrate 10 - 60 gph this generator gave film thicknesses between .007 and .010 mm in excess of the mean of the flow recordings taken. In this range therefore mean film thicknesses measured at the 0° generator position are approximately .009 mm in excess of the true mean, that is between 4% and 7% high.

Mean Film Thickness at 4 Quadrature Points

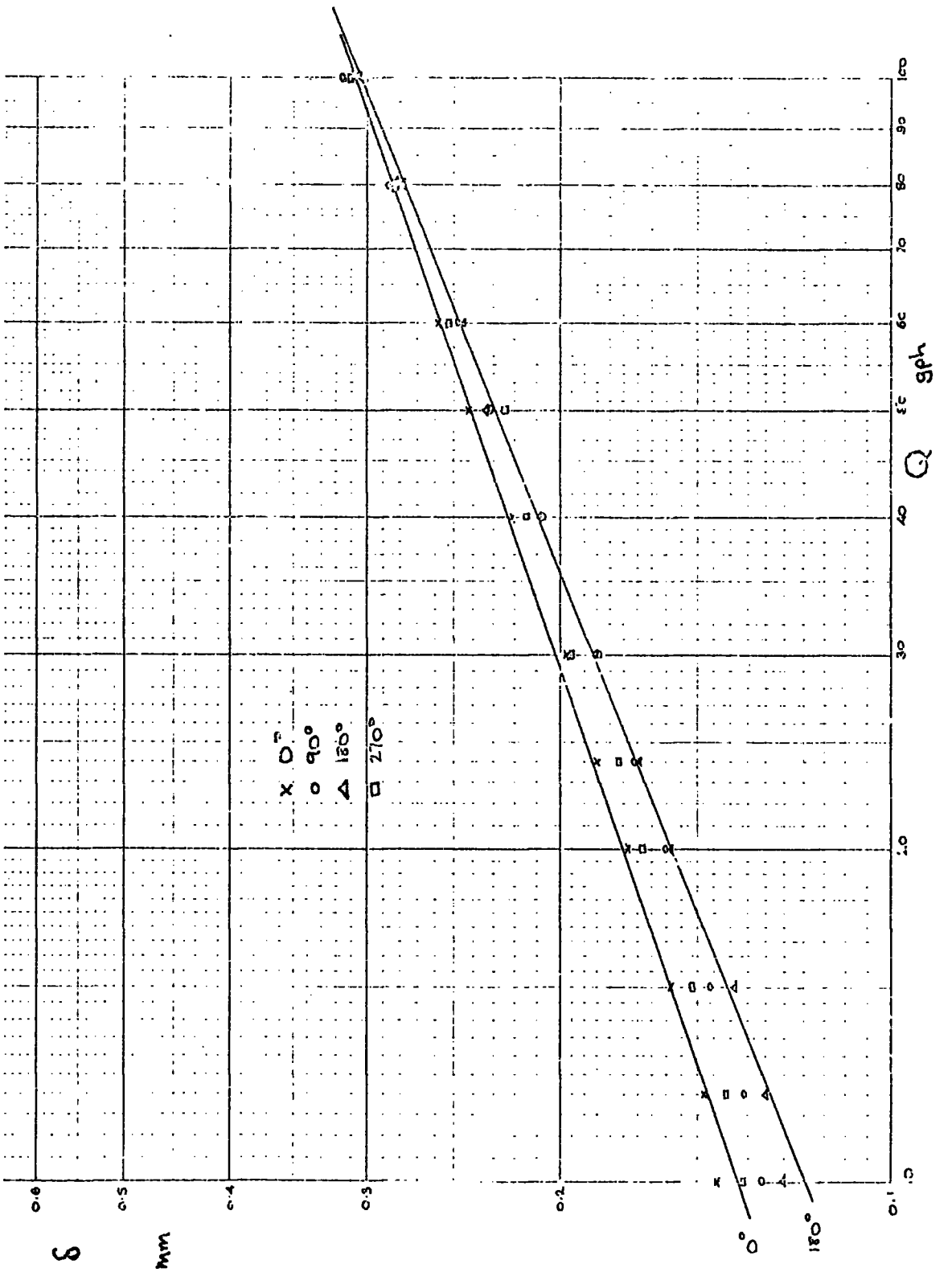

Fig

A final experimental check was made to see if any indication could be found of mean flow not following the cone generator. This was done by introducing a fine filament of dye into the film high on the cone. The dye spread out in a fan shape as the film 'stretched' over the expanding cone surface. Both visual observation at the time, and later measurement of photographs taken, showed equal spread of the dye to both sides of the line of introduction, at all stations tested. It was therefore concluded that any tangential movement could be discounted and that any pattern of non-uniform film thickness around the cone did not change appreciably with progress from top to bottom.

3.5 Calibration of the Instrumentation

3.5.1 Static Voltmeter Calibration

Calibration presented a number of problems. For a directly comparable static calibration, it would be necessary to produce water films of similar thickness to those found on the cone. Now films of this thickness (0.2 - 0.5 mm) are not easily formed except in flow situations where their thickness is uncertain. However the expression for the dependence of capacitance on this film thickness suggests that the actual film has little effect except in so far as it modifies the size of the air gap. Initial calibration therefore proceeded on the assumption that it was the air gap thickness that was being measured.

Firstly a simple air gap was created between the probe and an opposing parallel metal sheet. The metal sheet was arranged so that it could be raised or lowered under the probe by means of a micrometer height gauge. A series of several such tests carried out at intervals over a period of a few weeks yielded excellently consistent results. There was a very clear linear relationship between voltage across a 1 kΩ resistive load and the air gap. The constant of proportionality varied only between 0.361 and 0.363 V/mm, and 0 V output corresponded to 0 mm air gap.

Similar tests carried out over the same period with the probe facing a horizontal water surface proved far less satisfactory. Not only was the constant of proportionality different but it was so by a varying amount. No apparent pattern was discernible. Although the thickness of the underlying water layer could not be easily reduced to the size of that found on the cone, widely varying values of 0.62 mm, 0.805 mm and 6.2 mm were all found to have the same calibration factor of 0.386 V/mm when successive tests were run one day.

This supported well the suggestion stated above that it is really the air gap that counts. Again the tests were carried out in such a way that the water layer had sufficient time to reach room temperature; and this in a room situated deep in the heart of a large building, where the temperature remained remarkably constant. Nevertheless, it was decided that calibration by moving a fixed thickness layer of water to and from the probe did not perhaps sufficiently simulate the situation on the cone, where it is a variable thickness film of water which modifies the capacitance between opposing fixed metal plates. It should be pointed out that the layer of water used in the tests above was not of fully constant thickness, a small amount of evaporation generally took place, but this was allowed for in the calculations it being assumed to have been at a constant rate.

Next, therefore, calibration tests were carried out with the probe fixed with vertical axis above a horizontal dish of aluminium, the cone material, Fig. 3.5.1. The dish was formed by turning a recess in a piece of aluminium plate. Three sizes of dish were used, the smallest with a 3 inch diameter recess gave results significantly different from those obtained from 4 inch and 5 inch diameter dishes which were closely similar. It was concluded that the 3 inch recess was insufficiently large compared with the probe size and that some fringing effects of the lines of flux were taking place. Later tests were therefore carried out on the 4 inch dish in which it was somewhat easier to create an unbroken film than in the 5 inch one. To facilitate this film formation at the lowest feasible film thickness the dish was thoroughly cleaned with concentrated sulphuric acid and ethyl alcohol shortly before calibration runs.

Calibration Arrangement

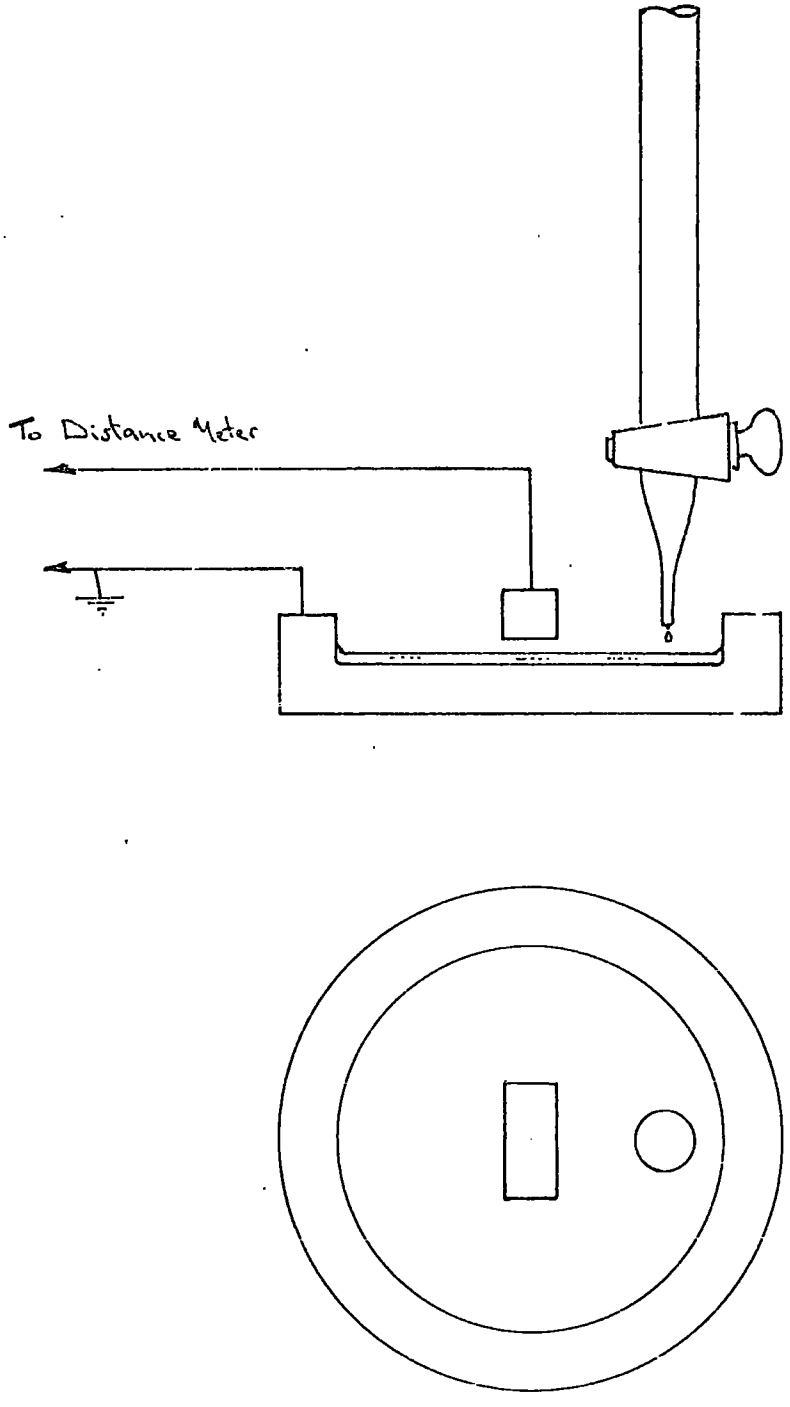

Fig. 3.5.1

Water was dripped into the dish from a 10 ml burette graduated in .02 ml . From knowledge therefore of the quantity added and the cross sectional area of the recess the film thickness could in theory be calculated. However, uncertainty as to the exact thickness arises through the existence of the meniscus region. It was necessary with the 4 inch dish to add initially about 3 ml of water before a continuous film over the whole recess could be formed at all. The earliest readings then tended to be erratic until a proper meniscus was formed after the addition of about 3.5 ml in all. This is equivalent to a film thickness of approximately 0.43 mm making no allowance for the fluid contained in the meniscus. Tests by evaporation and weighing with the 3 inch dish suggested that that had a meniscus region which contained 1.1 ml water. A pro rata increase suggests that approximately 1.5 ml would be contained in the 4 inch dish meniscus. Making this allowance gives approximately 0.25 mm as the lowest reliable film thickness that could be obtained using the 4 inch dish. This is well within the range of film thickness measured on the cone, although still somewhat greater than the minimum thicknesses encountered.

A series of tests with the above arrangement carried out over a period of 10 days yielded the following calibration factors :-

0.379	0.392	0.398
0.386	0.391	0.387
0.394	0.395	0.392

These give an average of 0.390 with a range of - 2.8% to + 2.1% of this.

Probe Calibration Factor v Check Circuit Voltage

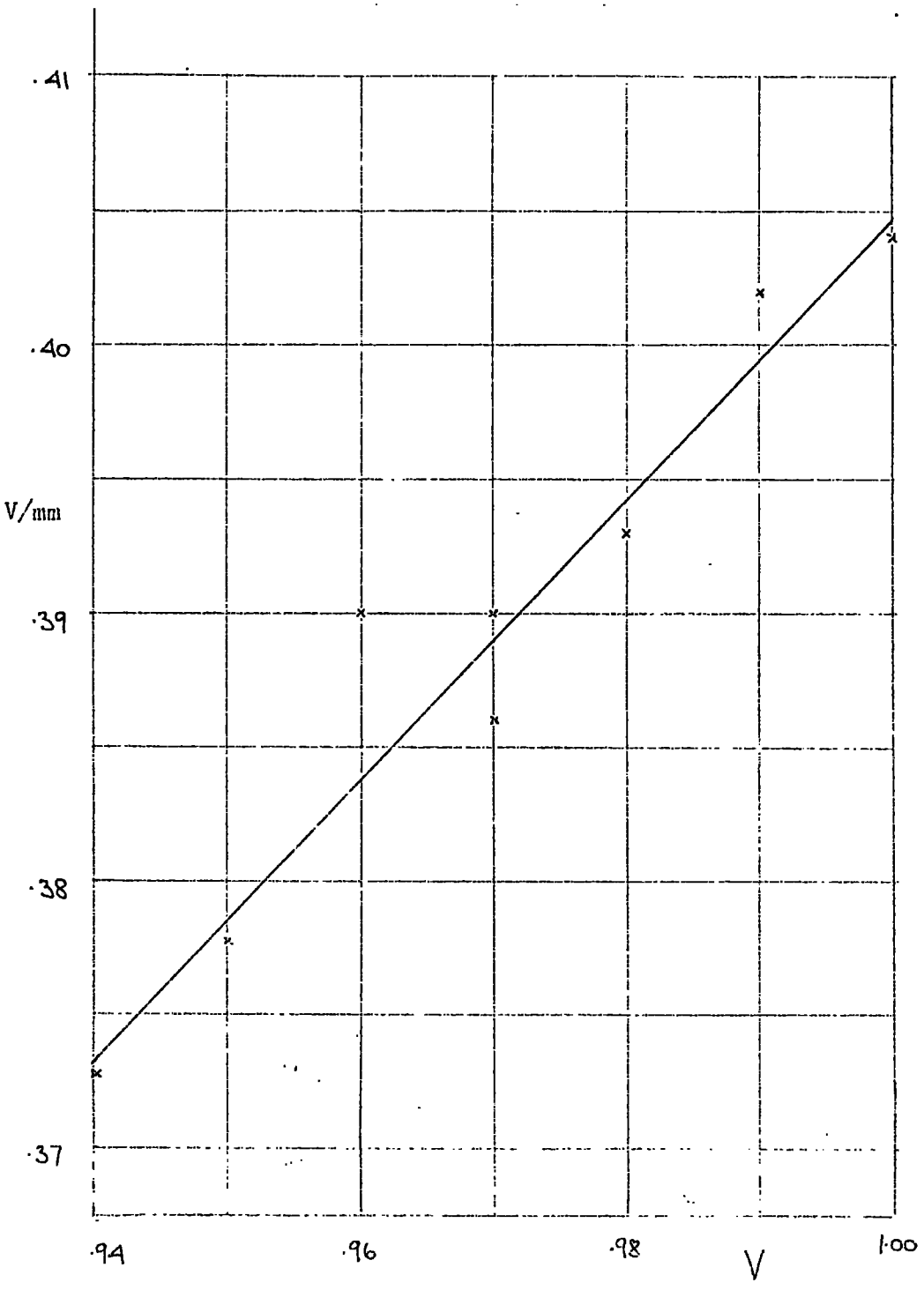

Fig. 3.5.2

About this time it was noticed that over a long period of testing, the output of the Wayne Kerr instrument, as evidenced by the output of a standard check circuit provided within the instrument, was liable to drift. Insufficient notice had been taken of the constancy of the check circuit output up till then. A series of calibrations was therefore carried out at different values of check circuit output, and a consistent pattern observed. Graph 3.5.2 shows the variation of calibration factor with check circuit output as measured with the digital voltmeter across the standard 1 kΩ resistance. The line drawn on this graph was obtained by a linear regression analysis.

All subsequent testing was carried out with a check circuit output maintained at 0.980 V and the corresponding calibration factor of 0.394 V/mm or 2.54 mm/V used.

3.5.2 Static Recorder Calibration

The instrumentation was next completed by the addition of the amplifier and recorder circuits as shown in the block diagram, Fig. 3.2.6. A calibration was then undertaken of the recorder deflection against film thickness using the 4 inch dish and water supplied by burette as before. The voltmeter was kept in the circuit so as to again check its own calibration, and also as a means of monitoring the check circuit output. Since the output from the Wayne Kerr instrument, in both operating and check modes, was a current output, the addition of the amplifier circuit, with its high but still finite input impedance, slightly reduced the check voltage recorded across the 1 kΩ reference resistor from 0.980 V to 0.974. Bearing in mind the dependence of the calibration upon this check circuit output,

care was taken to maintain this check voltage at 0.974 V with the amplifier in circuit, and 0.980 V with the amplifier absent.

The results of four successive calibration runs were as follows :-

		Voltmeter		Recorder	
RUN	1	.391	V/mm	179	mm deflection/mm
	2	.402		185	
	3	.390		182	
	4	.392		185	
	mean	.394		183	

This therefore gave a result in good agreement with the voltmeter calibration already established, and a value consistent within 2½% for the recorder deflection calibration.

It is interesting to observe that the value of 183 mm/mm also approximates reasonably well to the value that might have been predicted by the circuit parameters. The amplifier gives a nominal amplification of 10 and in 3.2.4. the recorder circuit is shown to have a nominal sensitivity of 48.8 mm/V output. These combine to give a nominal recorder sensitivity of 0.394 x 10 x 48.8 = 192 mm/mm; within 5% of the actual value.

It should at this point be noted that, while throughout the calibration testing, good agreement was always obtained between the gradients of different calibration runs, far less consistency of intercept on the axes was obtained. With reference to the use of

the dish for calibration this might be explained in terms of uncertainty as to the amount of fluid occupying the meniscus region. It is however difficult to see how this would vary very widely between runs, particularly in view of the cleaning precautions taken. Another possible source of variation is adsorption into the metal surface. Unfortunately aluminium represents a poor choice of material in this respect, a fact unknown at the design stage when it was chosen on grounds of weight and cost.

3.5.3 Dynamic Voltmeter and Recorder Comparison

It was thought desirable to have some form of check that static calibrations did produce values that were valid for dynamic measurements made with actual films on the cone. While no direct absolute check of the 2 calibrations was possible, a comparison of corresponding voltmeter and recorder readings was thought to be better than no check at all. Consequently readings obtained during the mean film thickness testing period were plotted in the form of voltmeter reading against an estimated mean UV recorder trace deflection. The result, Fig. 3.5.3. shows that these points lie in a band fairly evenly distributed about the line given by points obtained from the static calibrations. A certain amount of scatter is inevitable bearing in mind that the mean recorder trace deflection is obtained by a subjective visual estimate of what is in some cases a highly irregular trace. Nevertheless it is apparent from this graph that points representing different flowrate values taken successively at a given diameter conform generally well to a line of their own parallel to the calibration line. The scatter therefore is not an entirely

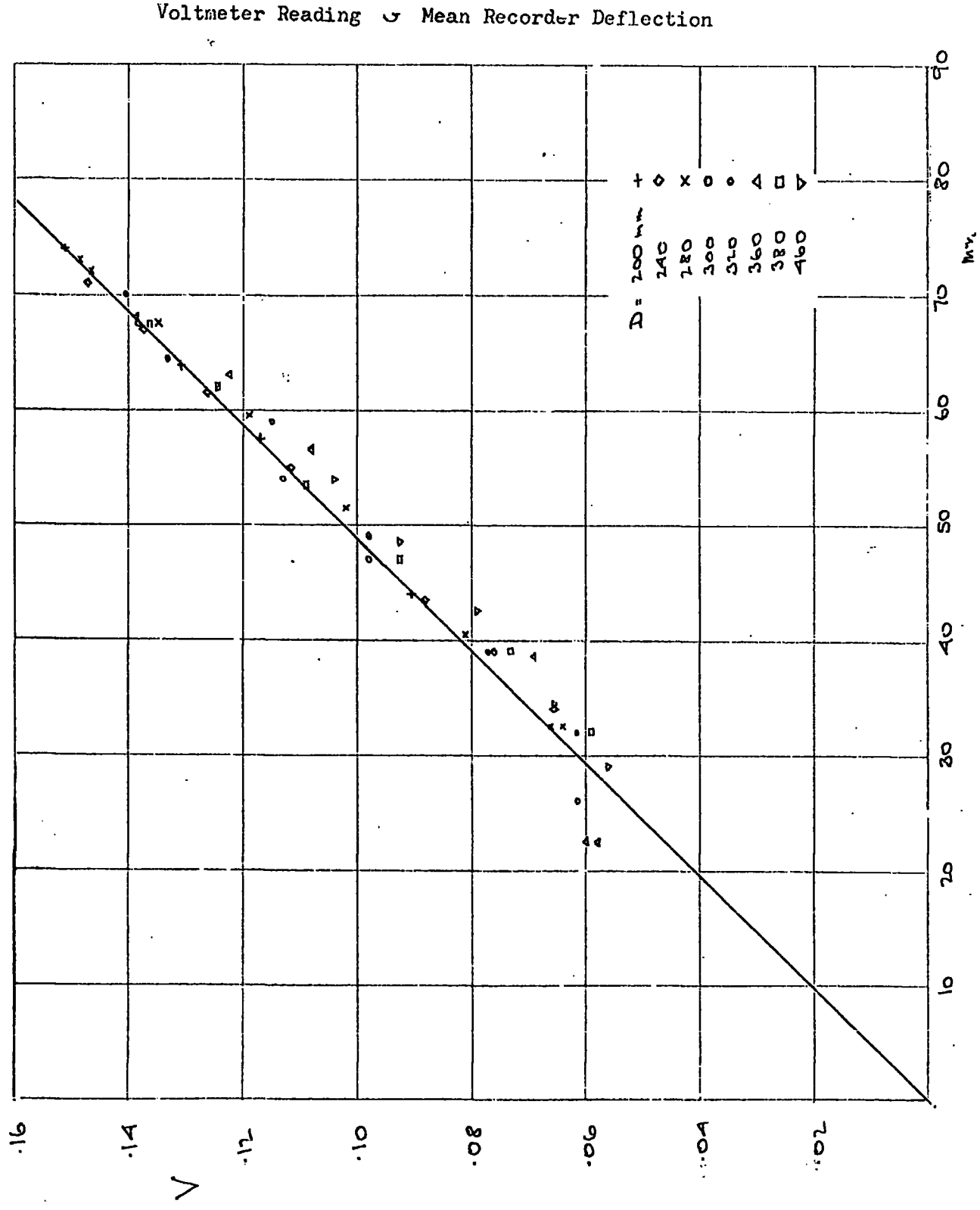
Voltmeter Reading ∽ Mean Recorder Deflection
λ = 200 mμ
240
280
300
320
360
380
400
mv.
V
.16
.14
.12
.10
.08
.06
.04
.02
90
80
70
60
50
40
30
20
10

Fig. 3.5.3

random one but stems from the uncertainty in zero reading referred to at the end of the previous section.

It is also worthy of note that there is a rather greater scatter towards the right of the calibration line suggesting that the recorder will tend to give a somewhat higher mean film thickness reading than the voltmeter. This was found to be so in later experiments. Also the scatter is greater the smaller the reading; and again in later experiments it proved more difficult to obtain consistent results at the lower flowrates despite the more irregular waveforms found with high flowrate values.

3.6 Tests

3.6.1 Mean Film Thickness

With the apparatus set up as described in the foregoing sections, a series or tests was carried out to determine the pattern of mean film thickness variation. The voltmeter only was used, with sufficient damping in its internal circuitry it registered a sufficiently steady mean value. The variation of mean thickness with both flowrate and diameter was studied for constant values of the other variable.

The range of diameter available on the cone was from 135 mm to 464 mm these being the extreme values that could be reached with the rail mounted probe. Measurements were therefore made at the following values of diameter : 140, 180, 220, 260, 300, 340, 380, 420, 460 mm. As previously stated, the range of flowrate was 10-100 gallons/hour or 12.6×10^{-6} to 126×10^{-6} m^3/s. The non standard unit of gallons/hour in which the rotameter was calibrated was retained for convenience during the experiments chiefly because it represented a complete single cycle on logarithmic graph paper. Since the theoretical relationship between mean film thickness and flowrate is cubic in form, logarithmic plotting to verify this relationship was convenient. With such plotting in mind the values of flowrate chosen were : 10, 12, 15, 20, 24, 30, 40, 50, 60, 80, and 100 gph.

The test procedure was as follows :-

(1) · The cone was cleaned with firstly a small amount of detergent solution, and secondly with light rubbing with 600 grade 'wet and dry'. The use of the latter being mainly confined to any areas where difficulty was being experienced in forming a continuous film. Care was also taken

to clean thoroughly the lip and underside of the cap at the water entry point. Throughout most of this process and for some 15-20 minutes after, a high flowrate was maintained over the cone in order to both wash away any trace of the detergent and also to bring the cone to water temperature.

(2) The probe was brought into position at one of the values of diameter listed above. The water flow was stopped and the area of cone surface immediately under the probe dried with a broad jet of cold air.

(3) The Wayne Kerr check circuit voltage was read, and adjusted if necessary to the chosen value of 0.980V. A zero reading was then taken corresponding to the air gap between the probe and the dry cone.

(4) The supply of water was resumed and the flowrate steadily increased to the maximum value of 100 gph. A check was made to see that the underside of the probe was still dry. Occasionally small drops were found to have splashed on to it in the starting period. When this happened it was necessary to start all over again. A check was also made that a complete film had been formed all over the cone. Little difficulty was experienced with this if step (1) had been properly carried out. After one or two minutes running any small air bubbles that tended to collect in the larger casting blowholes were removed by wiping the cone under the film with a piece of stiff paper. After a check that the water temperature was steady, this and the voltmeter reading were recorded.

(5) Thereafter the flowrate was reduced by successive steps to the values listed above. The flow showed a rapid response to the changes. The voltmeter reading was recorded at each flowrate value, and a check was kept on water temperature. The latter showed little variation, not more than $0.1^{o}C$

during the run. As the flowrate reached the smaller values, care was taken to check that a complete film around the cone was being maintained. This was found to be easier when starting with a high flowrate and successively reducing it, than when forming a film at a low flowrate from scratch.

(6) After readings had been obtained at all flowrate values, the supply was turned off. The area of cone immediately under the probe was again dried with the air jet, and the zero reading with the dry cone repeated. This reading was then compared with that taken at the start of the test. Some difficulty was experienced here in that sometimes discrepancies existed. Some of these were the result of electronic drift in the Wayne Kerr instrument circuitry. These were revealed by also re-checking the check circuit output voltage. Only where the zero readings and check circuit voltages were in agreement to within .001V were the results for that run accepted.

(7) If unacceptable agreement of zero readings was obtained, the run was repeated until satisfactory. The probe was then moved to a different diameter and the procedure from (2) onwards repeated until runs had been made at all the diameters listed.

The readings thus obtained were then processed as follows :-

1. Subtracted the voltages recorded at the various flowrates from the zero reading to give the voltage equivalent to the mean film thickness.

2. Divided by the calibration factor 0.394 V/mm to give the apparent mean film thickness.

3. For diameters up to 260 mm applied the appropriate conical surface correction as outlined in 3.2.1 and Appendix I . For the higher diameters this correction would have been very small (< 1%).

4. Calculated the corresponding values of Reynolds number using the kinematic viscosity of water at the mean temperature for the run.

For results and discussion see section 4.1.

3.6.2 Wave Measurements - Amplitude and Frequency

The basic test procedure was identical to that adopted in 3.6.1 except that now the instantaneous film thickness was continuously recorded for a short period when all conditions were steady. This required the full amplifier and recorder instrumentation as shown in Fig.3.2.6. As noted in 3.5.2 the Wayne Kerr check circuit output voltage was maintained at 0.974V. A number of different recorder paper speeds were tried. The slowest speeds were unsuitable for giving any indication of wave shape but indicated well the pattern of peak size variation. Early records taken like this emphasised the difficulty of getting an exact measure of amplitude. They also showed that no simple measure of frequency was entirely satisfactory either due to the complexity of the waveform. Consequently it was decided to subject records to a full Fourier analysis. For this, traces at a much higher paper speed were necessary and 400 mm/s was found most suitable. At this relatively high speed, the paper acceleration and deceleration periods at the two ends of the record must be avoided when analysing the trace. An internally generated 0.1 sec. interval timing mark on the paper margin made this simply done, and gave a ready check of the constancy of paper speed. As with the mean film thickness measurements, a trace corresponding to the dry cone reading was taken at the beginning and end of each run. These served as zero lines from which the deflection could be measured. Small zero drifts were sometimes found (2-3 mm) between beginning and end of a run. If the voltmeter readings were otherwise satisfactory, this drift was divided into equal intervals of drift between each

record in between, and allowed for thus.

Wave records at the lower diameters showed very little disturbance as was expected, especially at low flowrates. Records for analysis were taken at diameters 240, 280, 320, 360, 400, 440, and 460 mm, and at flowrates of 10, 20, 40 and 100 gallons/hr. The analysis of the records is described in sections 3.7.1 and 3.7.2.

3.6.3 Wave Measurements - Wavespeed and Wavelength

These measurements were obtained from the cine photographs taken as described in 3.3.2. Not all of the length of the 0^{o} cone generator could be covered by one shot, so three overlapping series of films were taken to cover the range of diameter from 160 mm to 460 mm. Initially films were taken at flowrates at 40, 20, and 10 gph only. The last of these proved very difficult to analyse and since it is only at the lower flowrates that fully developed waves were found to be obtained, a further series was taken at a flowrate of 15 gph. The water temperature was measured to allow the water properties to be determined. No direct measurement was made of the film thickness at the time, since the probe and measuring station had been removed to give the camera a clear view. By this time however enough was known about the flow to enable an indirect calculation of mean film thickness to be made.

Strips of four successive frames were enlarged and printed and from these measurements made. The movement of the waves down the cone could be clearly seen and at 30 frames/s the time interval covered by the 4 frames was 0.1 s. Measured changes of wave position in the range 15 to 40 mm then corresponded to wavespeeds of 0.15 to 0.4 m/s. A considerable number of such measurements were made, the wave being

credited with that mean speed at the mid-point of the travel measured.

The measurement of wavelength was much less simple as could be predicted from the traces obtained in 3.6.2. No clear regular wavelength was apparent, and the distance between successive wavefronts varied widely. A number of specific diameters were chosen, such as D = 320 mm. Measurements were then made of the distance between the wavefronts either side of this diameter and a number of such measurements averaged to give a mean wavelength at that diameter. Care was taken to pick wherever possible the distance between two roughly parallel wavefronts. This procedure was most difficult at low flowrates and high diameters where the recorded wavefronts were not at all clear against the patchy grey cone background. While the larger waves could be fairly confidently picked out for wavespeed measurement, less confidence was possible in picking two successive wavefronts.

3.7 Wave Analysis

3.7.1 Trials with a Wave Analyser

A Muirhead-Pametrada wave analyser type D-489-GH was brought into the instrumentation in an attempt to determine if any single dominant frequency was present in the wave readings. As the lower frequency limit of the analyser was 15 Hz, it was necessary to record the output from the operational amplifier over a period of time using an Epsylon-Labcorder. The recording was made at a lower speed and played back into the analyser at the maximum speed available, 15 inches/s thus increasing all frequencies.

The analyser consists essentially of a series of adjustable filters which permit examination of the energy content of the waveform at any specified frequency. The band width of the filters could be varied from 'in tune' to one-third octave. It was found in practice that energy content thus measured fluctuated considerably as the recording was played back. This indicated as might have been expected that the flow disturbances presented a by no means steady picture. Taking mean values, it was possible to build up a picture of frequency dependence which indicated no great dominant peak. A maximum was apparent, and this varied with flowrate. The maximum was not however sharply peaked and this method which was time consuming and necessitated the undesirable intermediate recording stage was not used further.

3.7.2 Fourier Analysis

Any complex wave pattern may be split into an approximating series of waves of different amplitudes and frequencies superimposed. If therefore we are able to define the wave pattern observed $x(t)$ over the period T, it can be expanded in the form of the Fourier series

$$x(t) = a_0 + \sum_{r=1}^{\infty} (a_r \cos rt + b_r \sin rt)$$

where $\omega = \frac{T}{2\pi}$

$$a_0 = \frac{1}{T}\int_{-T/2}^{+T/2} x(t)\,dt$$

$$a_r = \frac{2}{T}\int_{-T/2}^{+T/2} x(t)\cos r\omega t\,dt$$

$$b_r = \frac{2}{T}\int_{-T/2}^{+T/2} x(t)\sin r\omega t\,dt$$

The degree of excellence by which a series can be determined to approximate to the pattern of wave formation will depend on both the length, and the degree to which the period T over which $x(t)$ is known, is typical of the wave pattern as a whole. If the process is truly harmonic, then T will merely need to exceed the period of the fundamental component. If the process is random, then a true approximation is not possible since no pattern exists, and the longer T is the better. In the present, rather intermediate case, where successive waves are visibly present, but there is also apparent no truly regular pattern, then a value of T long enough to cover several of these waves might be expected to give useful information of the general pattern.

A computer program was available as part of the IBM 360 Scientific Subroutine Package to carry out an analysis of the above type. To define $x(t)$ over the period T it was necessary to divide T into $2n$ equal intervals and to measure $x(t)$ at each interval point. The input to the program consisted therefore of $2n + 1$ successive values of $x(t)$ including the end values. Examination of the recorder traces obtained suggested that the number of waves per second varied from about 8 to 30. Supported by the wave analyser experiments which gave peak frequency values in a similar range, a period of T = 1 sec. was chosen as suitable. Division of this period into 1 mm steps on

the paper trace, the smallest interval feasible, then gave $2n = 400$ since the recordings were made at 400 mm/sec paper speed. From these input data, the program could give values of a_0; a_r, b_r for $r = 1, 200$ i.e. values of the amplitudes associated with both the sin and cos component waves at frequencies from 0 Hz to 200 Hz at 1 Hz intervals.

It was found in practice, that only frequencies of less than about 40 Hz gave values of a_r, b_r that were of significance. Consequently the output program was written so as to print values up to 50 Hz only. Rather than print out the values of a_r and b_r, these were squared, added and rooted to give

$$c_r = \sqrt{a_r^2 + b_r^2}$$

i.e. the amplitude associated with that particular frequency, independent of phase. The values of c_r or perhaps more correctly c_r^2, thus obtained could be plotted against the associated frequency to give the spectral density of the waveform: Robson ('63). Also obtainable from these results was a mean square value. Using Robson's notation the mean square value of $x(t)$

$$\langle x^2(t) \rangle = a_0^2 + \frac{1}{2} \sum_{r=1}^{\infty} (a_r^2 + b_r^2)$$

In this instance a_0 represented the mean film thickness and it was preferred to exclude this and get a root mean square amplitude for the waves

$$A_{rms} = \left[\frac{1}{2} \sum_{r=1}^{\infty} (a_r^2 + b_r^2) \right]^{1/2}$$

This in turn could be made non-dimensional by dividing by a_0 to give a parameter indicating the degree of waviness or the wave intensity of the flow. This wave intensity parameter is somewhat similar to the turbulence intensity parameter often used and was defined as

$$I = A_{rms} \div a_0$$

$$= \left[\frac{1}{2}\sum_{r=1}^{\infty}(a_r^2 + b_r^2)\right]^{\frac{1}{2}} \div a_0$$

For a listing of the program written to provide input to the standard Fourier Analysis program and to provide the above manipulation of the output; See Appendix II

An analysis of this form was carried out on traces obtained at the following conditions

D \ Q	10	20	40	100
240		x	x	x
280	x	x	x	x
320	x	x	x	x
360	x	x	xx	x
400	xx	x	x	x
440	xx	x	x	x
460	x	x	x	xx

xx indicates 2 traces were analysed.

3.7.3 Statistical Analysis Program

Also available in the IBM 360 Scientific Subroutine Package was a simple statistical program. Use was made of this partly as a means of checking the results of the Fourier Analysis program and partly for the information in its own right. The input to both these programs consisted of a series of 401 successive 3 or 4 digit numbers. Though checked, there was a strong possibility of error remaining. The statistical program with its listing of maximum and minimum values

would have readily exposed any particularly gross errors. In addition to these values the output program was used to calculate their difference, the range over which the film thickness varied. Also determined by the program were the average film thickness as a direct mean of the 401 values constituting the input, and also the standard deviation of these values about that mean. This average was invariably slightly larger than its value of a_o determined above, the difference being generally between 1% and 2%, and never more than 2½%. The standard deviation was found to be identical to Arms as a consideration of their origin and significance suggests.

For a listing of the full program written to provide input and output manipulation of the standard program, see Appendix III

Analysis was carried out on the same traces as indicated in 3.7.2.

4

RESULTS AND DISCUSSION

4 Results and Discussion

4.1 Mean Film Thickness

In the experiment described in 3.6.1 the D.C. voltmeter gave a voltage reading corresponding to the mean film thickness, as the instantaneous voltage was averaged by the internal damping circuit. The converted results of nine runs at different diameters are given in Table 1.

Table 1

Measured Values of Mean Film Thickness (mm)

Q gph \ D mm	140	180	220	260	300	340	380	420	460
10	.212	.203	.185	.178	.169	.155	.147	.145	.141
12	.220	.213	.195	.187	.178	.163	.155	.151	.149
15	.235	.228	.210	.199	.191	.174	.168	.160	.157
20	.260	.248	.232	.220	.211	.192	.187	.175	.178
24	.270	.261	.246	.234	.222	.202	.196	.191	.191
30	.288	.279	.262	.253	.241	.219	.211	.205	.203
40	.320	.302	.284	.280	.266	.242	.231	.222	.222
50	.355	.327	.304	.305	.288	.263	.252	.240	.238
60	.379	.338	.320	.323	.306	.283	.269	.255	.256
80	.436	.373	.351	.356	.338	.310	.298	.287	.287
100	.483	.400	.374	.381	.367	.335	.322	.312	.316
Mean T ^{o}F	68.4	68.0	67.9	67.8	67.8	68.0	67.2	67.5	67.5
Variation ^{o}F	0.1	0.0	0.3	0.0	0.0	0.1	0.1	0.0	0.3

Table 2 gives the value of film thickness for undisturbed laminar flow given by expression 2.3.4 at the upper and lower ends of the flowrate range. The calculation was in each case based on a value of viscosity corresponding to the mean temperature of the particular experimental run.

Table 2

Theoretically Predicted Values of Mean Film Thickness (mm)

Q gph \ D mm	140	180	220	260	300	340	380	420	460
10	.216	.199	.186	.176	.168	.161	.156	.150	.146
100	.466	.429	.402	.380	.362	.347	.335	.324	.315

Since expression 2.3.4 gives a one-third power law relationship between film thickness δ and flowrate Q, δ plotted against Q on logarithmic scales will give a straight line of gradient $^1/_3$. Graph 4.1.1 shows every other set of both the experimental values of Table 1. and the corresponding theoretical lines defined by Table 2. The vertical (δ) scale of this graph has been cut and divided into sections to separate lines and points which would otherwise have been very crowded, so as to allow a clearer comparison between each set of experimental and theoretical results.

In determining the values set out in Table 1. experimental errors are inevitably involved. These are assessed as follows :-

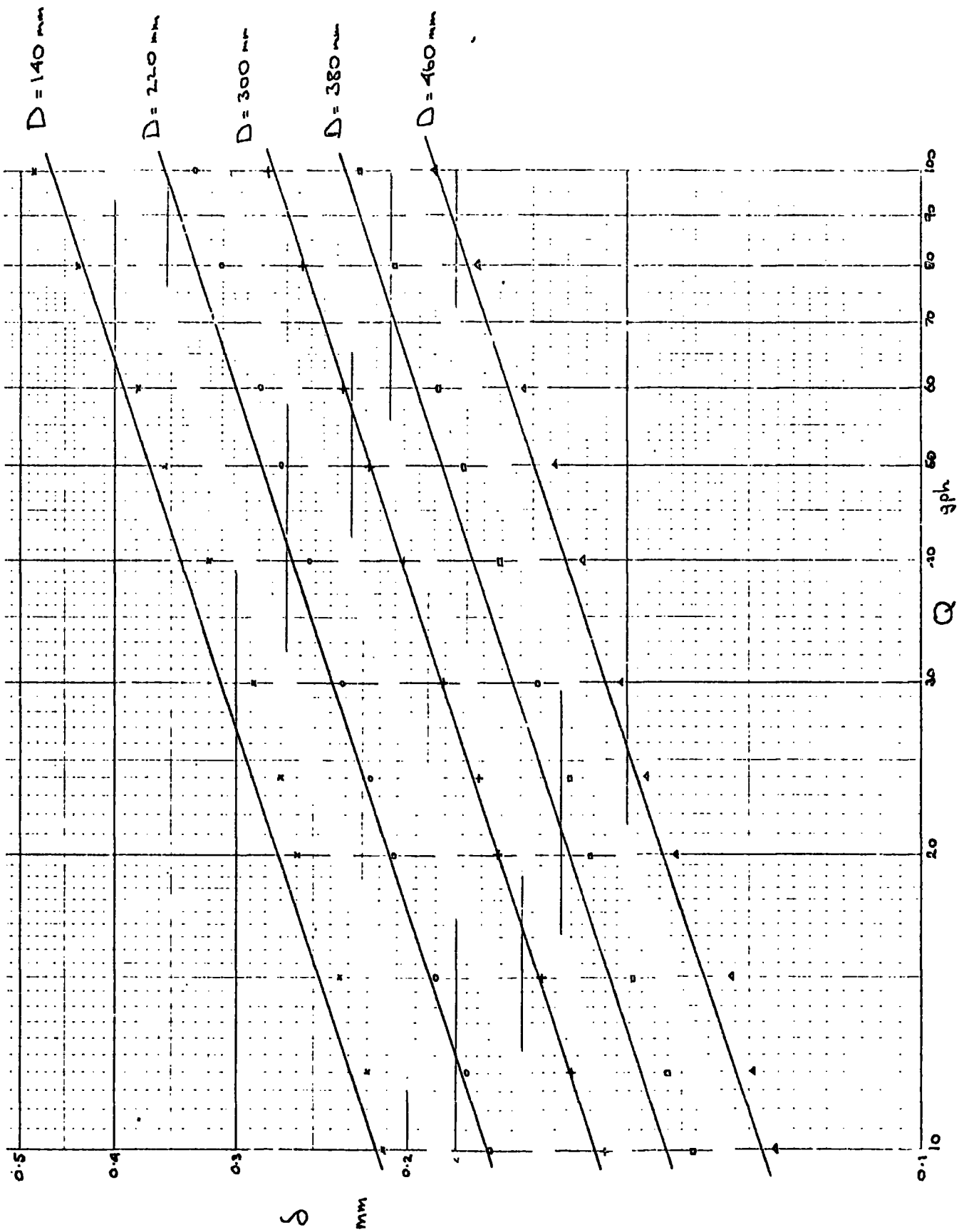

Fig. 4.1.1 Mean Film Thickness v Flowrate

Error in mean film voltmeter reading .001V

Error in zero voltmeter reading .001V

Hence error in voltage change is approx. 1.5%

Error in calibration factor approx. 0.5%

Hence error in experimentally determined mean film thickness should not exceed 2%.

Errors are also involved in the calculations leading to the values given in Table 2. These arise from

Error in $\sin 2\beta$ 0.1%

Error in viscosity from the temperature measurement — error approx. 1.5%

Error in D approx. 1% at worst. $(D = X)$

In comparing the experimental and undisturbed laminar flow values it is therefore necessary to allow the possibility of errors up to 4½% stemming from the measurements made. Examination of graph 4.1.1. suggests that this assessment of errors is a somewhat pessimistic one. In most cases the experimental points conform remarkably well to a line of similar gradient to that predicted for laminar flow but displaced a little vertically. After an uncertain start, and the highest flowrate readings at the 140 mm diameter indicate clearly that flow was not then properly established at that diameter, this vertical displacement corresponding to a mean film thickness smaller than that of an undisturbed laminar film, shows some signs of growth as the surface waves become fully developed. This is shown more clearly in graph 4.1.2. which shows mean film thickness δ against diameter of the cone D for four flowrates Q = 10, 20, 40 and 100 gph.

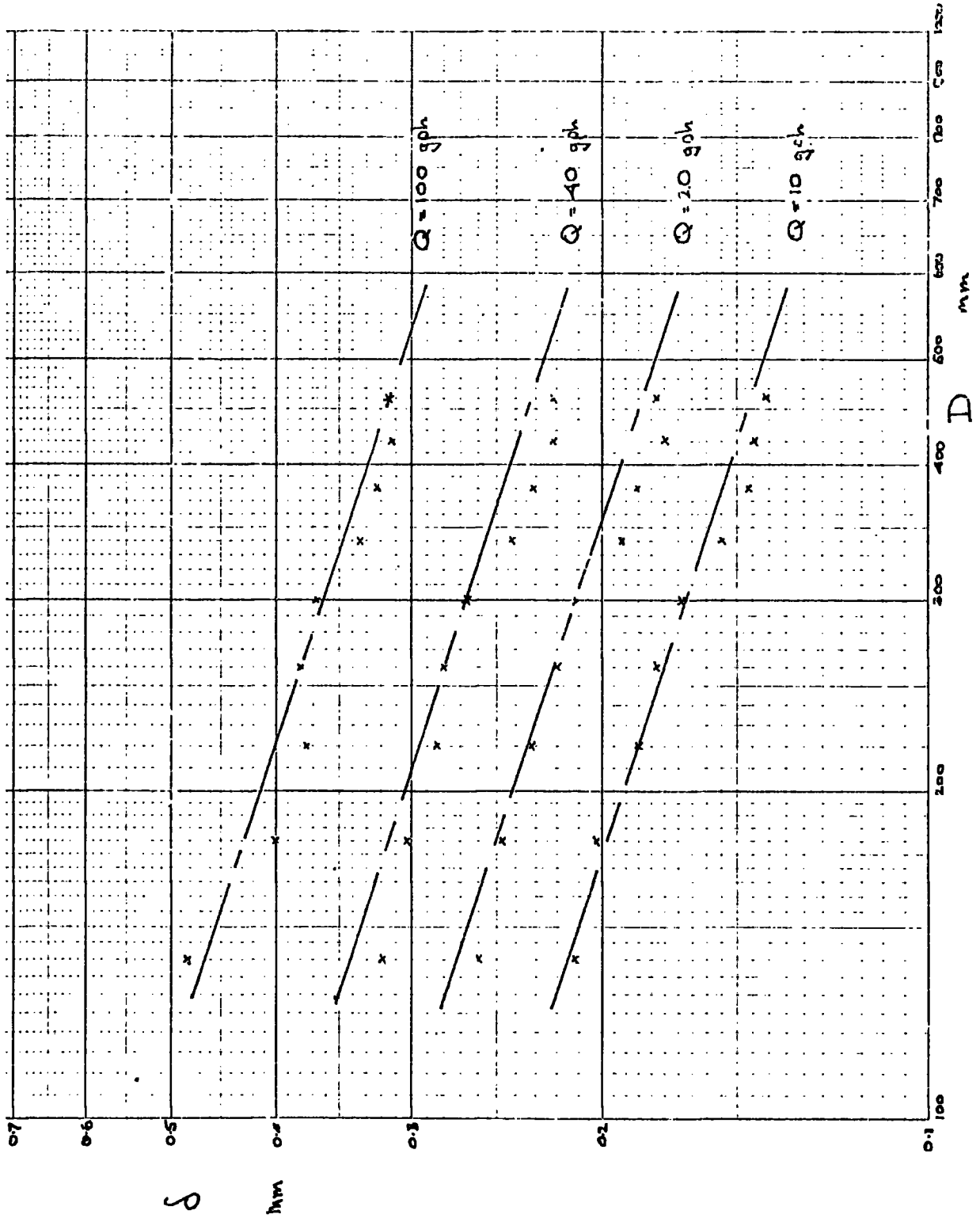

Fig. 4.12. Mean Film Thickness v Diameter

4.1.3

Graph ~~3.4.3~~. brings together all the results obtained at the different flowrates and diameters in a logarithmic plot of mean film thickness versus Reynolds number.

$$Re = \frac{Q}{2\pi D \nu \sin\beta}$$

Again for comparison the undisturbed laminar film thickness is plotted

$$\delta^3 = \frac{3\nu Q}{\pi g D \sin 2\beta} = \frac{3\nu^2 Re}{g \cos\beta}$$

This has been calculated for a value of water viscosity corresponding to a temperature of 67.8°F the mean water temperature during the experiments. On substitution of the numerical values

$$\text{laminar film thickness (in mm)} = 0.0710\ Re^{1/3}$$

Once more it is seen that the experimental points form a band below this line which fits well

$$\delta\ (mm) = 0.0685\ Re^{1/3}$$

That is to say the measured film had a mean thickness of $3\frac{1}{2}\%$ less than a laminar film.

In addition it has to be taken account that all these measurements were along a single generator of the cone. Tests reported in 3.4.2. showed that this generator carried a film thickness of 4-7% greater than the average taken at the four generators at quadrature. Hence it is seen that the mean film thickness of the wavy film is some 9% on average less than the undisturbed laminar film thickness. This is in good agreement with the difference of 7% deduced by Kapitza ([48 - 1) between laminar flow and regular sinusoidally wavy flow down a vertical surface.

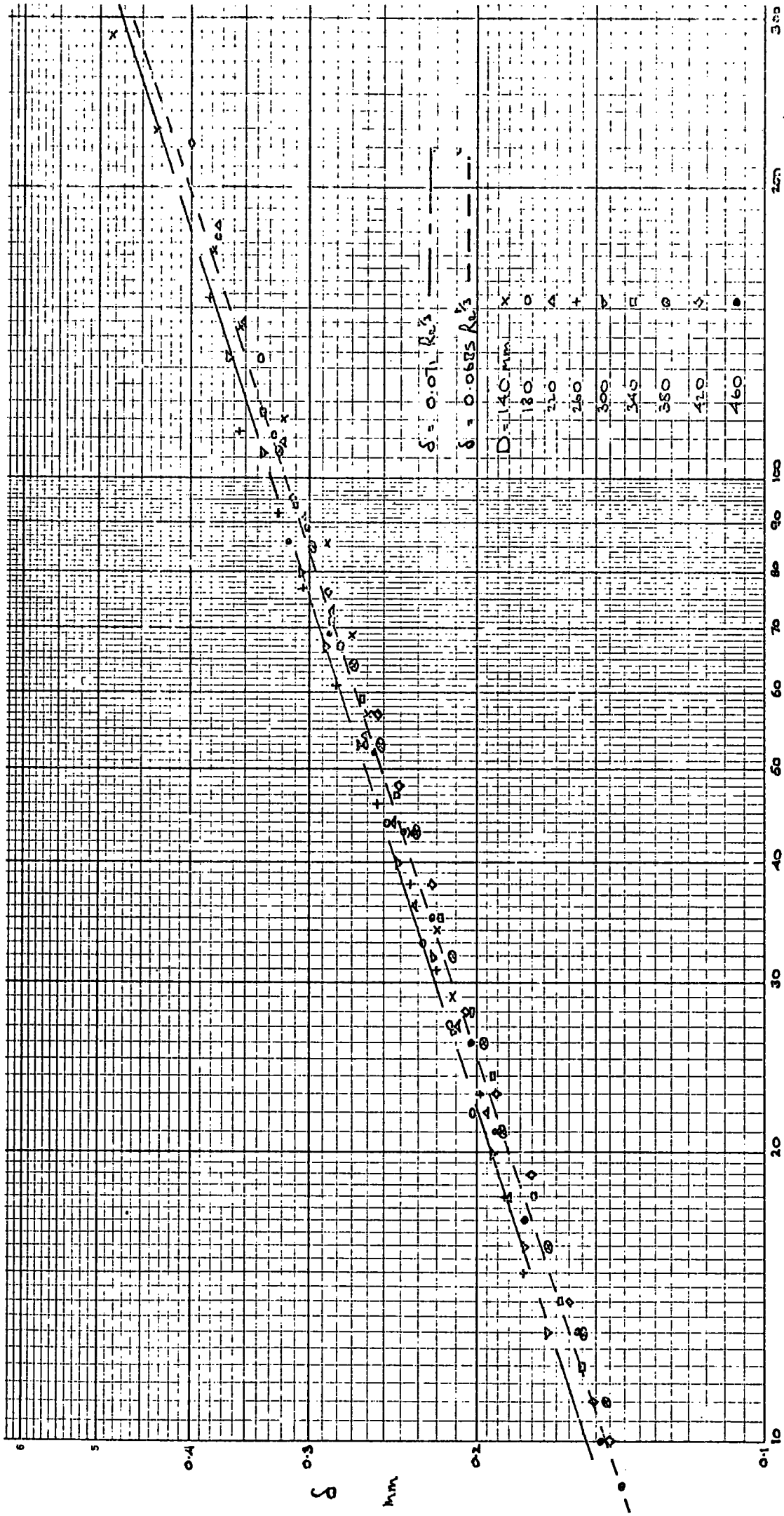

Fig. 4.1.3. Mean Film Thickness v Reynolds Number

It was found in the later experiments in which amplitude was studied, that the mean film thickness value calculated both as the zeroϕth order coefficient of the Fourier series and as a simple arithmetic mean of a large number of successive instantaneous thickness measurements, was slightly larger than that given directly by the voltmeter. In all cases the average of the 3 readings was in close agreement with that value obtained by Fourier analysis. The arithmetic mean was on average 2% higher, and the voltmeter reading 2% lower. If this additional 2% correction is made, then an exact agreement with Kapitza's 7% is found.

4.2 Wave Amplitude

4.2.1 Peak Amplitude

Section 3.6.2 described tests which yielded ultra violet trace records of instantaneous film thickness variation, which were then analysed as indicated in sections 3.7.2 and 3.7.3. The traces obtained were for the most part extremely complex. At higher Reynolds numbers they were jagged and showed little obvious regular periodicity. At intermediate values of Reynolds number 10 - 50 the variation was smoother and a harmonic variation more clearly apparent. This was still not truly regular however, the period between crests varying quite markedly. At low Reynolds numbers $\lesssim$ 10 the waveform is seen clearly to degenerate into single waves at intervals which are again somewhat irregular. Fig. 4.2.1 shows sample traces of the three kinds described.

Amongst the information yielded by the statistical analysis program, were the maximum and minimum values of film thickness for the film. Comparison of these values for the same flowrate at different cone diameters showed that while progress down the cone led to a steady reduction of minimum thickness, the maximum remained little changed. Fig. 4.2.2 shows for each trace taken the two highest peak values and the two lowest trough values. In addition to the lines drawn to indicate the trend of these values, the chain dotted line indicates the corresponding undisturbed laminar film thickness. It has to be remembered that these are the extreme values taken from generally irregular traces which themselves are samples of a not very large number of waves (approximately 15-30), hence a fair amount of scatter is to be expected in such graphs as 4.2.2 shows. Nevertheless

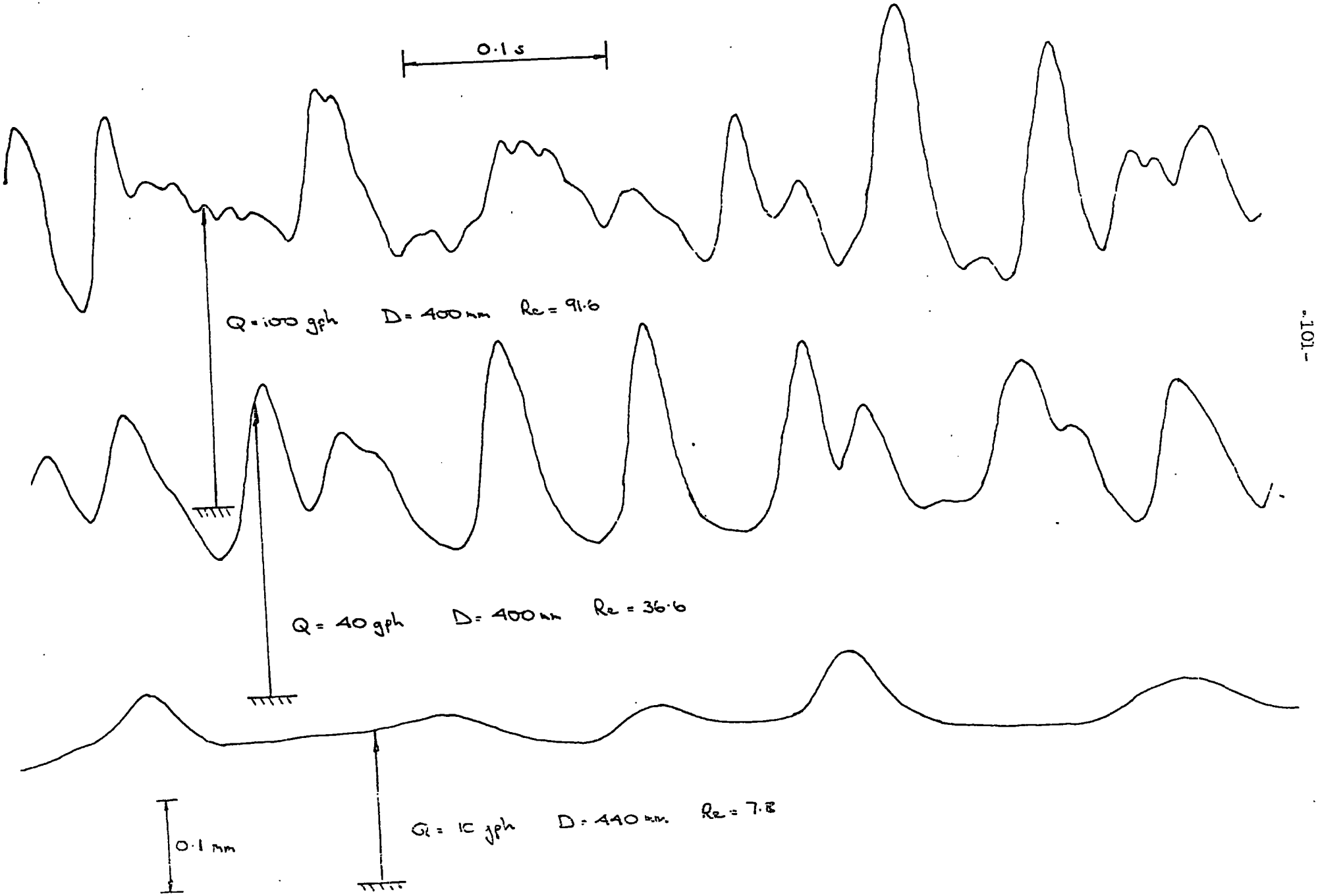

Q = 100 gph = 126 x 10^{-6} m^3/s

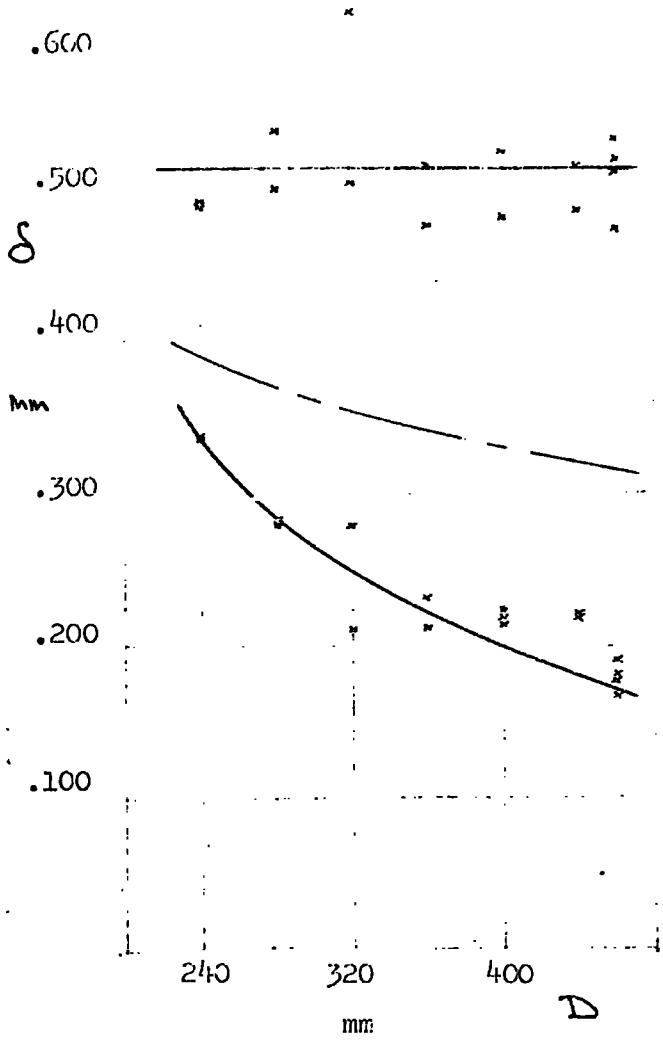

Q = 40 gph = 50.4 x 10^{-6} m^3/s

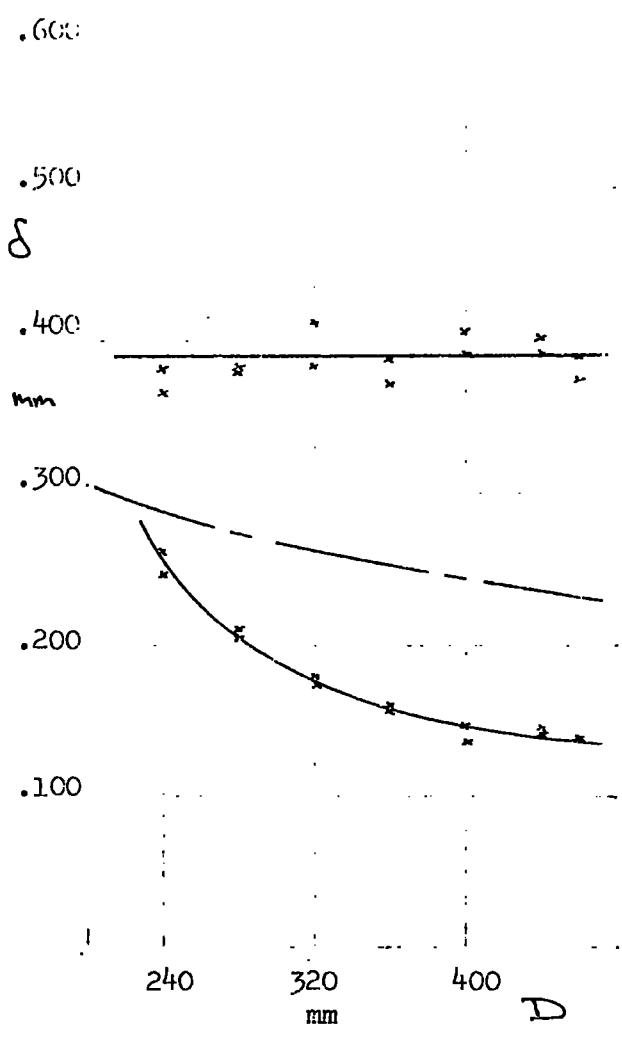

Q = 20 gph = 25.2 x 10^{-6} m^3/s

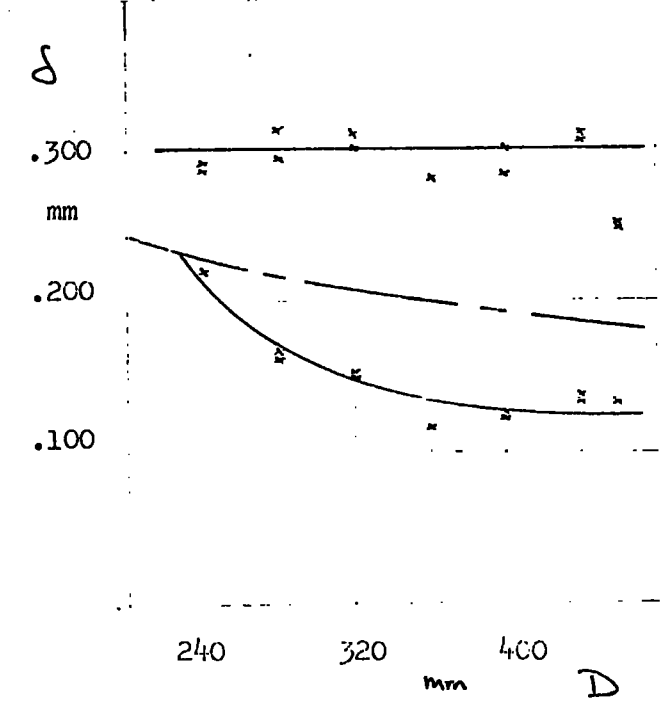

Q = 10 gph = 12.6 x 10^{-6} m^3/s

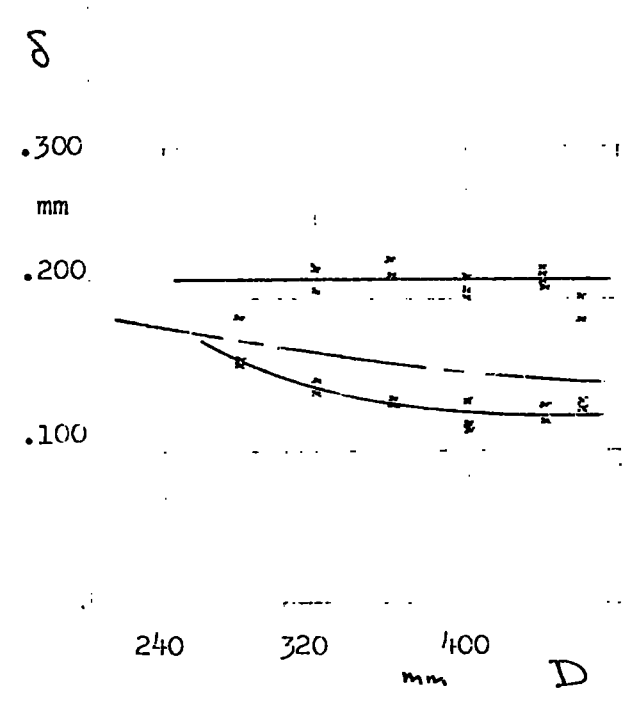

4.2.2. Peak and Trough Film Thicknesses

a few deductions can be fairly made from them.

The two lower flowrate graphs show a clear flattening of the trough thickness decline. What is more, despite the difference in flowrate, they do so at the same value of 0.125 mm, and the Q = 40 gph trough curve shows evidence of starting to flatten off at a similar thickness too. This suggests a minimum stable film thickness, and it was found in practice to be difficult to maintain films continous around the cone at the higher diameters for flowrates any lower than 10 gph. If the film were broken at any point it would remain so, and could only be re-established by increasing the flowrate to a higher value and drawing the film back over the dried area.

Accompanying this levelling out of the trough thickness curve, is a reduction of the difference between the trough thickness and the equivalent laminar film thickness. The gap between the crest curve and the laminar one however continues to widen, except for a suggestion from the last points that this trend may not continue indefinitely. From this one deduces that there must be more trough than peak in the waveform, especially when it is remembered that the mean wavy film thickness is somewhat less than the laminar film thickness which is plotted. This deduction is clearly reinforced by the traces themselves which show much flatter troughs and relatively sharp peaks. In the extreme case of low flowrate and high diameter that is so marked that the pattern appears to be more one of solitary waves on a continuous constant thickness film, than of a continuously wavy film.

There appears also to be a suggestion from the points plotted that as the trough thickness approaches that of the laminar film at the

lower diameters, so does the peak thickness decline to the central line. This is entirely in keeping with the observation that at lower diameters than those recorded here the waves are very small. No waves at all could be detected at D = 240 mm with the 10 gph flowrate. The interpretation is then that the film starts undisturbed and as the waves develop the two curves of peak and trough film thickness diverge from the undisturbed laminar film thickness curve, which is amply supported by simple visual observation. The subsequently almost constant peak film thickness leads to the interesting physical interpretation that it is perhaps more a case of troughs developing in the film than of waves doing so.

The information plotted in 4.2.2 permits also the determination of an amplitude like quantity. The two minimum film thickness values were averaged and subtracted from a similar average of the two maximum film thickness values. Halving this range value gives what the author has chosen to call a peak amplitude. This peak amplitude is plotted against diameter D in 4.2.3. for the four flowrates studied. The information derived from the points plotted in 4.2.2 has been augmented by readings from a second set of traces which were taken on a separate occasion to serve as a general check of repeatability. A good deal of scatter of experimental points is observed as is to be expected considering the variability of the waveforms observed. This scatter will also be aggravated to a small extent by the small but nevertheless finite temperature differences between the various tests for which no allowance is made in these graphs.

Despite the scatter, the graphs do yield a clear indication that the peak amplitude reaches a limiting value. The lower the

Q = 100 gph = 126 x 10^{-6} m^3/s

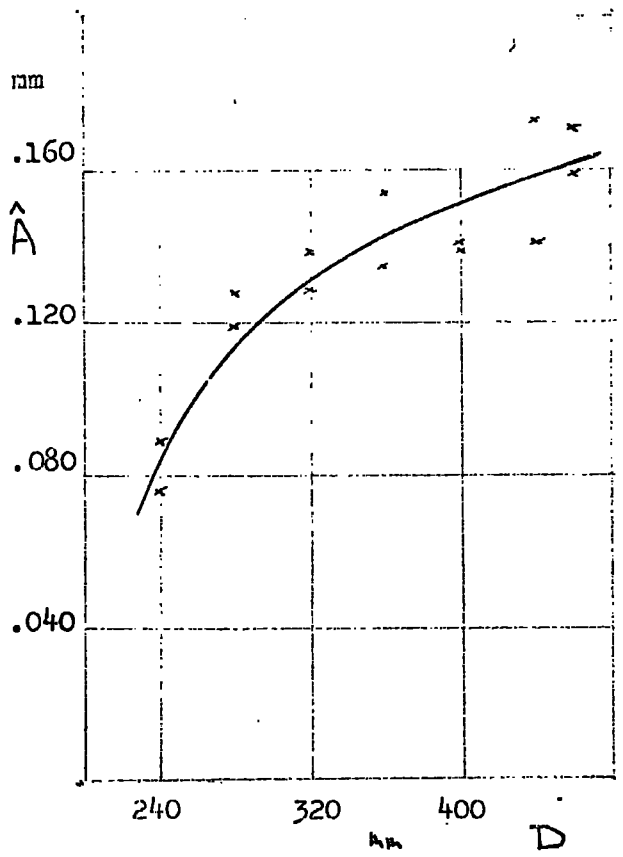

Q = 40 gph = 50.4 x 10^{-6} m^3/s

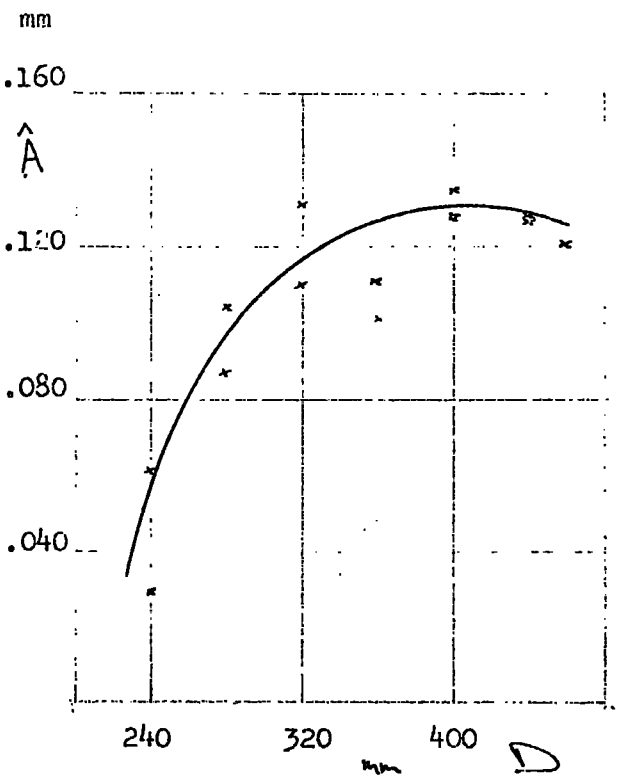

Q = 20 gph = 25.2 x 10^{-6} m^3/s

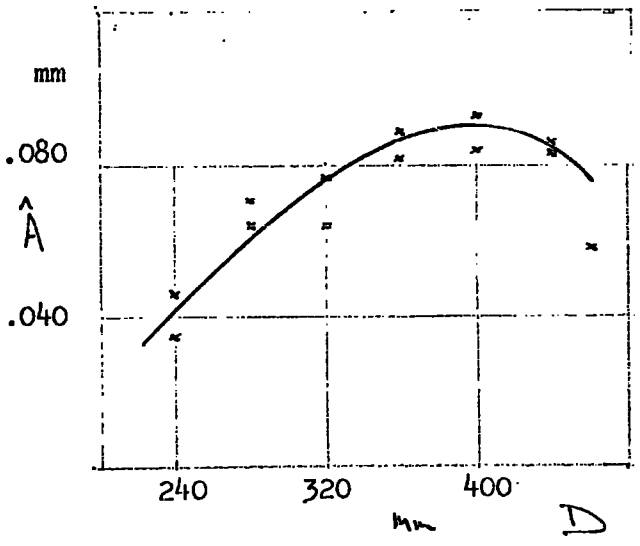

Q = 10 gph = 12.6 x 10^{-6} m^3/s

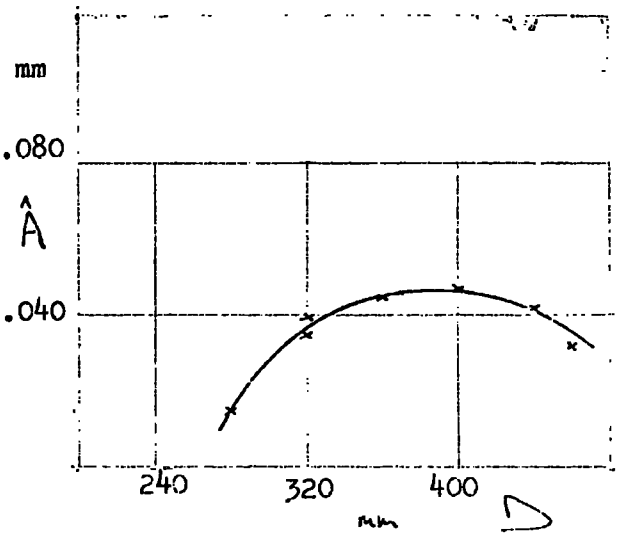

4.2.3 Peak Amplitude Variation

flowrate the sooner this limit is reached; in the highest flowrate case it has not been reached in the length of cone available for observation. They also point to a subsequent decrease of peak amplitude as the mean film continues to grow thinner with progress down the cone. The evidence for this last conclusion is limited to that provided by the readings at the two highest diameters and must therefore be treated with some caution at this stage.

4.2.2 Root Mean Square Amplitude

Another assessment of wave amplitude is provided by the Fourier analysis programme used. As reported in section 3.7.2 this was arranged to produce a root mean square amplitude.

$$A_{r.m.s.} = \left[\frac{1}{2} \sum_{r=1}^{\infty} a_r^2 + b_r^2 \right]^{\frac{1}{2}}$$

and a non-dimensional wave intensity.

$$I = A_{r.m.s.} \div a_0$$

Fig. 4.2.4. shows the variation of $A_{r.m.s.}$ with diameter for the chosen flowrates. It shows a general pattern similar to that obtained for the variation of peak amplitude, but shows more clearly the decline of amplitude after it has reached its limiting value. Fig. 4.2.5. which shows the pattern of change of wave intensity I further reinforces this conclusion in that it shows the decline is even one of amplitude expressed as a fraction of mean film thickness, that is the film is becoming less intensely wavy.

It is interesting and perhaps surprising to note that this maximum intensity is not the same independent of flowrate, for the two peaks clearly recorded differ and the peak not yet reached for Q = 40 gph must clearly be higher still.

Q = 100 gph = 126 x 10^{-6} m^3/s

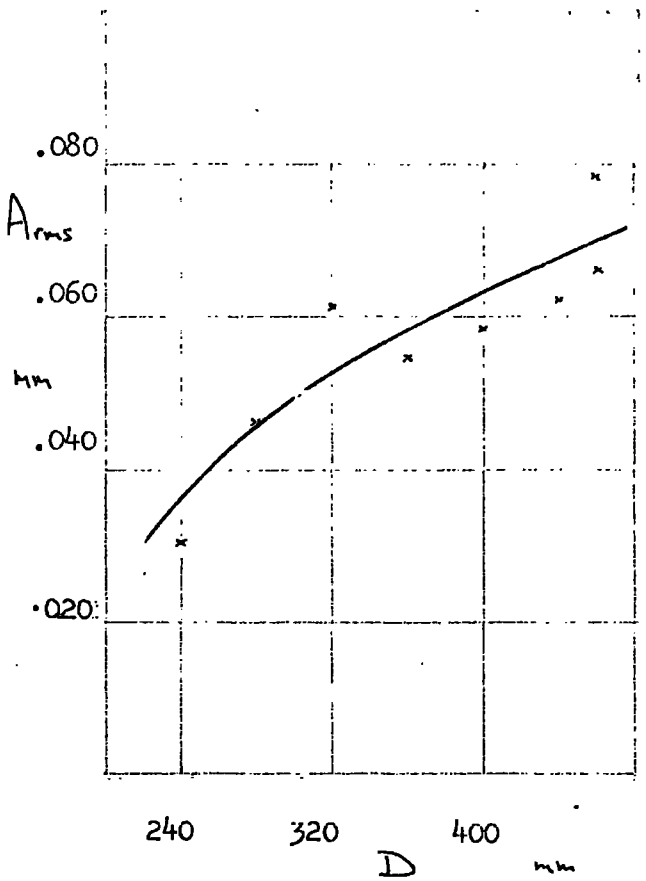

Q = 40 gph = 50.4 x 10^{-6} m^3/s

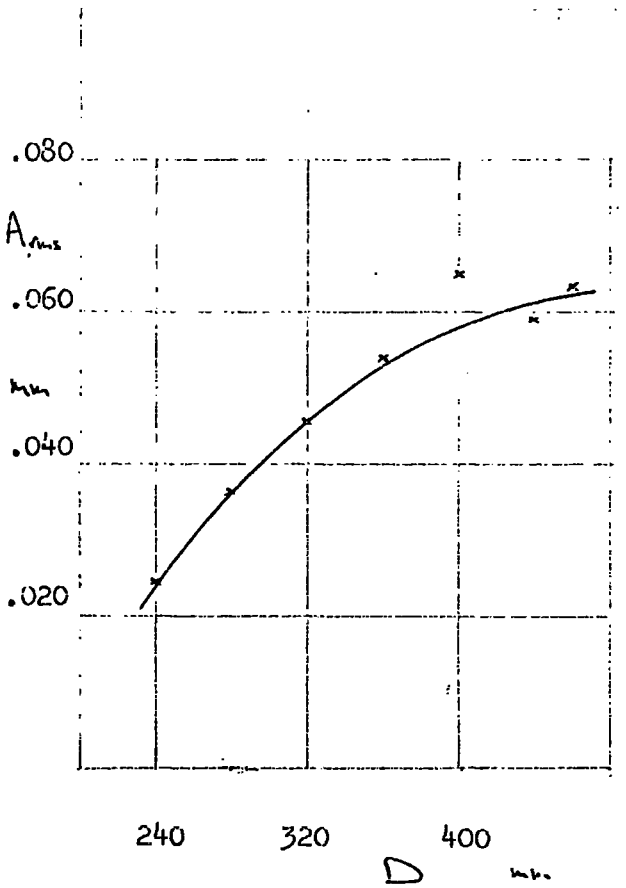

Q = 20 gph = 25.2 x 10^{-10} m^3/s

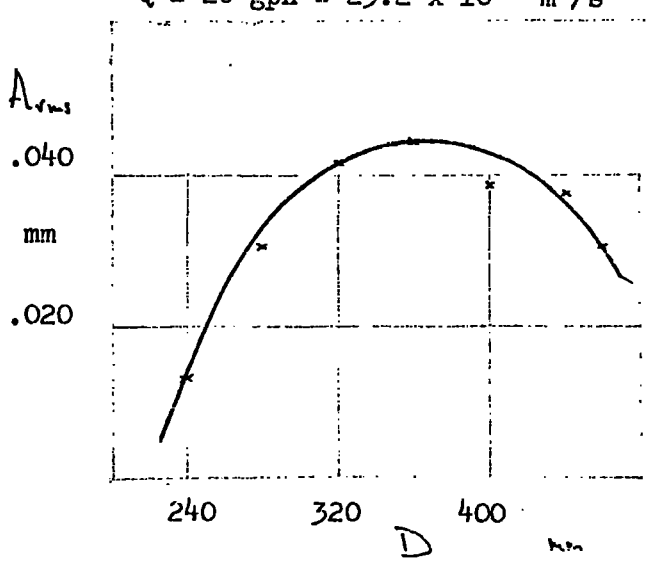

Q = 10 gph = 12.6 x 10^{-6} m^3/s

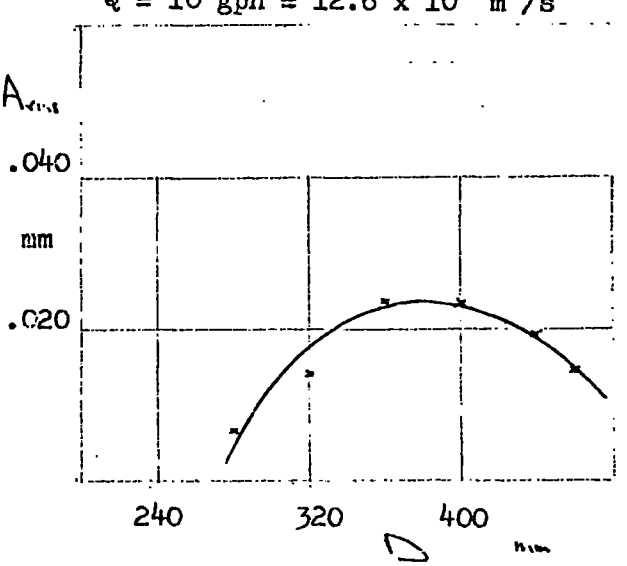

4.2.4 RMS Amplitude Variation

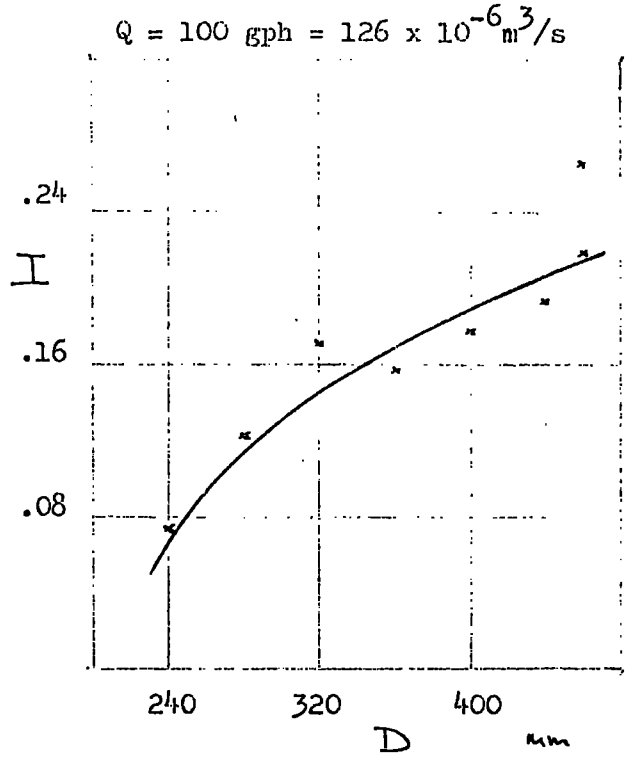

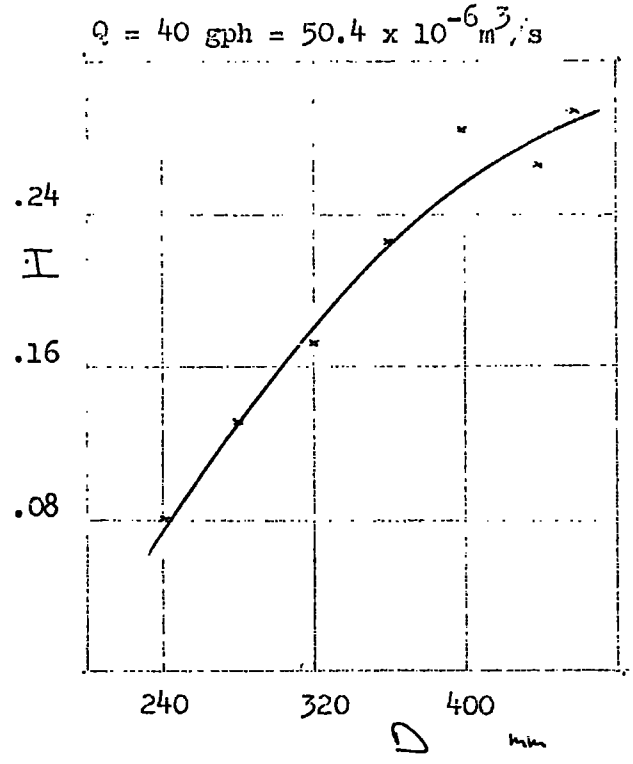

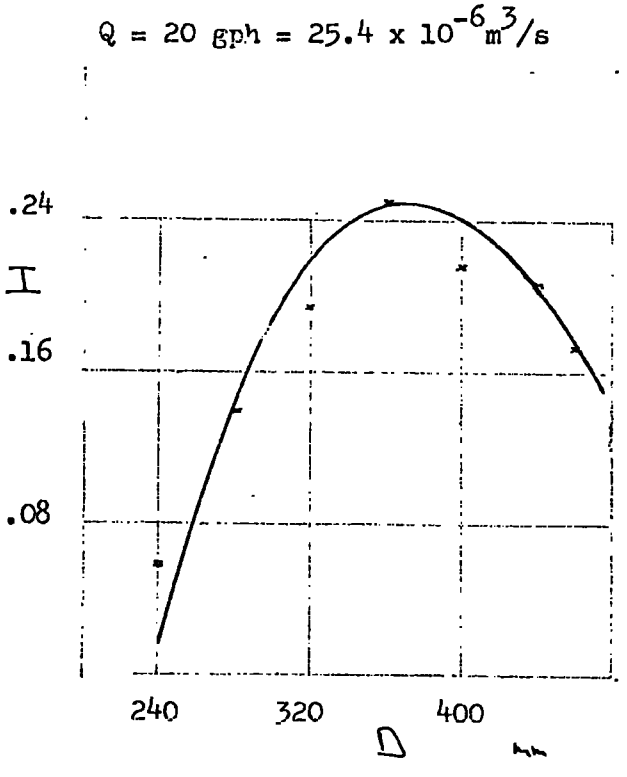

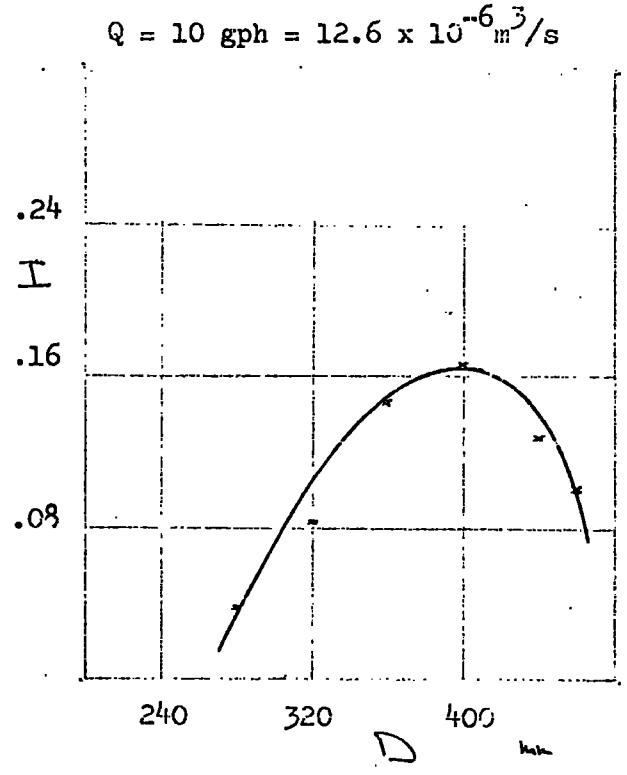

4.2.5 Wave Intensity Variation

4.2.3 Comparison with Inclined Plane Flow Predictions

A number of theoretical predictions for limiting wave amplitudes exist in the literature of film flow over inclined plane surfaces. The first is that of Kapitza ('48) who predicted a value of 0.46 for the non-dimensional amplitude which he defined as $\frac{1}{2}$ (peak to peak variation)÷ mean film thickness, which is equivalent to $\hat{A} \div \delta$ in the notation of this work. Bushmanov ('61) gave a revised value of 0.58 for the value of this ratio. Fig. 4.2.6 shows $\hat{A}/\delta$ plotted against Reynolds number for the results obtained on the cone. The curves for the four different flowrates show clearly the rise to a limiting value as Re decreases down the cone, and the subsequent amplitude decline. The limiting value of $\hat{A}/\delta$ is seen however to be dependent on the value of the flowrate, or of the Reynolds number at which it is reached. Clearly a single value such as that proposed by either Kapitza or Bushmanov does not sufficiently well cover what is happening here.

Both Berbente and Ruckenstein ('68) and Krantz and Goren ('70) sought to improve this limiting value estimate, and incorporated in both works is the effect of surface tension. Berbente and Ruckenstein suggested that it depended on the value of a complex non-dimensional group ψ_{BR}. This group may be reduced to

$$\psi_{BR} = Re^{7/6} S^{-1/2} F^{-1/3}$$

in the author's notation, that is it is a function of the Reynolds, Weber and Froude numbers. Although Berbente and Ruckenstein were considering a vertical plane, the effect of slope is to modify the component of gravity acting in the main direction of motion. This is reflected in the relationship between the Reynolds and Froude numbers 2.3.2.

$$3F^2 = Re \cos\beta$$

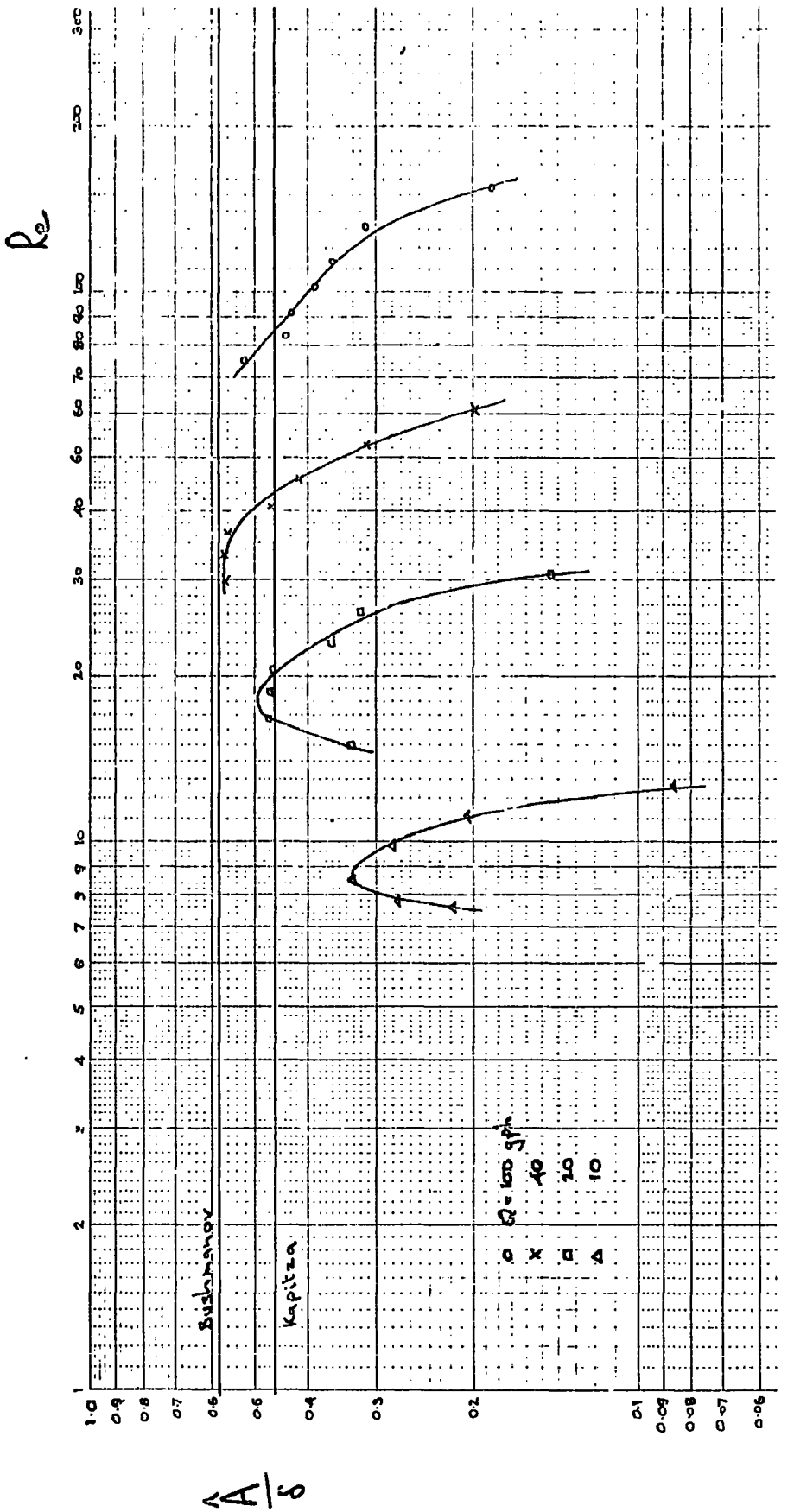

Fig. 4.2.6 Amplitude v. Reynolds Number

Substituting for this gives

$$\psi_{BR} = \left(\frac{3}{\cos\beta}\right)^{1/n} Re\, S^{-1/2}$$

Krantz and Goren also suggested a controlling non-dimensional group

$$\psi_{KG} = \frac{\left(\frac{6}{5} Re - \tan\beta\right)^3}{S\,Re}$$

This makes a more direct allowance for the effect of slope which they included in their considerations. However, the effect of β is very small unless either β is very large or Re is very small. If neither is the case then it reduces to a group closely similar to that of Berbente and Ruckenstein.

$$\psi_{KG} = 1.142\, \psi_{BR}^2 \qquad \text{for } \beta = 30°$$

Fig. 4.2.7 shows $\hat{A}/\delta$ plotted against ψ_{BR} for the four flowrates studied, as might be expected the general pattern is similar to that of 4.2.6. Also shown is the relationship between the quantities derived by Berbente and Ruckenstein, and it is seen that there is quite good agreement.

The relationship arrived at by Berbente and Ruckenstein based on the results of Kapitza and Kapitza ('49) fits much better than that derived by Anshus ('65) as reported in Krantz and Goren ('70). The latter predicts a limiting non-dimensional amplitude of approximately 1.0 for the whole of the range of ψ_{BR} shown in 4.2.7. Results of experiments by Krantz and Goren with oils of low surface tension gave quite good agreement with the Anshus theory. The results of Kapitza, and now these of the author, with water do not.
Krantz and Goren sought to explain the lack of agreement with Kapitza's results in terms of fluid impurities which might have affected the surface tension. The Kapitzas used distilled water,

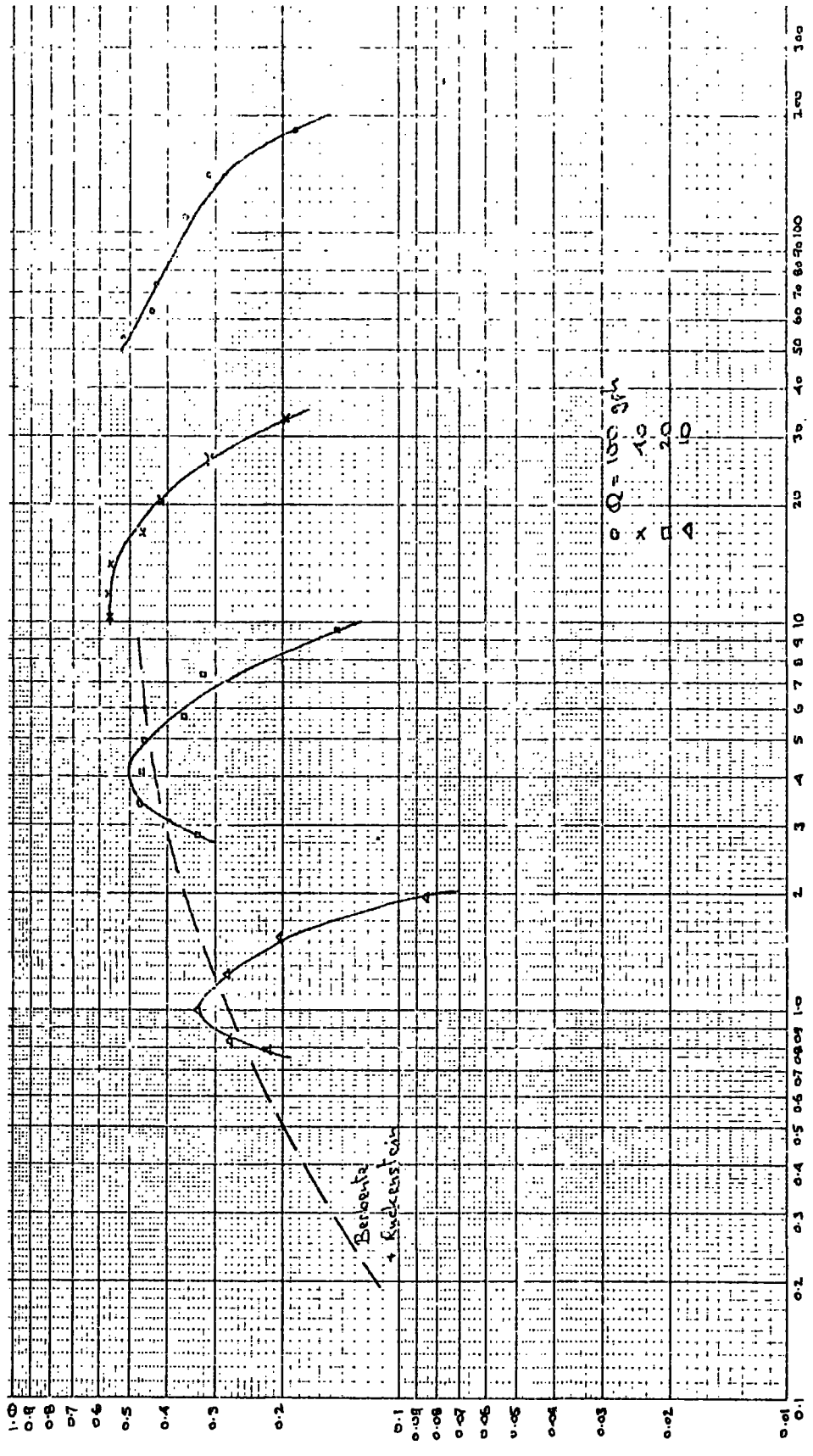

Fig. 4.2.7 Amplitude v. ψ_{BR}

and yet the present results obtained with ordinary tap water are closely similar. This would seem to suggest that some other explanation is required to satisfy this discrepancy.

While the results obtained on the cone fit the Berbente and Ruckenstein planar prediction well so far as the peak value of $\hat{A}/\delta$ is concerned, the behaviour at points further down the cone is less readily explained. It might be expected that once the waves had reached their limiting amplitude, this amplitude would then continue to be controlled by the Reynolds number of the flow. This would appear on the graph as a rise to the limiting curve and then a flattening out and steady fall along the limiting curve. Some lag effect might even be expected by which the amplitude would tend to remain higher than that predicted on a Reynolds number basis. What happens however is that the amplitude appears to decline more rapidly than is expected, suggesting that the steady decline in Reynolds number is having an even more powerful damping effect. This must not however be treated with undue emphasis since the number of points which suggest it are very small and they are the ones for which the film was thinnest and experimental error consequently highest.

4.3 Wave Speed and Wavelength

4.3.1 Wave Speed.

Benjamin ('57) quoting the work of Lighthill and Witham ('55) shows the velocity of a long kinematic wave to be 3 times the mean velocity in the film, or twice the velocity at the free surface. Although the waves observed did have wavelengths of up to 100 times the mean film thickness the long wave assumption is not entirely satisfied and some departure from the factor 3 might be expected especially for not fully developed waves. Figs. 4.3.1. (a) - (d) show the wave speeds measured plotted against the base of cone diameter, which is in turn equal to distance along the cone surface from the apex since it is a 60^{o} cone.

Considerable scatter of wavespeeds is apparent, but a number of points clearly emerge. Firstly, it is seen that during the period of wave development and growth the mean wave speed remains essentially constant. This continues until the speed of the faster waves reaches Benjamin's long wave velocity. Thereafter it appears that the faster waves decelerate to maintain a speed of 3 times the mean film velocity or slightly less, while the slower waves continue their progress until they are of similar speed. It was readily apparent when making the measurements of wave speed that those waves most clearly visible, i.e. the largest, were also the ones with the highest velocities at a given diameter, so that development of amplitude and wave velocity go hand in hand. The scatter of the velocities plotted also implies the possible existence of waves travelling at different velocities at the same point on the cone. This was indeed observed: fast waves do overtake and engulf smaller slower ones. This was one of the factors

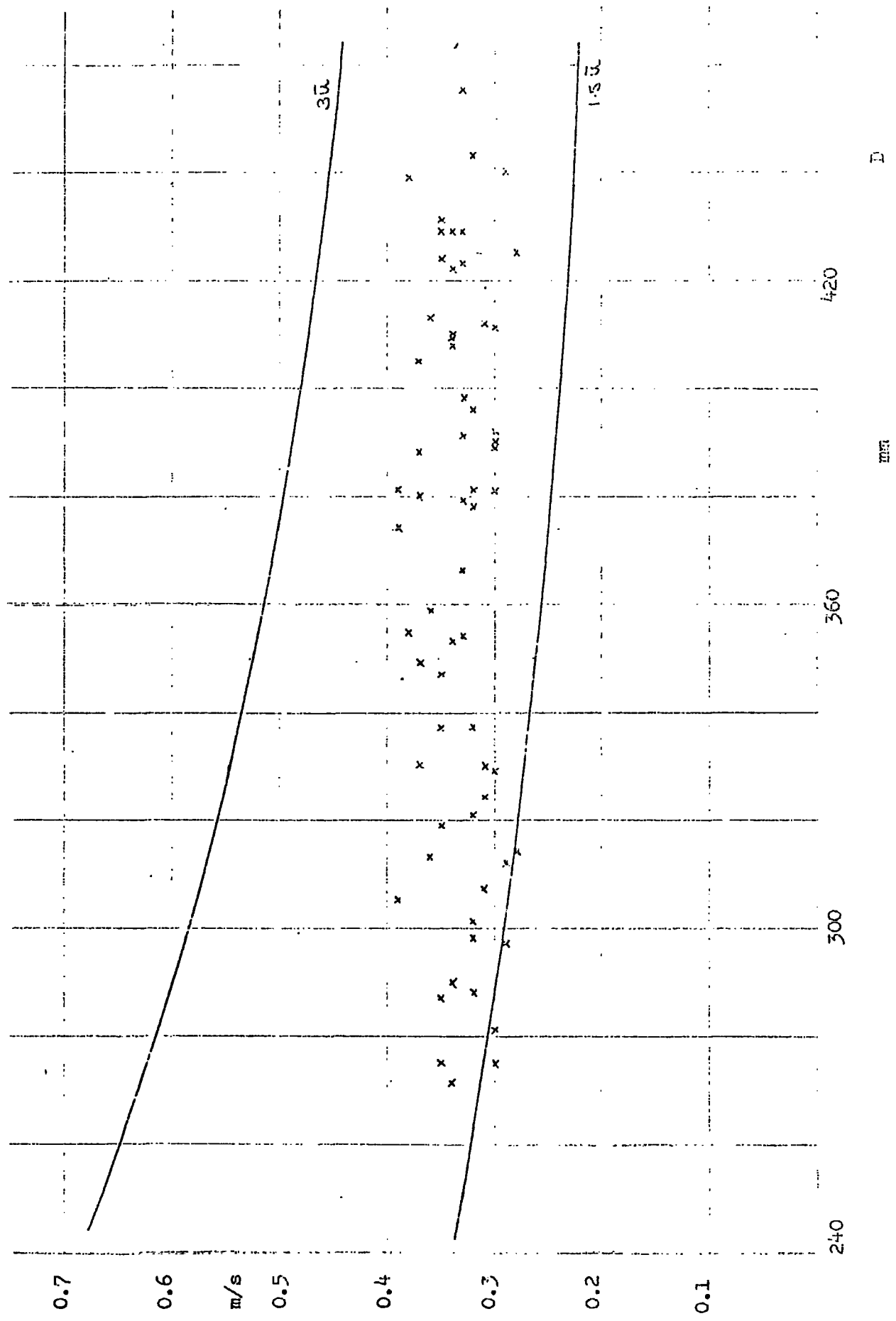

(a) Q = 40 gph

Fig. 4.3.1. Wave Speed Variation

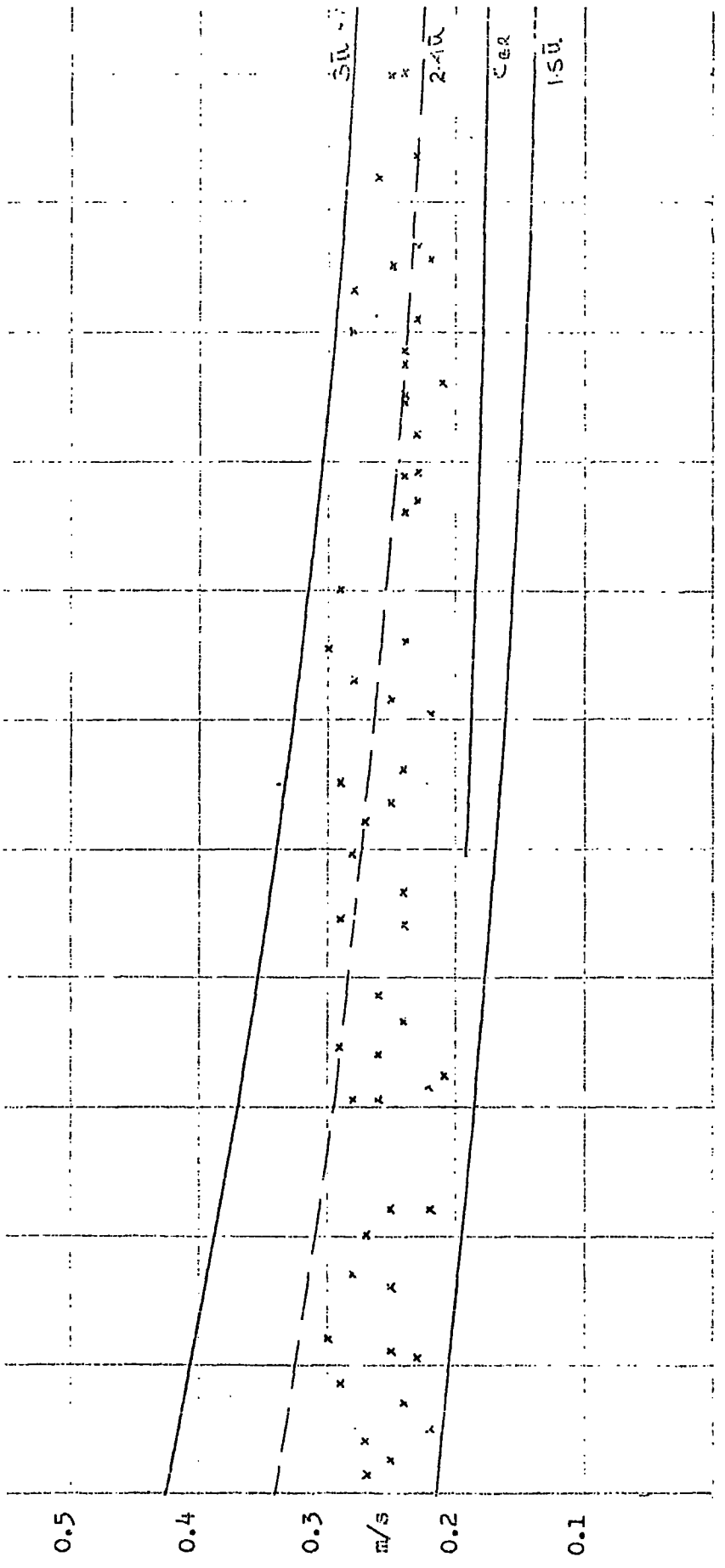

(b) Q = 20 gph

Fig. 4.3.1. Wave Speed Variation

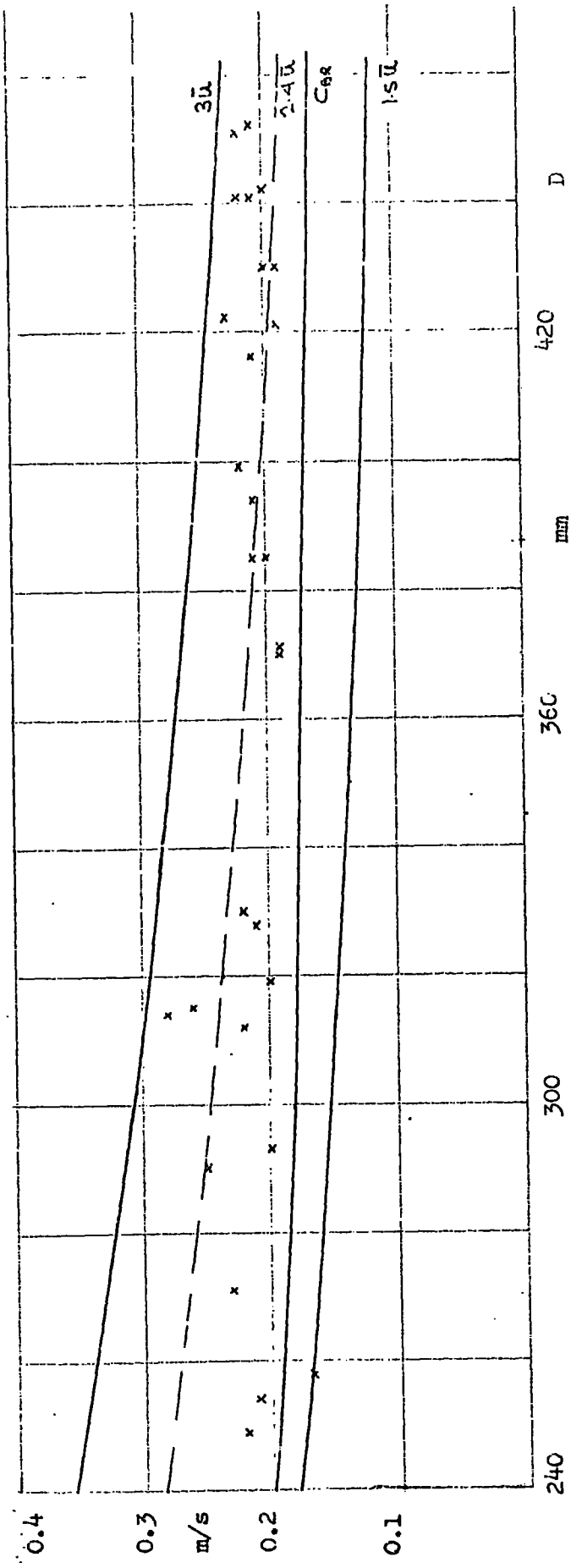

(c) Q = 15 gph

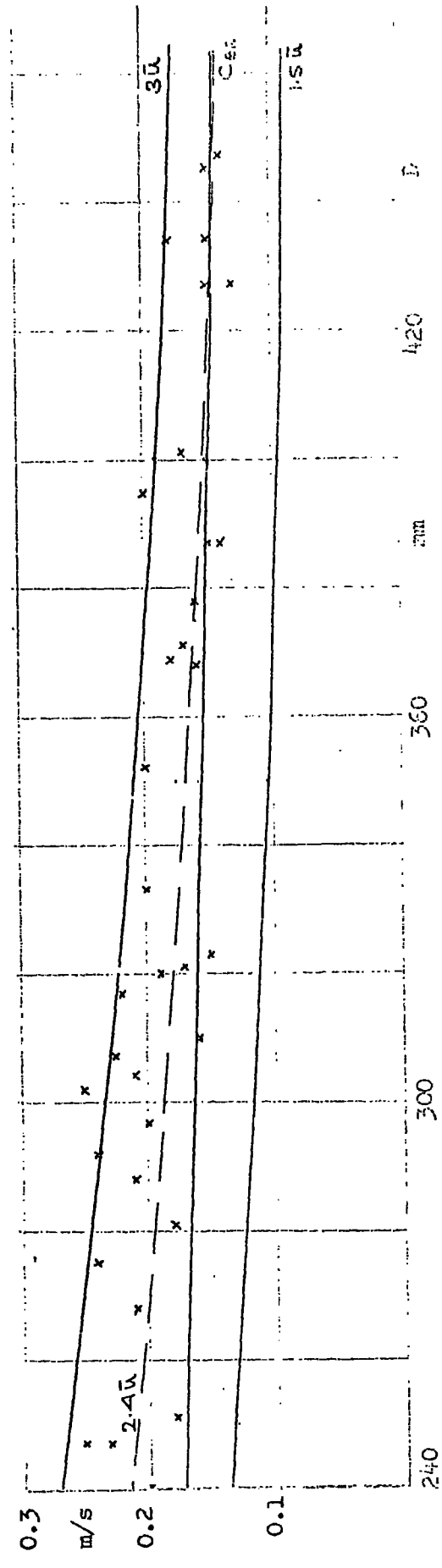

(d) Q = 10 gph

Fig. 4.3.1. Wave Speed Variation

making interpretation of the cine photographs difficult, especially where measurements of wavelength were concerned.

Plotted on graphs 4.3.1. (b) - (d) in addition to lines corresponding to the long wave speed and the undisturbed film surface speed, is a value of the wave speed C_{BR} predicted by Berbente and Ruckenstein ('68). They arrived at their prediction by a combination of theoretical analysis and the use of the amplitude results of Kapitza and Kapitza ('49). This produced a value for the ratio between wave speed and mean film velocity which varied with their non-dimensional group ψ_{BR} . This relationship they showed to be in good agreement with the experimental results of the Kapitzas, and also those of Jones and Whitaker ('66). It is seen that while their prediction of amplitude examined in section 4.2.3 was good, that of wave speed is far less so when applied to flow on the cone. It is only at the lower values of ψ_{BR} corresponding to the thinnest films examined that C_{BR} approaches the measured values. A much better prediction in the context of the cone is that of the simple relationship proposed by Kapitza ('48)

$$\text{wave speed} = 2.4 \times \text{mean film speed}$$

which is shown as a dashed line in Fig. 4.3.1. (b) - (d). Even this however tends to underestimate the speed of the fully developed waves which approach quite closely to the full long wave speed of $3\bar{u}$.

In section 4.2.3. it was remarked that once the wave reaches limiting amplitude the amplitude then decreases rather more rapidly than is suggested by the Berbente and Ruckenstein theory. The wave speed on the other hand retains a higher value than predicted. Thus the thinning of the film as it progresses down the cone is more effective in controlling wave amplitude than it is in limiting wave speed. The

wave as it were retains translational kinetic energy in preference to energy associated with amplitude.

4.3.2 Spectral Density

The results of the Fourier analysis program were of a form which allows the plotting of spectral densities. Fig. 4.3.2 shows two such specimen plots in which $C_r = \sqrt{a_r^2 + b_r^2}$ is plotted against a base of r. The program was arranged so that the number of input values, their time interval, and the order of the Fourier analysis, gave a unit interval of r which corresponded to 1 Hz. Thus the r axis is also identical to a frequency axis graduated in Hz. The two spectra shown correspond to the upper and lower traces of which samples are given in Fig. 4.2.1. The upper spectrum is that of a film at a relatively high Reynolds number with an irregular waveform that has not yet reached its limiting amplitude. The lower spectrum on the other hand is that of a low Reynolds number film where the amplitude has reached its limit and started to decline. Despite these differing circumstances, the two spectra have common features typical of all the analyses carried out.

Neither spectrum shows a clear single dominant peak frequency. Rather do they both possess peak regions formed by two or three pinnacles arising from low immediate surroundings. If the two spectra had been drawn against a 2 Hz base by averaging adjacent values then a much smoother pattern would have been obtained. This would not have shown a marked peak either, more a rounded hump, as was found with the electronic wave analyser. The peak value is seen to be small compared with that of $C_0 = a_0$, the mean film thickness. The peak value behaved in a

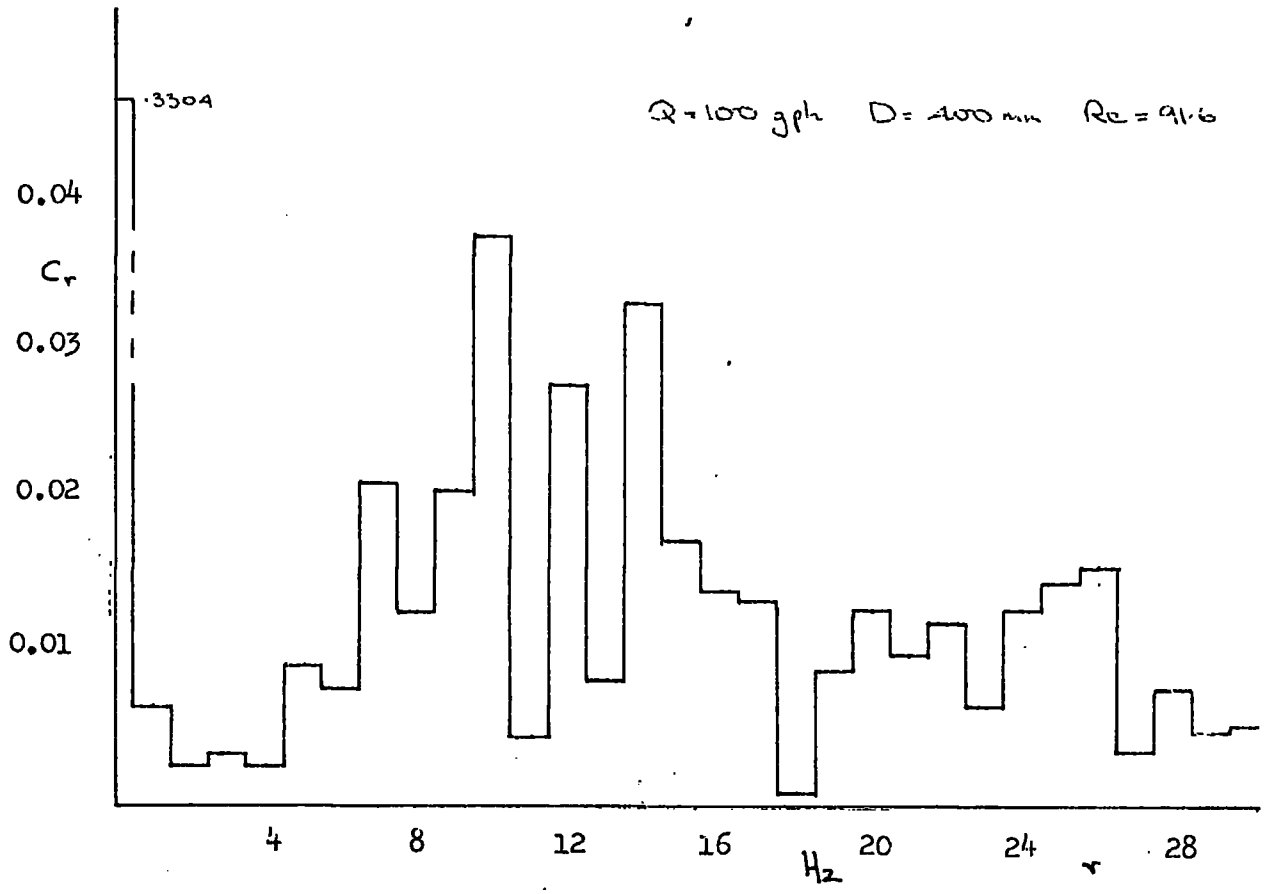

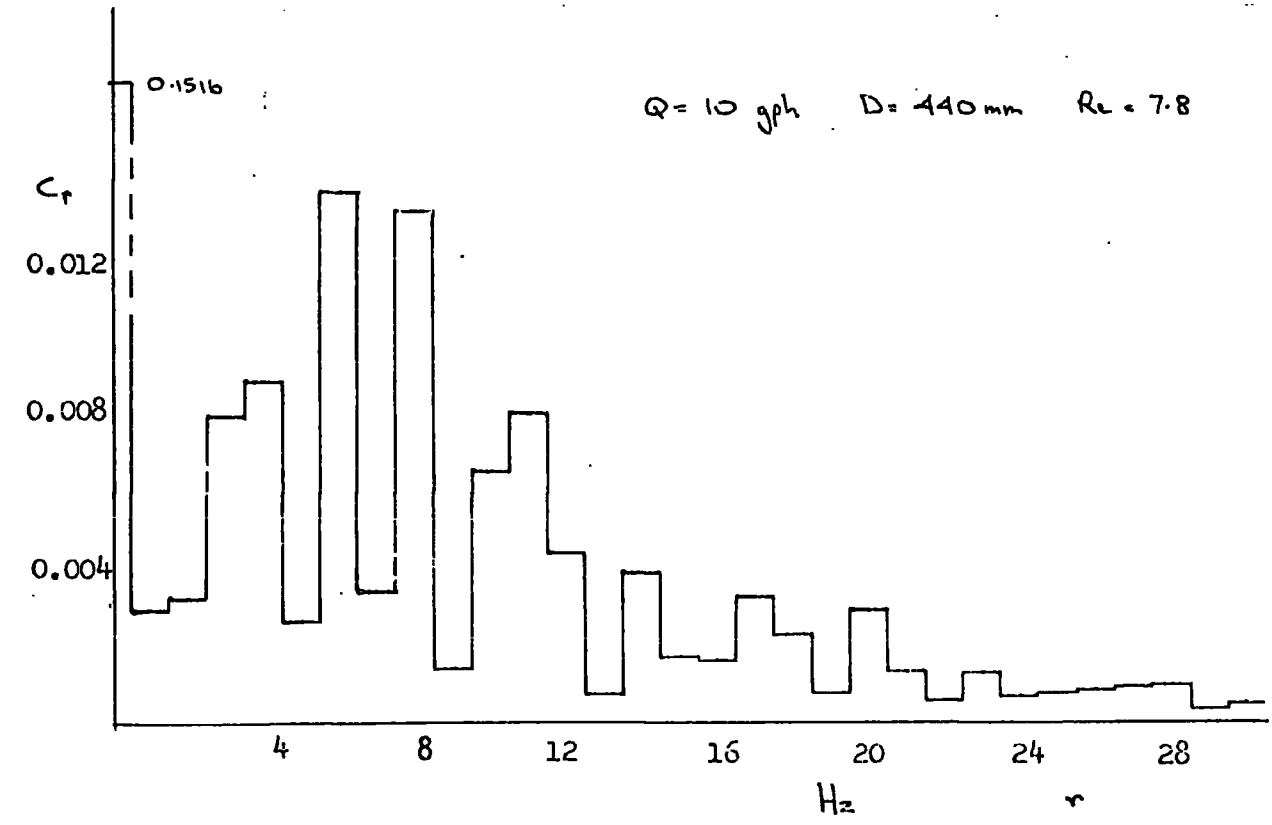

Fig. 4.3.2 Spectral Densities.

manner similar to that of the amplitude already discussed, rising to a maximum of about 18% of a_o and then starting to decline once the limiting amplitude had been reached. Beyond 30 Hz, the value of c_v remained at a fairly uniform low level.

From all the Fourier analyses it was possible to pick out an approximate frequency at which the peak power was concentrated for each film condition. These are plotted in figure 4.3.3. While the points plotted do exhibit a considerable scatter the general trend of frequency to decrease both with increasing diameter and with decreasing flowrate is clearly discernible. The Q = 100 gph curve appears to be exceptional, but these points were from analyses of highly irregular waves, where the spectra tended more to a uniform 'white noise' level and picking the peak became more than usually liable to subjective error. These frequency values may also be used in conjunction with the wave speeds reported to give an estimate of wavelength additional to that obtained by the photographic method.

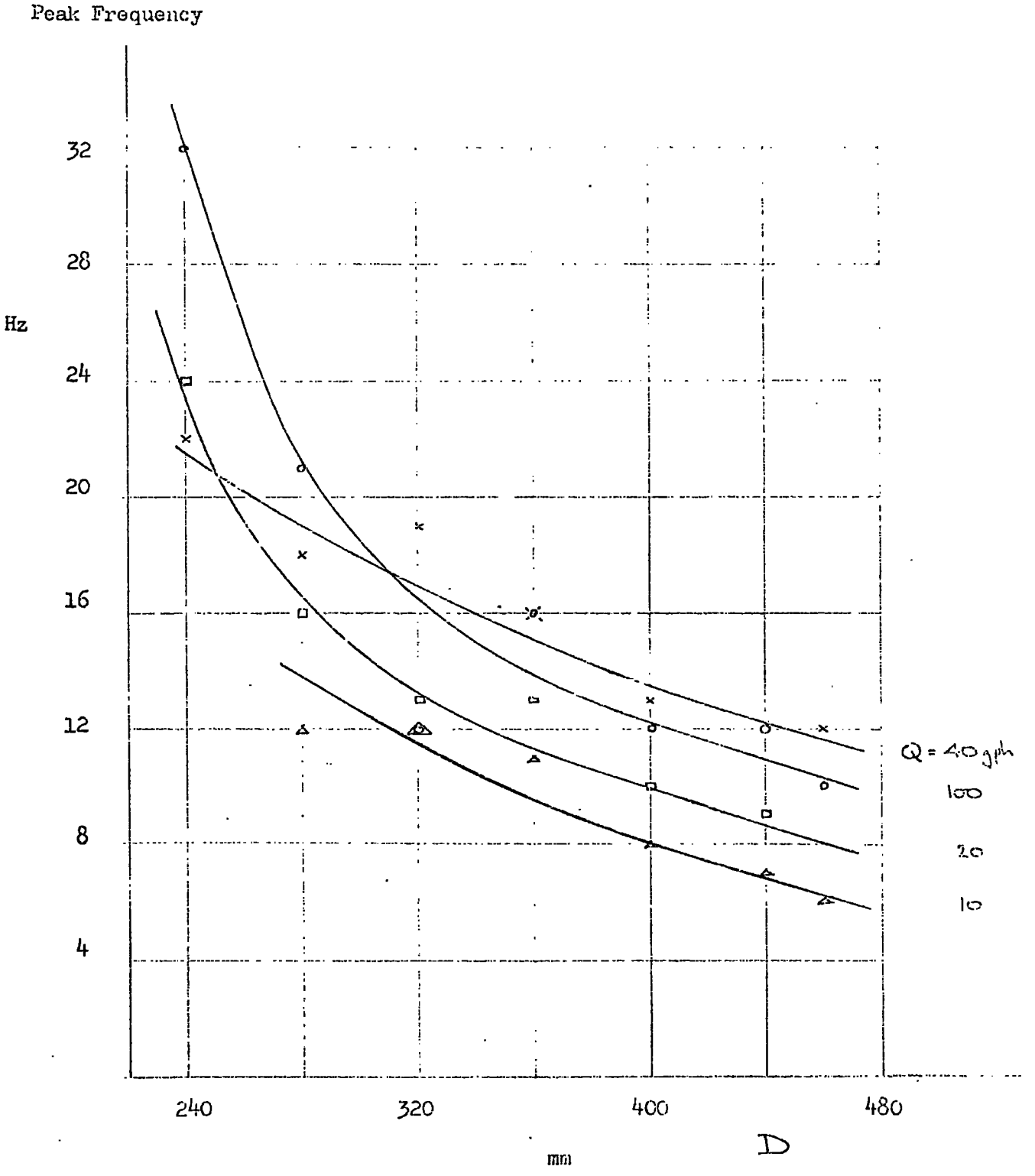

Fig. 4.3.3 Peak Frequency ơ. Diameter

4.3.3 Wavelength

Of all the quantities measured, wavelength was found to be most difficult for reasons already mentioned in 3.6.3. Although distances between wavecrests could be measured quite accurately (± 1 mm on wavelengths of 10 - 30 mm) and a mean was obtained of several such measurements (never less than 10), the difficulty lay more in the non-uniformity of the patterns recorded. Wavefronts were generally curved and crossed in places rather than being parallel and regularly spaced. Measurements must therefore have been unusually liable to subjective error in the choice of what looked like good pairs of parallel wavefront sections. The measurements obtained from the photographic analysis are shown plotted in Fig. 4.3.4. These show a general pattern of wavelength increasing with diameter, and doing so more rapidly at lower flowrates. Plotting these values logarithmically reveals no clear power law relationship; the gradients revealed in decreasing flowrate order are 1.09, 1.26, 1.88, 1.66.

Also shown on three of the graphs of Fig. 4.3.4. are dashed curves which were obtained by combining estimated mean wave speeds from Fig. 4.3.1. with frequency values from the smoothed curves of Fig. 4.3.3. using the relationship

$$\text{wavelength} = \text{wave velocity} \div \text{frequency}$$

No such estimate was available unfortunately in the Q = 15 gph case. While these dashed curves generally corroborate the pattern of behaviour, they indicate that the accuracy of the wavelength measurements might be less good than the accuracy of fit to the drawn curves suggests. It should be pointed out that the readings on which the frequency assessments are based were obtained at slightly different water temperatures

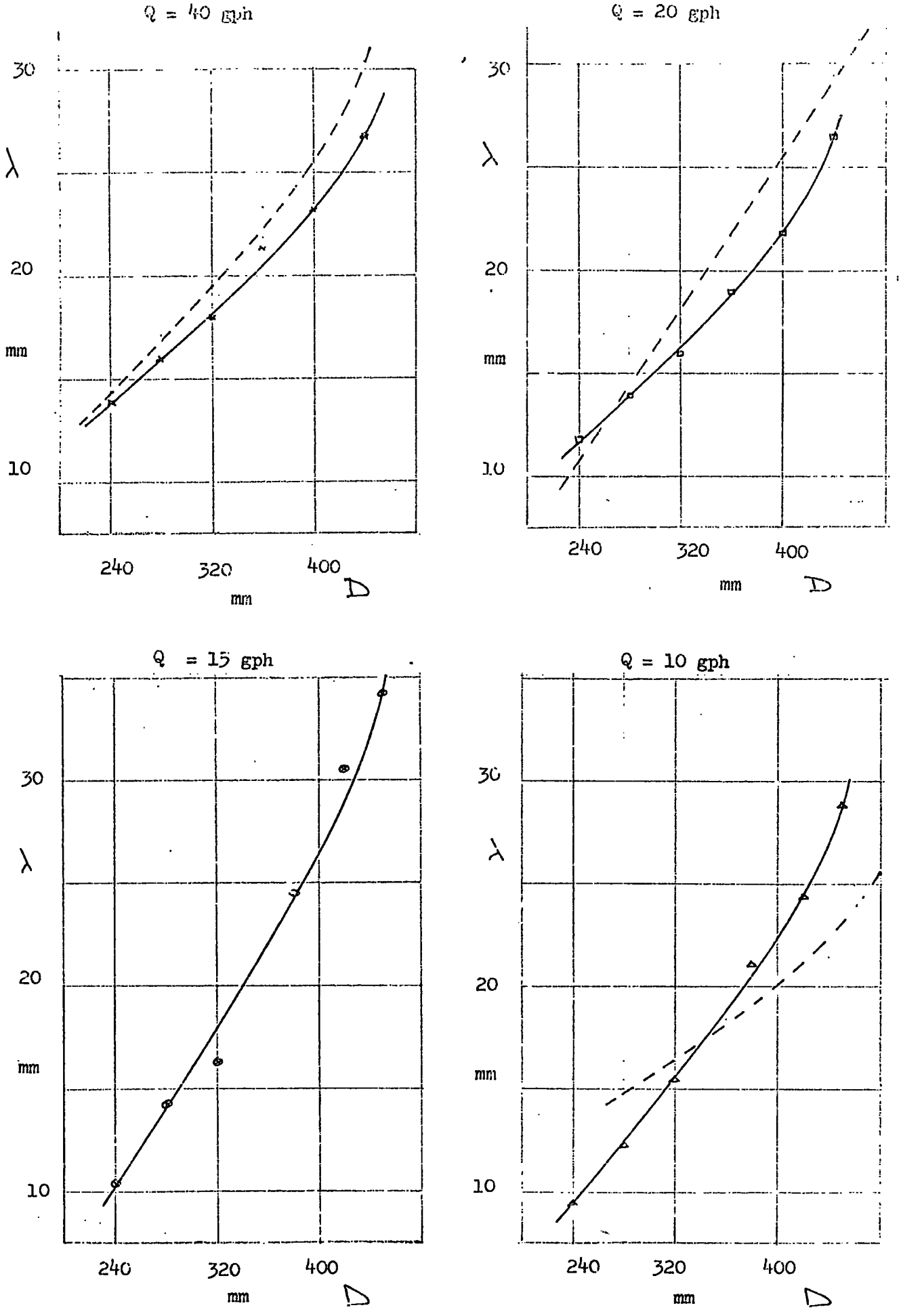

Fig. 4.3.4. Wavelength Variation

to those at which wavelength and wavespeed were measured. Nevertheless the temperature difference was equivalent to a viscosity change of at most 7% and for the most part less than 1%, which is small when the scatter of the frequency points is considered. Averaging the two differently obtained values of wavelength and plotting once more on logarithmic scales yields gradients for $Q = 40, 20, 10$ of 1.15, 1.54 and 1.33. The average of these values is 1.33 and one is tempted to conclude that a $^{4}/_{3}$ power law holds. The evidence however is slim and it is probably more appropriate to remark that where the waves are still growing to their limiting amplitude the rate of increase of wavelength is little more than linear, while after a limiting amplitude has been reached the wavelength grows more rapidly.

4.4 Wave Number

The wave number α is defined as 2π x mean film thickness ÷ wavelength; it gives a non-dimensional measure of wavelength, for long waves it is small as assumed in the solution of the modified Orr - Sommerfeld equation. Wave numbers have been calculated based on the mean wavelength derived in 4.3.3 and a value of δ calculated from

$$\delta = 0.0685\, Re^{1/3}$$

These wave numbers are shown plotted against a base of diameter D in Figure 4.4.1. This shows that at the point where waves are first clearly to be seen as waves they have the same wave number regardless of flowrate. Surface disturbances were visible at somewhat lower diameter values, ranging from 180 mm to 220 mm depending on flowrate, but 240 mm was the smallest diameter at which measurements could be sensibly made. Thereafter the wave number decreases with diameter at a rate which is dependent on flowrate. It would appear that the Q = 10 and Q = 15 gph have become interchanged. It must be remembered however that the Q = 15 gph points are based on a single assessment of wavelength and are consequently less reliable than the others.

Graph 4.2.3. shows that $\hat{A}$ reaches its limiting values at D = 410, 400, 390 mm approximately for Q = 40, 20, 10 gph respectively. At these diameters the wave numbers are 0.056, 0.048, 0.044 respectively. These are insufficiently similar to suggest that the limiting amplitude is reached at a critical value of wave number, despite the fact that waves start at such a closely similar value. However the difference is not great and the assessment of the diameter at which the limiting amplitude is reached is based on a curve smoothed by eye, so the idea

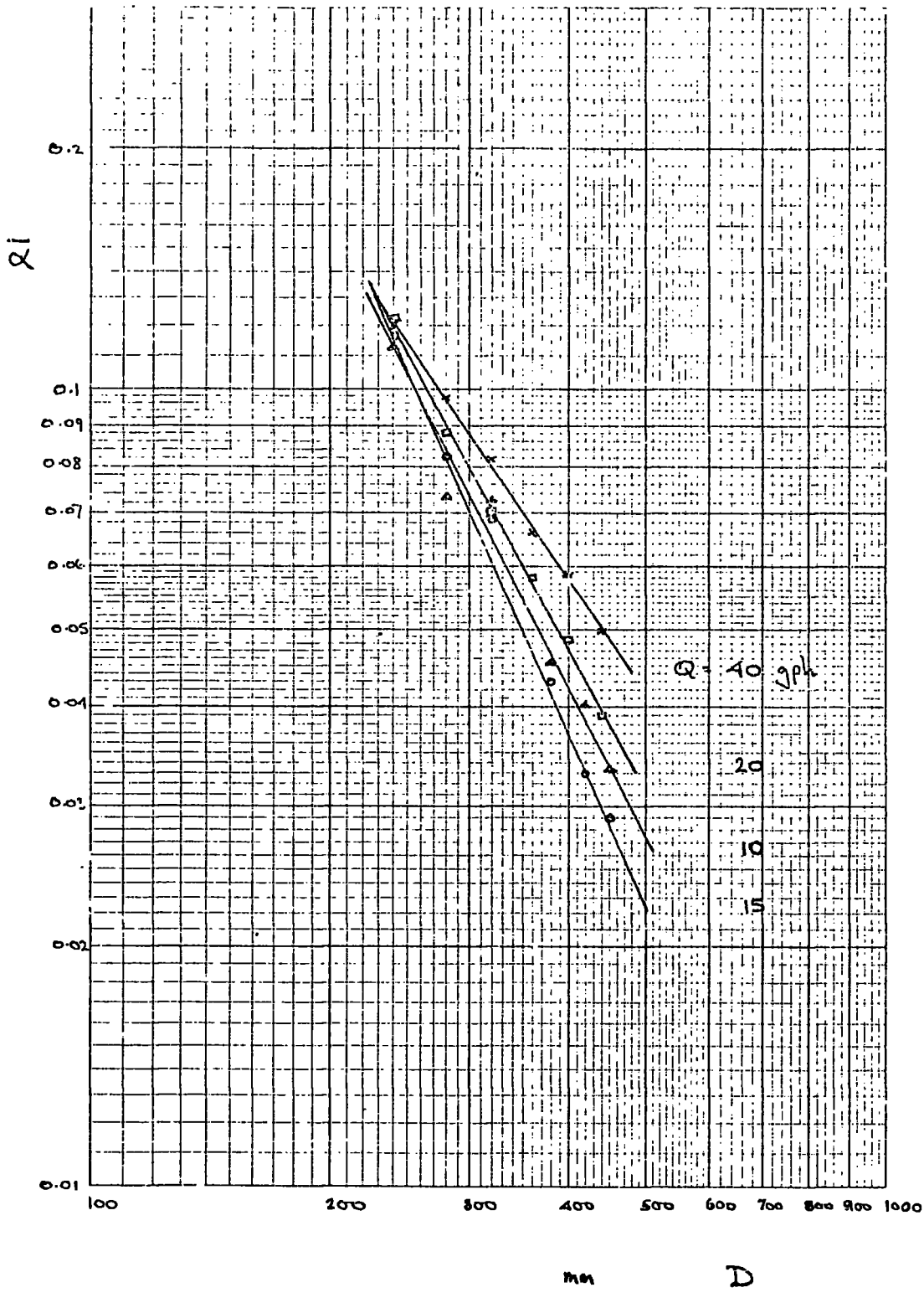

Fig. 4.4.1 Wave Number v. Diameter

of a critical wave number should not be ruled out.

Berbente and Ruckenstein's results were found to give good agreement with the amplitudes measured, though less good prediction of wavespeeds. Fig. 4.4.2. shows wave number plotted against the parameter ψ_{BR} . The lines for Q = 10, 20 gph are drawn at 45° and therefore strongly support a conclusion that a linear relation exists between α and ψ_{BR} . The Q = 40, 15 gph lines fit less well having gradients of 0.81 and 1.19. It has already been pointed out that the Q = 15 gph results are less reliable, and if a linear relationship is accepted they appear to fall into two sets of three points each, which fit well two separate 45° lines. As for the Q = 40 gph points, these correspond to less fully developed waves, and a 45° line could quite reasonably be drawn if the two highest points were discounted on this ground. If such a linear relationship is accepted, and revised 45° lines drawn as suggested, these yield values for the constant of proportionality which are plotted against flowrate in Fig. 4.4.3. The line made by these points has gradient - 1.56. The available evidence therefore strongly suggests that a relationship

$$\alpha \propto \psi_{BR}/Q^{3/4}$$

exists between wave number α and ψ_{BR} .

Seeking further evidence for the existence of a critical wave number, Fig. 4.2.7. gives ψ_{BR} = 10, 4.1, 1.0 as the values at which limiting amplitude is reached for the three flowrates. Fig. 4.4.2. shows the corresponding wave numbers to be .043, .049, and .037. Once again no firm conclusion can be drawn, though of the six values thus obtained only two differ by more than $6\frac{1}{2}\%$ from their mean value of .046.

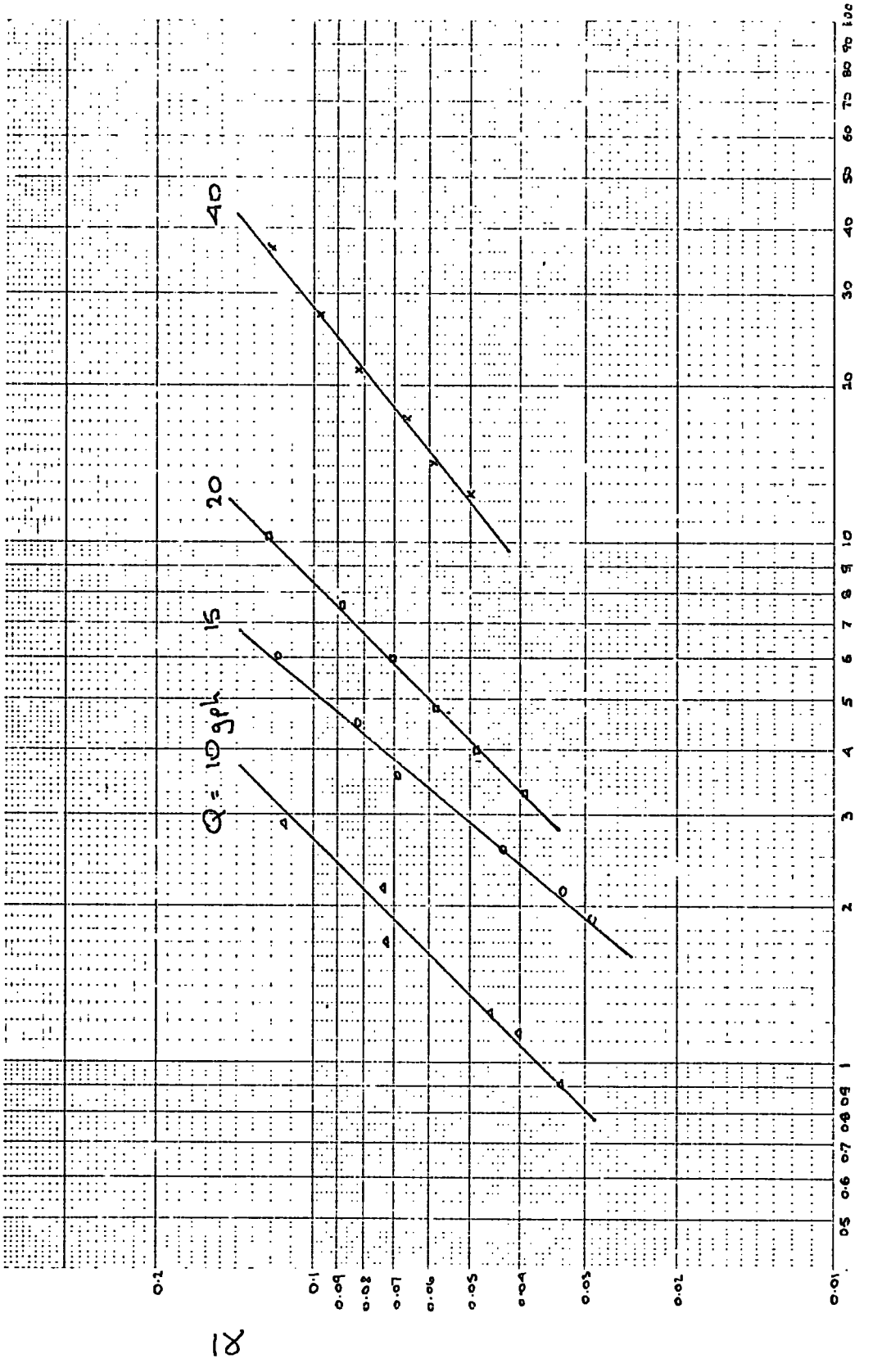

Fig. 4.4.2. Wave Number α. ψ_{BR}

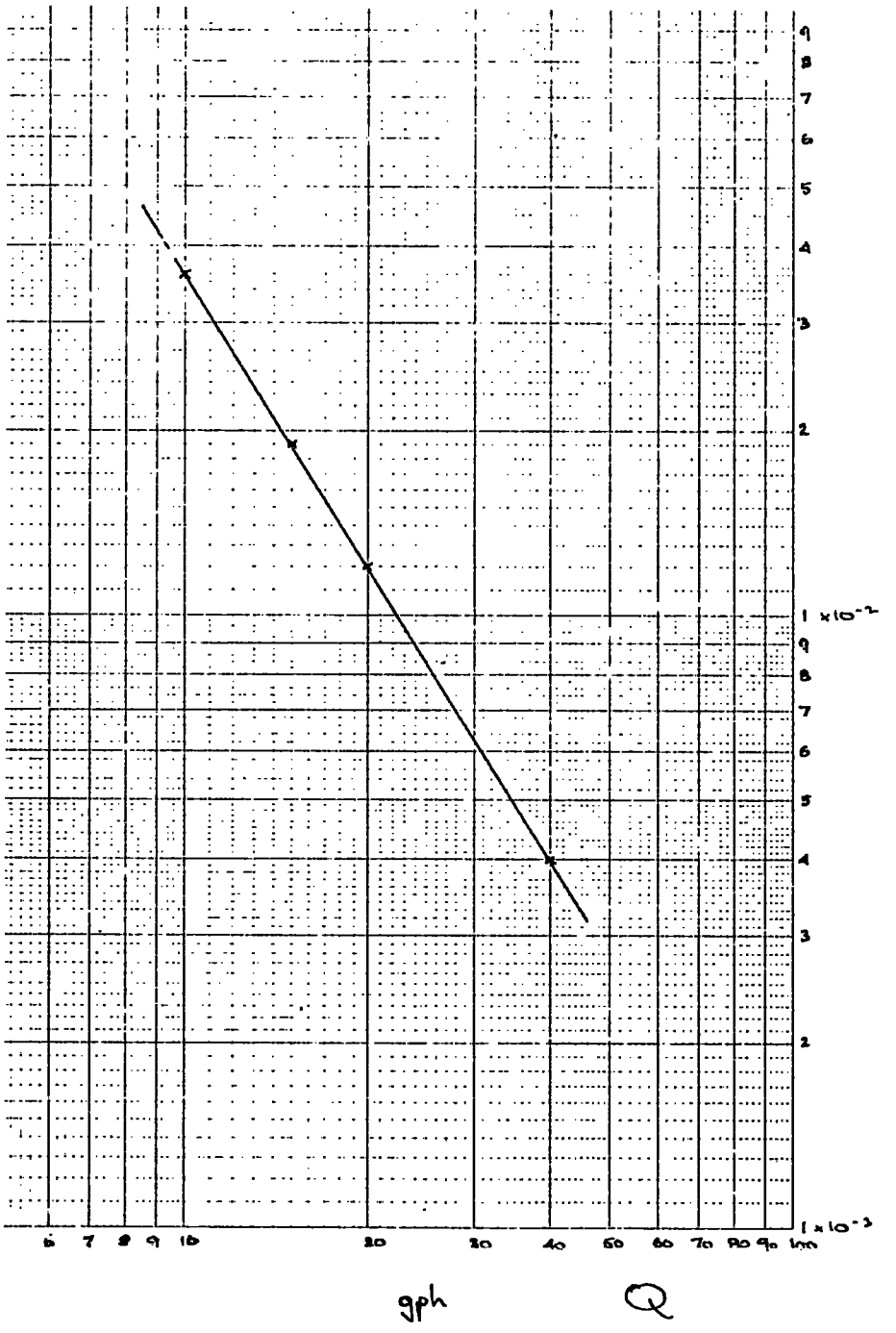

Fig. 4.4.3. Constant of Proportionality v. Flowrate

5

CONCLUSIONS

5 CONCLUSIONS

The following is chiefly a summary of the conclusions reached at various stages of this report. Further discussion may be found in the corresponding earlier sections.

On the theoretical side, an equation of motion and its appropriate boundary condition, derived for the flow over the cone, did show a dependence on the position on the cone in terms of non-dimensional distance $\varkappa$ along the cone generator. The effect of curvature and expanding surface width thus introduced is however small, since $\varkappa$ appears only in the form $1/\varkappa$. This may be related to physical lengths as $\frac{1}{\varkappa} = \delta/x = \frac{2\delta \sin\beta}{D}$ which is seen to be small since the mean film thickness δ is very small compared with the cone diameter D and becomes increasingly smaller with progress of the film down the cone. The solution of the system of equations produces a criterion of stability which shows that instability exists for

$$R_e > \frac{\tan\beta + \frac{7}{4\varkappa}}{\frac{9}{8}\varkappa\tan\beta + \frac{9}{4} + \frac{2\cot\beta}{\varkappa} - \frac{1}{3}\alpha^2 S}$$

This places a very low limit on the critical Reynolds number. It shows that for long waves (small α) of the type observed, the flow would only be stable at a value of Reynolds number so low that a film could not in practice be formed.

Experimentally also, the behaviour of the film was found to bear similarities with flow down an inclined or vertical plane. As in these cases there was an initial apparently undisturbed region for which Benjamin's('57) explanation must be assumed to apply, namely that while the flow is unstable, the rate of amplification there is too low to produce measurable waves. One striking advantage of the

cone was that, due to the thinning of the film produced, a whole range of Reynolds number was available for study at a single flowrate setting. The chief parameters of the basic flow, and the waves upon it, were found to behave as follows

Mean Film Thickness - was found to be expressible as a function of Reynolds number alone,

$$\text{mean film thickness in mm} = 0.0685\ R_e^{1/3}$$

Since Reynolds number is in turn directly proportional to flowrate, and inversely proportional to diameter and kinematic viscosity, one-third power law relationships hold for these also. The mean film thickness was found to be less than that of an undisturbed laminar film by some 7%, a figure in exact agreement with that deduced theoretically by Kapitza ('48).

Amplitude - three different measures of amplitude were employed, peak amplitude, root mean square amplitude, and a non-dimensional amplitude, wave intensity; all of these showed that a limiting value of amplitude was reached after a sufficient distance down the cone. This distance increases with increasing flowrate. The limiting amplitude agreed well with that predicted from the theory of Berbente and Ruckenstein ('68) based on a parameter incorporating both Reynolds and Weber numbers. After the limiting amplitude had been reached, the available evidence showed a more rapid decline of amplitude with further passage down the cone than Berbente and Ruckenstein's theory suggests.

Wave Speed - in the region of amplitude growth this was found to be essentially constant, starting at a value equivalent to the local free surface velocity and increasing to a value averaging around 2.5 to 2.6 times the local mean film velocity. This is a little greater

than the 2.4 times mean velocity proposed by Kapitza ('48) but is still less than the long wave speed of 3 times mean velocity deduced by Benjamin ('57). This long wave velocity appeared to act as a limiting value, several measured speeds came very close to it, but the very few that exceeded it were most probably the result of combined experimental errors. Berbente and Ruckenstein's theory did not predict wave speed at all well; this was most probably due to an effect of the slope for which they made no direct allowance.

Wavelength - no precise pattern of behaviour could be determined. The whole wave pattern was insufficiently regular for the determination of other than mean values. Fourier analysis to give spectrum densities for the related frequency values confirmed visual and photographic evidence in this respect. Nevertheless a clear trend was observed of wavelength increasing with passage down the cone, and doing so more rapidly at lower Reynolds numbers, particularly after the limiting amplitude had been reached.

Wave number - while no clear cut conclusions emerged for wavelength itself, its non-dimensional equivalent, the wave number, gave rise to some most interesting results. That they are based on mean wavelength values suggests caution in giving them too much weight, but they are nevertheless strongly supported by all the evidence available. Firstly it was found that at that point on the cone where measurements were first possible of the emergent waves, the value of wave number was closely similar, (.114 - .122) over the whole range of flowrate (10 - 40 gph) studied. Thereafter the wave number decreased with passage down the cone, and did so more rapidly at lower flowrates. Secondly the evidence strongly suggests that a linear relationship exists between the wave number and

a non-dimensional parameter:-

$$\psi_{BR} = \left(\frac{3}{\cos\beta}\right)^{1/6} Re\, S^{-1/2}$$

derived from that proposed by Berbente and Ruckenstein which also gave good correlation with the limiting amplitude results. Further consideration of the constant of proportionality involved showed it to be inversely proportional to (flowrate)$^{3/2}$. There was also some evidence to suggest that the limiting amplitude might be reached at a single critical value of wave number, but further evidence is needed to prove or disprove this.

While much basic information on the behaviour of the fluid film has been presented, a good deal remains that could usefully be investigated. Some of the above conclusions are presented somewhat tentatively, experiments with improved instrumentation, taking further flowrate values, and concentrating particularly on waves past the point of limiting amplitude, would yield valuable extra evidence. One most effective improvement would be the addition of a second instrumentation channel, feeding from a second identical probe a short distance down the cone generator from the first, on to a second channel of the recorder. This would give two broadly similar waveform traces displaced in time, and offer easily measurable wave velocities and rates of amplitude growth. More elaborate systems giving direct waveform analysis, or coded output for computation can be imagined, but they would be vastly more expensive and costly in development time also.

NOTATION

a_0, a_r, b_r	Fourier series coefficients
A	Area
A_{1-6}	Area of numbered face of element
$\hat{A}$	Peak amplitude $\pm \frac{1}{2}$ max. 'trough to crest' measurement
A_{rms}	Root mean square amplitude
A, B, C, D	Constants of integration
$c = c_r + ic_i$	Non dimensional wave velocity
$c' = c - 3/2$	
$c_r = \sqrt{a_r^2 + b_r^2}$	
c_{BR}	Wave velocity predicted by Berbente and Ruckenstein
C	Capacitance
D	Cone diameter
D	Differential operator
f	Pressure disturbance function
F	Froude number
$\tilde{F}$	Body force/unit mass vector
$F_{x,y,\Theta}$	Components of body force in directions X, Y, Θ.
g	Acceleration due to gravity
$h_{1,2,3}$	Rates of increase of length in directions α, β, γ
$i = \sqrt{-1}$	
i	Current
$I = A_{rms}/a_0$	Wave intensity
L, M, N	Integration coefficients
n	$2n + 1$ = number of points subjected to Fourier analysis
$O( )$	Of the order ( )
p	Non-dimensional pressure
P	Pressure
P_0	Atmospheric pressure above the film

q	Flow/unit width
Q	Total flowrate
$R = X\sin\beta + Y\cos\beta$	Distance from axis of cone
R	Resistance
$R_{1,2}$	Radii of curvature of free surface
$Re = \bar{u}\delta/\nu$	Reynolds number
$S = T/\rho\delta\bar{u}^2$	Non-dimensional surface tension parameter, the reciprocal of Weber number
t	Time
t	Probe - cone separation
T	Surface tension
T	Period of Fourier analysis
u, v, w	Non-dimensional velocities in directions x, y, Θ
U, V, W	Velocity components in directions X, Y, Θ
$\bar{U}$	Mean film velocity
$\tilde{v}$	General velocity vector
V	Voltage
V_{1-6}	Velocity normal to numbered face of element
$x(t)$	Equation of wave trace subjected to Fourier analysis
x, y, Θ	Non-dimensional cone coordinates
X, Y, Θ	Cone coordinates
$\alpha = 2\pi\delta/\lambda$	Wave number
$\bar{\alpha}$	Mean wave number, based on mean of wavelength estimates
α, β, γ	General curvilinear coordinates
β	Cone half angle
δ	Mean film thickness
Δ	Small change in value associated with higher approximation

ε	Relative Permittivity
ε_0	Permittivity of free space
η	Displacement of free surface coordinate
$\theta = \Theta$	Non-dimensional cone coordinate
Θ	Cone coordinate
$\kappa = \cot\beta/\pi$	
λ	Wavelength
μ	Dynamic viscosity
ν	Kinematic viscosity
ξ, η, ζ	Components of vorticity in directions X, Y, Θ
ρ	Density
σ_y	Normal stress in y direction
τ	Non-dimensional time
ϕ	Stream function disturbance function
ψ	Stream function
ψ_{BR}	Non-dimensional group proposed by Berbente and Ruckenstein
ψ_{KG}	Non-dimensional group proposed by Krantz and Goren
$\omega = T/2\pi$	Circular frequency of Fourier analysis
$\hat{\omega}$	General vorticity vector

Subscripts

x, y, z	Indicate partial differentiation with respect to
$0, 1, 2$	Indicate order of approximation
1	Indicates value at $y = 1$
P_1	Indicates particular integral

Superscripts

0	Indicates undisturbed flow quantity
$'$	Indicates differentiation with respect to y
$\bar{}$	Indicates mean value

BIBLIOGRAPHY

Anshus, B.E. '65. Ph.D. Thesis, Univ. of California, Berkeley.

Anshus, B.E. and Acrivos, A. '67. Chem. Eng. Sci., 62, 389.

Benjamin, T.B. '57. J. Fluid Mechanics, 2, 554.
'64. Archiwum Mechaniki Stosowanej, 16, 615.

Berbente, C.P. and Ruckenstein, E. '68. A.I.Ch.E.Jnl. 14, 772.

Betchov, R. and Criminale, W.O. Jr., '67. "Stability of Parallel Flows", Academic Press.

Binnie, A.M. '57. J. Fluid Mechanics, 2, 551.

Brauer, H. '56. V.D.I. Forchungsheft, 457.

Buevich, Y.A. and Gupalo, Y.P. '67. Fluid Dynamics, 1. translation of Mekh. Zhidk. i. Gaza, 1, 105, 1966.

Charvonia, D.A. '59. Purdue Univ. Jet Propulsion Lab. Rept. 1-59-1.

Chien, S-F. and Ibele, W.E. '67. Int.Jnl.Mech.Sci., 9, 547.

Collier, J.G. and Hewitt, G.F. '61. Trans.I.Chem.E., 39, 127.

Cooper, C.M. Drew, T.B. and McAdams, W.H. '34. Ind.Eng.Chem. 26, 428.

Espig, H. and Hoyle, R. '67. Proc.I.Mech.E., 182 (3H), 406.

Fallah, A., Hunter, T.G. and Nash, A.W. '34. J.Soc.Chem.Ind., 53, 369T.

Friedman, S.J. and Miller, C.O. '41. Ind.Eng.Chem. 33, 885.

Fulford, G.D. '64. in "Advances in Chemical Engineering 5". Academic Press.

Grimley, S.S. '45. Trans.I.Chem.E., 23, 228.

Gupta, A.S., '67. J.Fluid Mechanics, 28, 17.
'68. Canadian Jnl. Physics, 46, 2059.

Gupta, A.S. and Rai, L. '67. Proc.Camb.Phil. 63, 527.

Hinze, J.O. and Milborn, H. '50. J.Appl.Mech. 17, 145.

Hopf, L., '10. Ann.Physik (4), 32, 777.

Howe, M. and Hoyle, R. '70. Proc.I.Mech.E., 184 (3G).

Hoyle, R. and Matthews, D.H. '64. J.Fluid Mechanics, 22, 105.
'64. Int.J.Heat. Mass Transfer, 7, 1223.

Jones, L.O. and Whitaker, S. '66. A.I.Ch.E.Jnl. 12, 525.

Kamei, S. and Oishi, J. '56. Mem.Fac.Eng. Kyoto Univ.18, 1.

Kapitza, P.L. '48. Zh. Eksparim i. Teor. Fiz. 18, 3.
" " " " " 18, 19.
" " & Kapitza, S.P. '49. " 19, 105.
translated in "Collected Papers of Kapitza", Pergamon, 1965.

Kirkbride, C.G. '34. Trans.Am.Inst.Chem.Engrs. 30, 170.

Krantz, W.B. and Goren, S.L. '70. I. & E.C. Fundamentals, 9, 107.

Lamb, H. '32. "Hydrodynamics". Camb. Univ. Press.

Lee, J. '69. Chem.Eng.Sci. 24, 1309.

Levich, V.G. '62. "Physicochemical Hydrodynamics". Prentice-Hall.

Lighthill, M.J. and Witham, G.B. '55. Proc.Roy.Soc. A.229. 281.

Lin, S.P. '69. J.Fluid Mechanics, 36, 113.
" " '70. Personal communication of paper to be published.

Loitsyanskii, L.G. '66. Mechanics of Liquids and Gases" Pergamon.

Massot, C., Irani, F. and Lightfoot, E.N. '66. A.I.Ch.E.Jnl. 12, 445.

Nikolaev, V.S., Vachagin, K.D. and Baryshev, Y.N. '67. Int.Chem.Eng. 7, 595.

Nusselt, W. '16. Zeit. Ver. Deut. Ing. 60, 541, 569.

Orr, W. McF. '27. Proc.Roy.Irish Academy A. 27, 69.

Portalski, S. '64. I. and E.C. Fundamentals, 3, 49.
" " '64. Chem.Eng. Sci. 19, 575.

Robson, J.D. '63. "Random Vibration". Edinburgh Univ. Press.

Robson, B. '70. M.Sc. Thesis. Univ. of Durham.

Ruckenstein, E. and Berbente, C.P. '65. Chem.Eng.Sci. 20, 795.

Sommerfeld, A. '08. Atti del Cong. Int. dei Matematici, 3, 116.

Squire, H.B. '23. Proc.Roy.Soc. A., 142, 621.

Telles, A.S. and Dukler, A.E. '70. I. & E.C. Fundamentals, 9, 412.

Van Rossum, J.J. '59. Chem.Eng.Sci. II, 35.

Voinov, A.K. and Khapilova, N.C. '67. PMTF. Zh.Prikl.Mekh.Tech.Fiz. 2, 107.

Warden, C.P. '30. M.S. Thesis, Mass. Inst. Technology.

Whitaker, S. '64. I. & E.C. Fundamentals, 3, 132.
and Jones, L.O. '66. Am. Inst.Chem.Engrs. Jnl. 12, 421.

Yih, C-S '54. Proc.2nd U.S.Cong.Appl.Mech., ASME, 623.
" " '63. Phys. Fluids, 6, 321.
" " '65. " " 8, 1257.
" " '67. J.Fluid Mechanics, 27, 337.

APPENDIX I

Shape Correction for Capacitance Probe

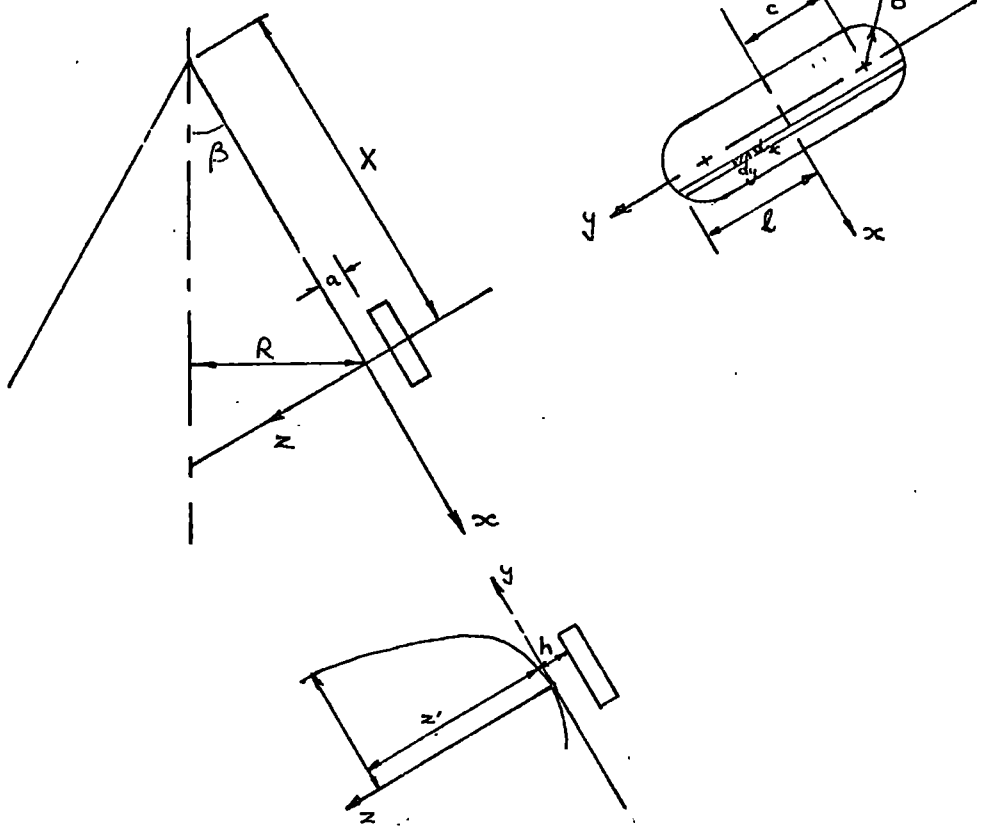

Capacitance of small element $dx \times dy = \varepsilon\varepsilon_0 \frac{dx.dy}{h}$

assuming roughly parallel plates, and parallel lines of flux which the guard ring should ensure. So for strip element dx wide

$$dC = 2\varepsilon\varepsilon_0 dx \int_0^{\ell} \frac{dy}{h}$$

But $h = R\sec\beta + a - z'$

and $\frac{z'^2}{R^2\sec^2\beta} + \frac{y^2}{R^2} = 1$

$$\therefore \quad dC = \frac{2\varepsilon\varepsilon_0 dx}{a} \int_0^{\ell} \frac{dy}{1 + \frac{R\sec\beta}{a}\left[1 - \sqrt{1 - y^2/R^2}\right]}$$

y/R has a maximum value which is small, expanding binomially and integrating gives

$$dC = \frac{2\varepsilon\varepsilon_0}{a}\sqrt{2Ra\cos\beta}\ \tan^{-1}\frac{l}{\sqrt{2Ra\cos\beta}}\ .\ dx$$

Now $l = c + \sqrt{b^2 - x^2}$ and $R = (X+x)\sin\beta$ for the strip

$$\therefore\quad dC = 2\varepsilon\varepsilon_0 b\sqrt{\lambda(K+t)\sin 2\beta}\ .\tan^{-1}\frac{\frac{c}{a} + \lambda\sqrt{1-t^2}}{\sqrt{\lambda(K+t)\sin 2\beta}}\ .\ dt$$

where $t = x/b$, $K = \frac{X}{b}$ and $\lambda = b/a$

The capacitance of the whole probe C is given by the integral of this between the limits $t = \pm 1$. For the same probe opposite a flat surface, as when calibrating

$$C_0 = \varepsilon\varepsilon_0 \cdot \frac{4bc + \pi b^2}{a}$$

Now if, as is the case, $C < C_0$ it leads to an apparent value for a greater than the true one. A correction factor of $C \div C_0$ must therefore be applied to the apparent a to yield the true value. After some manipulation

$$\text{correction factor} = \frac{2}{\pi + 4\frac{c}{b}} \int_{-1}^{+1} f(t)\tan^{-1}\frac{\frac{c}{b} + \sqrt{1-t^2}}{f(t)}\ .\ dt$$

where $f(t) = \left[\frac{a}{b}\left(\frac{X}{b} + t\right)\sin 2\beta\right]^{1/2}$

The following is a listing of a computer program used to carry out the integration, and calculation of this correction factor. The numerical integration is done by means of a combined Laplace forward and backward difference method. The accompanying graph, App.I.1. shows the magnitude of the correction for a range of values of X and a. In assessing the effect of this on readings taken, it must be remembered that correction factors must be applied to both 'wet' and 'dry' readings, so that it is only where such correction factors differ markedly that much effect results from their use.

```
C       PROBE H CORRECTION
C       MAIN PROGRAM
      1 FORMAT (4F8.5)
      2 FORMAT (13H SIN 2 BETA =,F8.5,5H  B= ,F8.5,5H  C =,F8.5,
     15H  H =,F8.5////)
      3 FORMAT (20(3H X=,F5.1,4H  A=,F4.2,7H  CORR=,F7.5)///)
        READ (5,1) TRIG,B,C,H
        WRITE (6,2) TRIG,B,C,H
        DO 500 J=1,20
        X=100.+20.*J
        DO 400 K=1,10
        A=1.40+0.10*K
        CALL CORREC(X,A,TRIG,B,C,H,CORR)
  400   WRITE (6,3) X,A,CORR
  500   CONTINUE
        STOP
        END


C       SUBPROGRAM
        SUBROUTINE CORREC(X,A,TRIG,B,C,H,CORR)
        DIMENSION S(1010),U(1010),V(1010),W(1010),Y(1010),Z(1010)
        Q=X/B
        P=A/B
        N=1.0/H+5.0
        T=-1.0
        SUMS=0
        SUMU=0
        SUMV=0
        SUMW=0
        SUMY=0
        SUMZ=0
        DO 10 I=1,N
        G=P*TRIG*(Q+T)
        IF(G) 11,11,12
   11   F=0
        GO TO 13
   12   F=SQRT(G)
   13   IF (1.-T**2) 14,14,17
   14   S(I)=0
        GO TO 18
   17   S(I)=F*ATAN((C/B+SQRT(1.-T**2))/F)
   18   IF (I-N+5) 15,15,16
   15   SUMS=SUMS+S(I)
   16   IF (I-2)    10,20,20
   20   U(I-1)=S(I)-S(I-1)
        IF (I-N+4) 25,25,26
   25   SUMU=SUMU+U(I-1)
   26   IF (I-3)    10,30,30
   30   V(I-2)=U(I-1)-U(I-2)
        IF (I-N+3) 35,35,36
   35   SUMV=SUMV+V(I-2)
   36   IF (I-4)    10,40,40
   40   W(I-3)=V(I-2)-V(I-3)
        IF (I-N+2) 45,45,46
   45   SUMW=SUMW+W(I-3)
   46   IF (I-5)    10,50,50
   50   Y(I-4)=W(I-3)-W(I-4)
        IF (I-N+1) 55,55,56
   55   SUMY=SUMY+Y(I-4)
   56   IF (I-6)    10,60,60
```

```
 60 Z(I-5)=Y(I-4)-Y(I-5)
    SUMZ=SUMZ+Z(I-5)
 10 T=T+H
    TINT=H*(SUMS+SUMU/2.-SUMV/12.+SUMW/24.-SUMY*19./720.)
    TINT=TINT+H*SUMZ*3./160.
    T=1.0
    SUMS=0
    SUMU=0
    SUMV=0
    SUMW=0
    SUMY=0
    SUMZ=0
    DO 110 I=1,N
    G=P*TRIG*(Q+T)
    IF(G) 111,111,112
111 F=0
    GO TO 113
112 F=SQRT(G)
113 IF (1.-T**2) 114,114,117
114 S(I)=0
    GO TO 118
117 S(I)=F*ATAN((C/B+SQRT(1.-T**2))/F)
118 IF (I-N+5) 115,115,116
115 SUMS=SUMS+S(I)
116 IF (I-2)   110,120,120
120 U(I-1)=S(I)-S(I-1)
    IF (I-N+4) 125,125,126
125 SUMU=SUMU+U(I-1)
126 IF (I-3)   110,130,130
130 V(I-2)=U(I-1)-U(I-2)
    IF (I-N+3) 135,135,136
135 SUMV=SUMV+V(I-2)
136 IF (I-4)   110,140,140
140 W(I-3)=V(I-2)-V(I-3)
    IF (I-N+2) 145,145,146
145 SUMW=SUMW+W(I-3)
146 IF (I-5)   110,150,150
150 Y(I-4)=W(I-3)-W(I-4)
    IF (I-N+1) 155,155,156
155 SUMY=SUMY+Y(I-4)
156 IF (I-6)   110,160,160
160 Z(I-5)=Y(I-4)-Y(I-5)
    SUMZ=SUMZ+Z(I-5)
110 T=T-H
    BTINT=H*(SUMS+SUMU/2.-SUMV/12.+SUMW/24.-SUMY*19./720.)
    BTINT=BTINT+H*SUMZ*3./160.
    CORR=2.*(TINT+BTINT)/(3.141592+4.*C/B)
    RETURN
    END
```

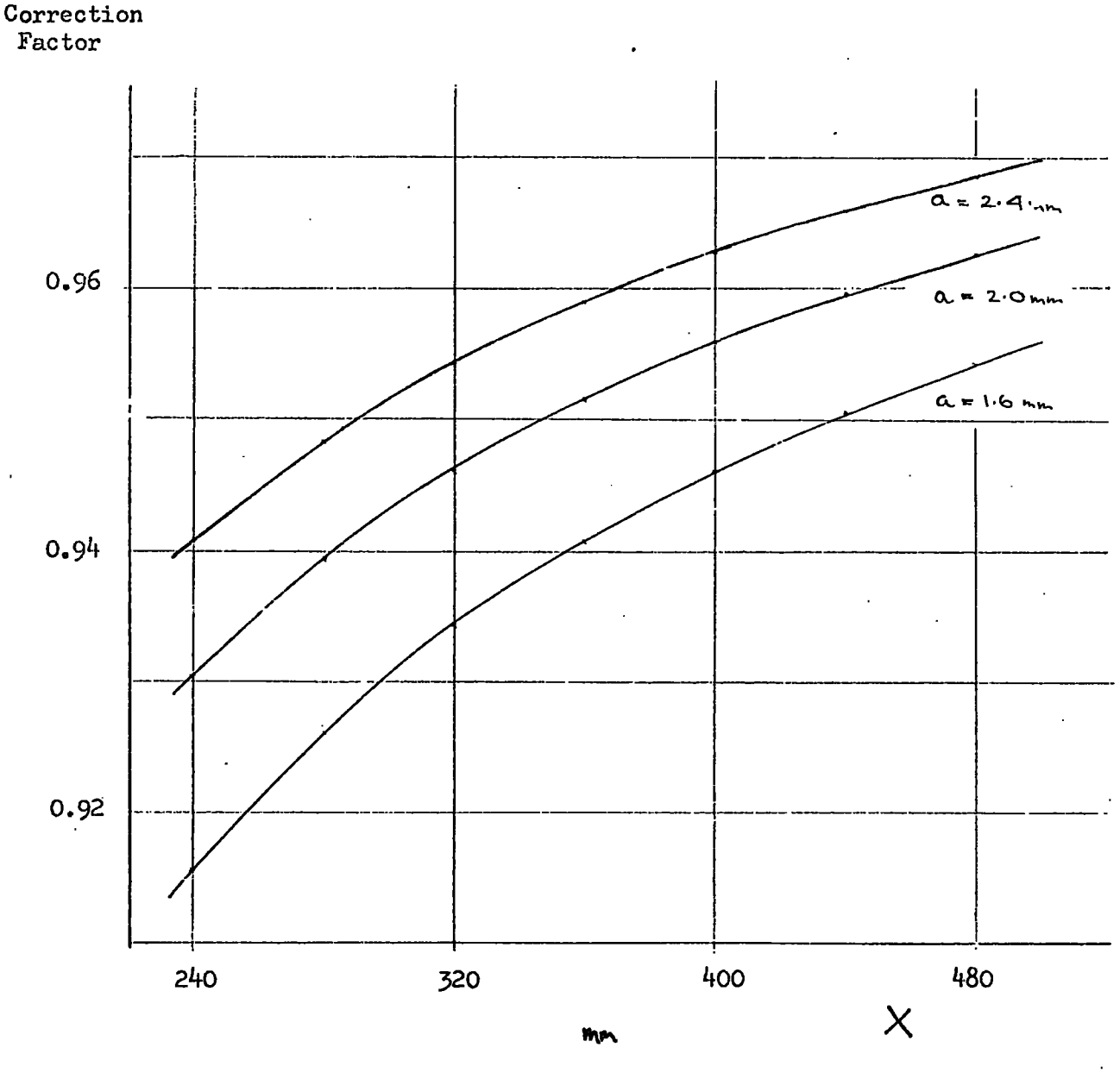

Fig. App.I.1 Correction Factor Variation

APPENDIX II

The following is a listing of the program used to carry out the Fourier analysis of the recorder traces. It is based on the IBM 360 SSP subroutine FORIT, and is written in Fortran to give the desired input and output manipulation. It produces a Fourier analysis of order 201 of the 401 successive trace ordinates which constitute the input data.

```
1     FORMAT(20F4.0)
3     FORMAT(' NO OF POINTS =',I5,' ORDER =',I3//)
4     FORMAT(' FREQUENCY =',I3,' AMPLITUDE =',F7.5)
5     FORMAT(' IER =',I1)
6     FORMAT(//'MEAN SQUARE =',F7.5,' RMS =',F7.5,' WAVE INTENSITY =',F7
     ..5)
      N=200
      M=N
      K=1330
      SUM=0
      DIMENSION FNT(401),A(201),B(201),C(201),D(201),NFREQ(201)
      READ (5,1) FNT
      CALL FORIT(FNT,N,M,A,B,IER)
      IF (IER) 8,9,8
8     WRITE (6,5) IER
9     NN=2*N+1
      NN1=N+1
      WRITE (6,3) NN,NN1
      DO 10 I=1,201
      D(I)=A(I)**2+B(I)**2
      C(I)=(SQRT(D(I)))/K
      IF (I-1) 11,11,12
12    SUM=SUM+D(I)/(2.*K**2)
11    NFREQ(I)=I-1
      IF (I-51) 13,13,10
13    WRITE (6,4) NFREQ(I),C(I)
10    CONTINUE
      RMS=SQRT(SUM)
      WI=RMS/(A(1)/K)
      WRITE (6,6) SUM,RMS,WI
      STOP
      END
```

APPENDIX III

The following is a listing of the program used for statistical analysis of the recorder trace. It is based on the IBM 360 SSP subroutine STAT, and is written in Fortran to give the necessary input and output manipulation. It produces mean, standard deviation, maximum, minimum and range values from the 401 successive trace ordinates which constitute the input data.

```
1     FORMAT (20F4.0)
2     FORMAT ('STAT YIELDS'//'AVERAGE=',F7.5,'  STD DEVN=',F7.5/)
3     FORMAT ('MIN=',F7.5,'  MAX=',F7.5,'  RANGE=',F7.5)
      DIMENSION A(401),S(401)
      K=1330
      NO=401
      NV=1
      READ (5,1) A
      DO 10 I=1,401
      S(I)=A(I)
10    CONTINUE
      CALL TALLY(A,S,TOTAL,AVER,SD,VMIN,VMAX,NO,NV)
      AVE=AVER/K
      SIGMA=SD/K
      YMIN=VMIN/K
      YMAX=VMAX/K
      DIFF=YMAX-YMIN
      WRITE (6,2) AVE,SIGMA
      WRITE (6,3) YMIN,YMAX,DIFF
      STOP
      END
```